Quality monitoring in extrusion-based bioprinting: From defect formation to AI-driven detection and correction

Md Asif Hasan Khan[1], Md Anisur Rahman[1], and Jinki Kim[1]

[1] *Department of Mechanical Engineering, Georgia Southern University, Statesboro, GA, USA 30458*

Abstract

Extrusion-based bioprinting is widely used to fabricate cell-laden three-dimensional constructs, yet its structural integrity remains difficult to ensure because interactions among bioink rheology, process parameters, hardware and construct design produce defects that compromise the dimensional accuracy and cell viability of the bioprinted samples. This review organizes the structural defects along a causal chain, from root-cause factors to nozzle-level failures (clogging and buckling-induced filament curling), filament-level defects (size inconsistency, fusion, delamination, sagging, collapse and breakage) and construct-level inaccuracy. It then maps each defect class to the sensing modalities that have been shown to observe it, spanning surface imaging (optical and machine-vision imaging, microscopy, thermography, video-based vibrometry and laser profilometry), volumetric analysis (optical coherence tomography, X-ray computed tomography, magnetic resonance imaging and ultrasound) and process sensing (dielectric impedance spectroscopy and flow sensing). The methods are compared in terms of processing stage, reported resolution and target object. The evidence linking each defect class to each method is also mapped. Machine learning is assessed as an interpretation layer on these data, distinguishing classification, segmentation, anomaly scoring, open-loop prediction, and assisting corrective measures in printing. Key open challenges include the scarcity of shared, standardized datasets, limited external validation and regulatory frameworks, the absence of standardized defect definitions and the coupling between structural fidelity and cell viability, which together define the requirements for quality-assessment frameworks that can support clinical translation. Collectively, this review aims to provide a structured foundation for developing quality assessment frameworks capable of supporting the translation of extrusion-based bioprinting from laboratory research toward consistent, clinically viable fabrication.

Keywords: Extrusion-based bioprinting; Defect detection; Process monitoring; Quality assessment; Closed-loop control; Machine learning

1. Introduction

1.1. Background

Organ transplantation represents one of the major advancements of modern biomedical science, with the number of transplants increasing steadily over the last two decades [1]. Nevertheless, the organ shortage remains a critical challenge worldwide. In the United States alone, more than 100,000 people are waiting for an organ transplant , and thousands of patients die each year while waiting [2]. Three-dimensional bioprinting has emerged as a transformative technology to tackle this challenge by enabling the fabrication of complex tissue and organ constructs using bioinks composed of living cells, hydrogels, and biochemicals, deposited in a precise, layer-by-layer manner [3, 4].

Bioprinting integrates principles from engineering, chemistry, biology, and materials science to create biomimetic structures. Bioprinting technologies can be broadly classified into extrusion-based, droplet-based, and light-based bioprinting [5]. Extrusion-based bioprinting dispenses a continuous filament driven by pneumatic pressure or by piston or screw displacement [6]. Droplet-based (jetting) bioprinting deposits discrete volumes of bioink through inkjet, acoustic or microvalve mechanisms [7]. Light-based bioprinting, such as vat photopolymerization (VP), utilizes light to crosslink photosensitive bioink, enabling rapid fabrication with high spatial resolution [8]. Among these, extrusion-based bioprinting accommodates the widest range of bioink viscosities and the highest cell densities, at the cost of relatively coarse resolution and lower reported cell viability [9, 10]. The same versatility, however, makes its outcomes particularly sensitive to process-induced defects, because filament formation depends directly on the interplay of bioink rheology, process parameters and hardware.

Clinical and preclinical milestones illustrate both the promise and the current limits of the bioprinting field: a full-size model of the human heart has been printed with the FRESH method [11]; acellular 3D-printed implants have been used for ear reconstruction [12]; experimental advances have extended to esophageal tissue regeneration [13], and a cell-seeded bionic ear has been printed and cultured in vitro [14]. Bioprinting, beyond its applications for organ transplantation, has been applied in diverse fields, including drug-toxicity testing [15], tissue engineering and wound healing [16], cancer research, and disease modeling [17–19]. Collectively, bioprinting holds significant potential for tissue engineering, drug delivery, and regenerative medicine, offering a pathway to create functional tissue constructs from patient-specific cells that could alleviate the organ shortage [20, 21]. However, the lack of process reproducibility and structural integrity remains one of the major barriers hindering the clinical translation of bioprinted constructs, as variations in bioink properties and printing conditions can introduce defects that compromise the function of bioconstruct. These limitations weigh most heavily on extrusion-based bioprinting because of its sensitivity to process-induced defects, and addressing them requires in-line monitoring and closed-loop quality control strategies. This review therefore focuses on extrusion-based bioprinting and examines how structural defects form, how they can be identified, and how AI can support reliable fabrication toward clinical practice.

1.2. Importance of process monitoring and defect detection in bioprinting

Bioprinted constructs must meet stringent criteria for clinical applications, particularly in organ transplantation. Along with critical factors including biocompatibility and functional performance, the structural integrity, including the architecture, mechanical strength, stiffness, and both micro- and macro-scale composition of the target tissues or organs [22], is critical to the successful clinical application of bioprinted constructs. Defects in the printing process, such as geometrical inaccuracies

(e.g., layer misalignment), inconsistent material deposition (e.g., nozzle clogging), or compromised cell viability due to shear stress, can severely undermine the quality and functionality of the final construct [23]. These challenges are particularly important for hydrogel-based bioinks, whose limited mechanical strength can lead to failures in maintaining structural integrity [24]. Moreover, because constructs are built layer by layer, a small deviation in one layer alters the substrate for the next and can propagate through the build, resulting in the loss of valuable bioinks, cells, and bioactive molecules [25]. In addition to the outer shape fidelity, internal features such as interconnectivity and porosity significantly influence structural stability, cell behavior, and tissue functionality [26, 27].

Process monitoring and defect detection in bioprinting are therefore essential to identify anomalies during fabrication and evaluate resulting constructs [28]. This is particularly relevant because cell-laden bioinks are costly and time-consuming to prepare, so early defect detection is economically as well as technically imperative. By implementing robust monitoring systems, researchers can enhance printing efficiency, reduce material and cellular waste, and improve the reliability and quality of bioprinted constructs. Furthermore, beyond detection alone, implementing closed-loop feedback control is necessary to autonomously mitigate subtle, early-stage defects and maintain print continuity without disruption. Ultimately, these approaches not only strengthen the structural integrity of the bio-constructs but also advance their readiness for clinical and industrial deployment.

1.3. Objective and scope of the review

The increasing demand for bioprinting, driven by its potential to transform organ transplantation and regenerative medicine, has fueled extensive research into its technologies, bioinks, and applications. Previous reviews have broadly explored bioprinting techniques [21, 29, 30], bioink development [31, 32], tissue-specific applications, including skin [16, 33], cornea [34, 35], and orthopedic structures [36, 37], as well as ethical considerations [38]. Former reviews have also discussed process monitoring, defect detection, and quality control. Yu et al. [39] reviewed defect monitoring and AI-enabled control across soft-material additive manufacturing, of which extrusion-based bioprinting is one process among several. Matavosian and Bonassar [40] examined real-time monitoring for the quality control of bioprinted constructs, with an emphasis on the design of future bioprinters. Bonatti et al. [41] and several reviews focused on artificial intelligence (AI) [42–44] surveyed machine learning (ML) across the bioprinting workflow, and Ke [45] described AI-driven closed-loop extrusion bioprinting from dynamic regulation to medical translation. Collectively, these works treat defects, sensing techniques and learning-based methods largely as parallel topics: defects are catalogued by their appearance, sensors by their modality and machine learning studies by their algorithm. The links among them, namely which process factor produces a given defect, and which sensing modality has been utilized to observe it and at what processing stage are seldom made explicit.

The present review complements these works by providing a focused synthesis of defect formation and identification in extrusion-based bioprinting that makes these links explicit, in three respects. First, it analyzes extrusion defects by organizing along the causal chain: governing relations from root-cause factor to nozzle-level failure, filament-level defect and construct-level outcome (Section 2). Second, it maps each defect class to the sensing modalities that have been shown to observe it, with the processing stage, reported resolution, and target object of each demonstration (Section 3.5, Tables 4 and 5). Third, this review assesses machine learning studies by task, validation design and whether a control action was demonstrated (Section 4.2, Table 6 and Section 4.3,Table 7), rather than by model architecture alone. Taken together, these three layers connect defect

mechanism, observability and learning-based detection within a single framework, so that the review both consolidates the existing literature and offers a structure against which new monitoring strategies can be positioned.

The scope is bounded in two respects. First, the review focuses on literature published mostly between 2014 and 2026, retaining earlier sources where they report foundational methods, definitions or regulations, and concentrates on extrusion-based bioprinting, which is widely utilized owing to its versatility, compatibility with a broad range of bioink viscosities, and capacity to create complex tissue constructs. Second, within this modality, the review addresses structural quality, namely filament geometry, internal architecture and dimensional fidelity, and the process signals that govern it. Cellular responses and tissue- and application-specific requirements, although important determinants of the overall quality of bioprinted constructs, are discussed only where they are coupled to structural defects or constrain the choice of monitoring method. Biological and cellular assessment is beyond the scope of this review.

The remainder of this review is organized as follows. Section 2 examines the key factors and failure modes governing defect formation and resulting filament- and construct-level defects. In Section 3, the process monitoring and defect detection techniques reported for bioprinting are surveyed, and their observables, reported resolution, and processing stage are evaluated and compared. Section 4 reviews artificial intelligence and machine learning approaches to defect detection and process monitoring. Section 5 examines how structural and cellular quality are coupled, Section 6 summarizes the open challenges and research gaps that must be addressed to build reliable monitoring frameworks, and Section 7 concludes.

2. Overview of defects in extrusion-based bioprinting

Defects in extrusion-based bioprinting primarily originate from multiple interdependent sources, including bioink material properties, hardware configurations, process parameters, and construct design. To understand the origins of defects in bioprinting, it is useful to examine them at two hierarchical scales: the global construct level and the local internal structural level. Defects manifest as macroscopic geometric inaccuracies at the global level [39], which are typically the cumulative outcome of instabilities occurring within the local internal structure. At the local internal level, defects typically originate at the filament scale before propagating through the structure. Commonly reported filament-level defects include inconsistent strand width and diameter, filament fusion, filament delamination, filament collapse. These defects primarily occur due to imbalances between the material's rheological properties, printing conditions, and construct design [3, 46].

Understanding the defects requires a systematic examination of how each root-cause category results in observable print defects. Bioink material behavior, particularly rheological instability, is one of the major factors behind most of these defects. Bioink with low viscosity tends to spread upon deposition, reducing shape fidelity [9], while viscoelastic materials may induce filament sagging and fusion [47]. Moreover, improper mixing of bioink, crosslinkers, and cells can introduce heterogeneity in bioink, leading to nozzle clogging and high shear stress, resulting in poor surface finish in filament and reduced cell viability [40]. Gelation kinetics further compound these issues: premature gelation weakens the interlayer adhesion, resulting in layer delamination [48], while the subsequent crosslinking process may alter the material properties of bioink, which may decrease the cell viability [46]. At the hardware and process level, nozzle geometry governs shear-induced reductions in cell viability and clogging [49, 50], nozzle misalignment introduces dimensional errors, instabilities in extrusion pressure, and unregulated temperature in bioprinting environment produce inconsistent filament dimensions. Moreover, design choices that ignore bioink rheology introduce geometric deposition errors, such as filament overlaps at sharp corners and insufficient filament gaps at high infill densities, which ultimately produce non-uniform layer heights and filament collapse. Cumulatively, these filament-level inconsistencies compromise the reproducibility of the microarchitecture, which presents a particularly critical challenge in extrusion-based bioprinting.

Collectively, these interdependent structural defects and deviations in geometrical fidelity underscore the necessity for real-time process monitoring. The following subsections systematically trace this causal chain along the process flow of extrusion-based bioprinting, as illustrated in Figure 1. Section 2.1 identifies the four major root-cause categories, highlighting the failure mechanisms associated with each. Section 2.2 focuses on the nozzle as the physical site where the mismatch between bioink rheology and process parameters and/or hardware configuration first manifests as failure in extrusion-based bioprinting. Section 2.3 describes the resulting filament-level defect types and explains how their accumulation compromises the integrity of the global construct. Section 2.4 synthesizes the causal chain and identifies the two considerations, the critical conditions of each defect and the stage at which it can be observed, that guide the choice of monitoring method.

Table 1 summarizes the cause-to-defect pathways across all four categories, while Figure 1 illustrates the relationship among different factors, failure mechanisms, and resulting defects.

Table 1. Relation between the cause and effect of major defects in extrusion-based bioprinting. Cellular outcomes coupled with the same factors are listed separately (Section 5).

Root-cause category	Contributing factor	Failure mechanism	Nozzle-level failure	Filament-level defect	Coupled cellular outcome (Section 5)	Reference
Material properties	Viscosity too high (or high yield stress)	Flow resistance exceeds the available pressure; air bubble trap	Nozzle clogging, filament curling at nozzle-tip	Filament size inconsistency, filament breakage	Higher wall shear stress at the pressure required for flow	[10, 24, 51–65]
	Viscosity too low	Spreading after deposition; sedimentation of cells and particles	—	Filament spreading, size inconsistency	Non-uniform cell distribution	
	Viscoelasticity, low elastic modulus	Self-weight not supported; excessive material accumulation	—	Filament fusion, sagging, and collapse	—	[24, 51, 56, 59, 66–69]
	Heterogeneity, improper mixing	High shear stress, fluctuating extrusion	Nozzle clogging	Rough surface	Low cell viability	[10, 50, 61, 64, 65, 70–72]
	Premature gelation, insufficient crosslinking	Weak adhesion and bonding	—	Filament delamination, fusion, and collapse	Low cell viability	[47, 68, 73–77]
Process parameter	Pressure/velocity mismatch	Over- and under-extrusion	—	Filament fusion, diameter/size inconsistency	—	[23, 28, 52, 55, 56, 69, 78–82]
	Nozzle tip-substrate gap	Gap too large: buckling or stretching; gap too small: compression and spreading	Filament curling at nozzle-tip (buckling)	Filament delamination, width deviation	—	[69, 74, 83–86]
	Temperature	Temperature-induced viscosity change, inadequate thermal stabilization (gelation)	Unstable extrusion	Filament spreading, size inconsistency, collapse	Thermal stress on cells	[87–92]
Hardware configuration	Nozzle shape/size	High shear stress	Nozzle clogging	—	Reduced cell viability (shear stress and exposure time)	[46, 49, 52, 60, 62, 69, 84, 93–96]
	Nozzle misalignment	Displacement error	—	Dimensional error	—	[97–99]
Design	Sharp corners	Excessive material accumulation	—	Filament fusion	—	[66, 67, 69, 97]
	Infill density	Large filament gap	—	Filament collapse	—	[67–69, 83, 100]

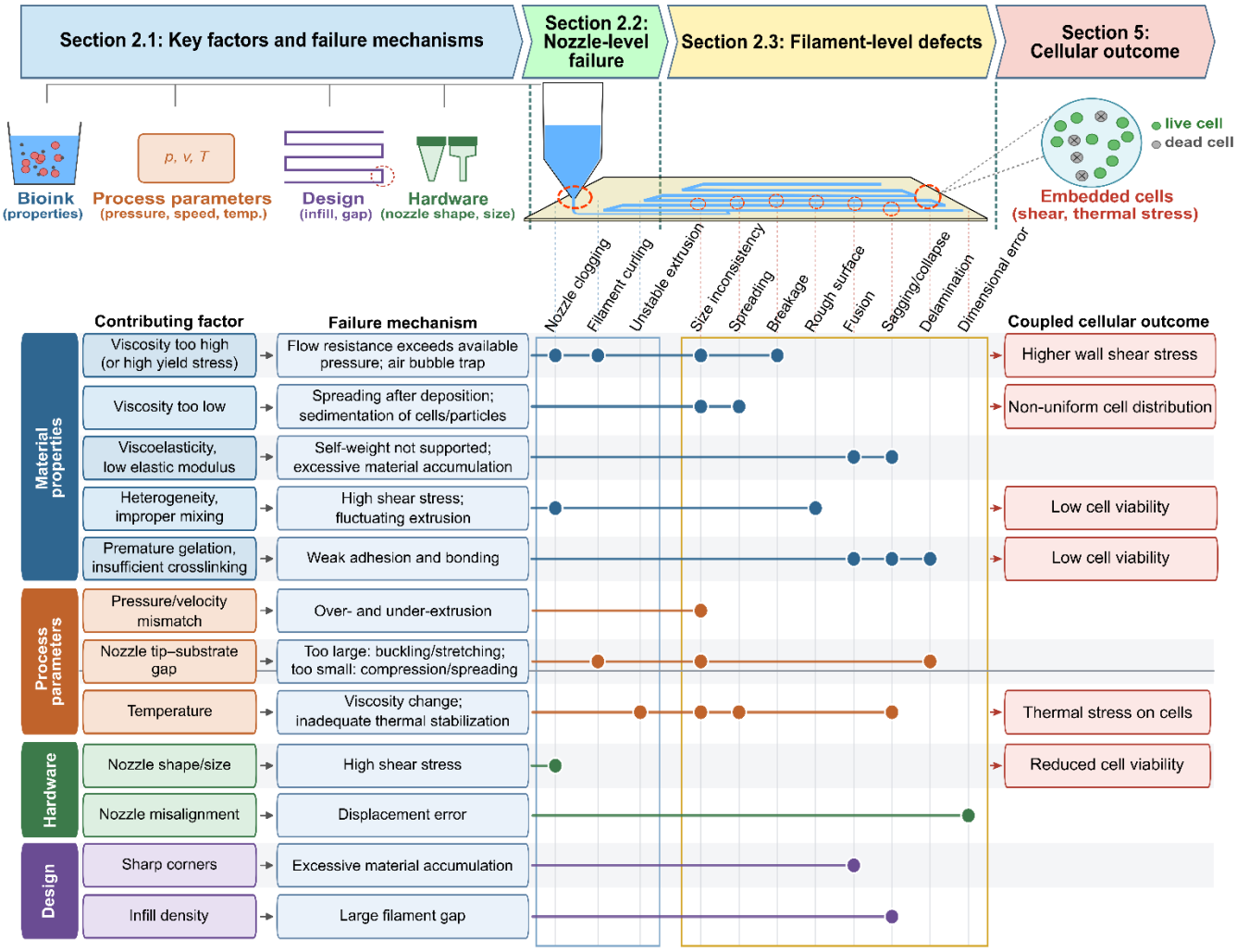


Figure 1. Defect propagation and failure analysis across the extrusion-based bioprinting workflow. Root cause factors (Section 2.1) act through nozzle-level failures (Section 2.2) to produce filament-level defects (Section 2.3), and, ultimately, construct-level inaccuracy.

2.1. Key factors causing defects

Defect formation in extrusion-based bioprinting is governed by the interplay of bioink rheology, printing parameters, hardware configurations, and design parameters [73], all of which shape how reliably a filament is deposited and how well the construct retains its intended geometry. Bioink rheology, particularly viscosity and viscoelasticity, governs the material's ability to flow through the nozzle and maintain its shape after deposition. Printing parameters such as extrusion pressure, flow velocity, temperature and layer height determine the consistency and continuity of the extruded filament. Hardware characteristics, including nozzle geometry and alignment, influence flow uniformity and deposition accuracy. Design parameters such as infill density and corner geometry further affect local support and filament deposition. Depending on how these factors interact, defects may emerge immediately after bioink deposition or after a certain printing process completion. Moreover, defects may also arise from multiple contributing factors, either independently or through their combined effects. For example, Figure 2

demonstrates different filament-level defects, such as size inaccuracy, filament curling, and filament fusion that can result from a combination of key factors. The core factors and the types of defects that arise from them are discussed in the following subsections.

2.1.1. Bioink material properties

Material rheological properties are pivotal contributors to defects in extrusion-based bioprinting [40]. Viscosity, viscoelasticity, gelation kinetics, and gel-like elasticity each govern a distinct failure pathway; the water content, polymer concentration, and crosslinker composition of the bioink collectively set these properties and therefore determine which failure modes are most likely. Viscosity strongly influences the printing quality and shape fidelity [54]. For instance, the water content in bioink influences filament spreading that can lead to fusion of adjacent filaments and consequently compromise the shape fidelity of bioprinted constructs, as illustrated in Figure 2(C) [28, 101]. Recent studies further emphasize the importance of bioink rheological properties in preventing nozzle clogging in extrusion-based bioprinting [24, 73, 102]. While highly viscous bioink may trap air bubbles, resulting in filament discontinuity when they pass through the nozzle [53], low viscosity may decrease the homogeneity in bioink, a cause for premature filament spreading and poor shape fidelity [24, 57]. Thus, applying constant extrusion pressure to such non-homogeneous bioink often results in increased strut diameter [52] and broken filament [10]. Additionally, bioink viscosity plays a critical role in filament curling at the nozzle tip after extrusion, as illustrated in Figure 2(B), which is further discussed in Section 2.2.2. While bioinks with a gel-like consistency exhibit improved shape fidelity, they can suffer from reduced cell viability due to raised wall shear stress on the cells in the nozzle [64].

Beyond the rheological properties, mechanical properties also contribute to printing defects; for example, a low elastic modulus often results in filament sagging [68] and fusion [24] that is shown in Figure 2(F). Moreover, the gelation process [47, 73] and cross-linking density [68, 75] are critical in balancing the shape fidelity and cell viability. A recent study indicates that increasing alginate concentration in cell-laden scaffolds can improve the shape fidelity and mechanical integrity and reduce swelling, yet this improvement may occur at the cost of cell viability [65].

Collectively, these findings demonstrate that printability arises from an interplay between rheological and mechanical properties of bioink. For instance, any changes in bioink formulation and processing conditions can result in under-, proper- or over-gelation, affecting the filament formation, pore geometry, and overall quality. Improving structural stability through increased viscosity, viscoelasticity, or crosslinking can introduce excessive extrusion resistance or affect deposition stability. The key challenge is, therefore, to maintain bioink properties within a printability window to enable smooth extrusion and stable deposition.

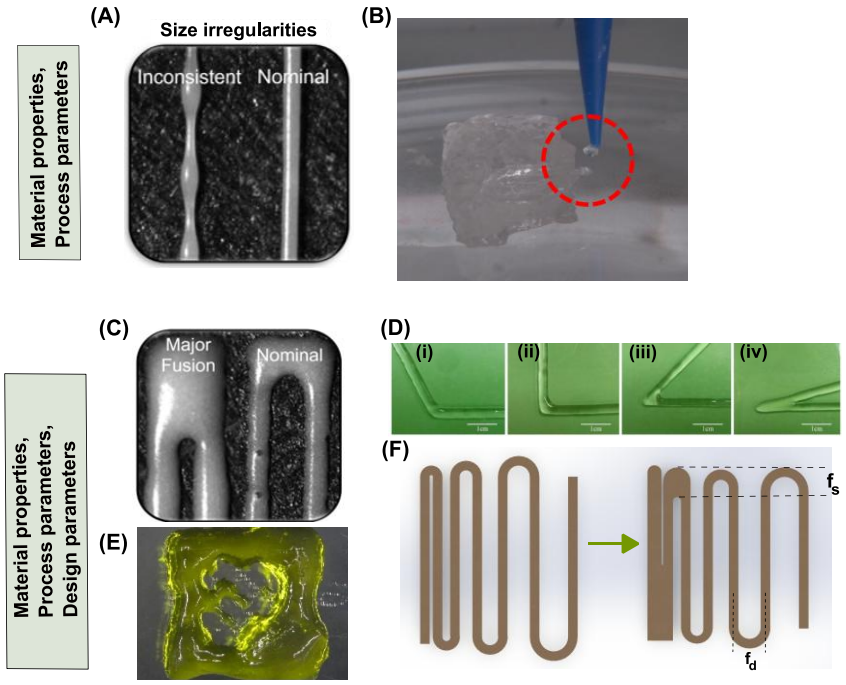


Figure 2. Filament-level defects in extrusion-based bioprinting with different combinations of key factors. (A) Filament size inconsistency results from mismatch among rheological properties, extrusion pressure, and printing speed [28] (B) Filament curling due to unstable rheological response and nozzle tip-substrate gap (C) Filament fusion due to spreading of bioink of adjacent strands due to material properties [28] (D) Filament fusion due to overlapping at sharp corners of design: (i) obtuse angle, (ii) right angle, (iii) acute angle, and (iv) sharp angle printing [69] (E) Filament fusion between adjacent layers due to over-extrusion, resulting from mismatch between extrusion pressure and material viscosity [103] (F) Filament fusion due to surface tension between bioink [68]; Bioink with lower yield stress obtains higher fused segment length (f_s) even at higher filament distance (f_d).

2.1.2. Process parameters

Process parameters, such as extrusion pressure, print speed, tip-substrate gap, and temperature, directly control the volumetric flow rate of bioink, the spatial accuracy of deposition, and the thermal environment in which crosslinking occurs. Mismatches among these parameters, or between any parameter and the rheological properties of the bioink, may produce a characteristic set of extrusion instabilities that resolve into filament-level defects [104].

Flow rate and printing speed represent a tightly coupled parameter pair: velocity and shear stress development form viscosity inside the extrusion needle has shown that any mismatch between flow rate and print speed causes over- or under-extrusion, which subsequently leads to deviations of the strand diameter from its target value [79, 80, 82], as depicted in Figure 2(A). In particular, because flow rate is dependent on extrusion pressure, increasing the pressure at a constant printing speed moves the process from under- to over-extrusion [81], resulting in filament fusion, as illustrated in Figure 2(E). Related work has also identified filament size and layer thickness deviations arising from pressure-velocity mismatches, with material deposition errors being especially pronounced at the start and stop points of each layer due to pressure hysteresis [23].

The gap between the nozzle tip and the substrate surface during deposition governs how the extruded filament contacts and adheres to the layer below. When this gap is too large, the extruded thread is deposited an unconstrained distance before contact, allowing it to deform under its own weight and buckle into coils (filament curling, Section 2.2.2). This filament curling may lead the filament away from its intended path. If the stage speed exceeds the extrusion velocity, the thread is stretched, thins, and if severe, may be pulled away from the previous layer, initiating deformation [84]. Conversely, a gap that is too small compresses the filament excessively, causing lateral spreading and an increase in strand width. The tip-substrate gap, therefore, together with the speed ratio, controls whether buckling or stretching occurs, while the resulting filament delamination is described further in Section 2.3.3.

The temperature profile of the bioprinting environment (bioink storage, syringe, nozzle, print bed) modulates the printing outcomes [91], especially by influencing the gelation of thermally responsive bioinks. For heat-gelling inks, such as chitosan-based thermosensitive formulations [88, 105], pluronic [106], and collagen [107], insufficient heat transfer from the print bed to the newly deposited layer can delay the gelation process, causing filament deposition instability [105]. In contrast, for cold-gelling inks, such as gelatin- and alginate-based formulations, lower print bed temperatures were found to stabilize crosslinking, yielding constructs with more consistent filament geometry [80]. Temperature also affects viscosity: as temperature increases, most hydrogel bioinks become less viscous, which shifts the system toward the low-viscosity failure mode of filament spreading and diameter inconsistency. In multi-material printing, differential thermal responses of co-extruded materials may introduce differential shrinkage or mismatched gelation timing, which could contribute to delamination at material interfaces [108].

Taken together, printing parameters greatly influence the outcomes of extrusion-based bioprinting because successful extrusion and stable deposition are often confined to a relatively narrow processing window. Insufficient pressure or excessive printing speed can result in under-extrusion or filament discontinuity, whereas excessive extrusion pressure or low printing speed promotes over-extrusion and dimensional deviation. The temperature profile further complicates this operating window by changing material properties, requiring adjustments in pressure and speed for accurate extrusion and deposition. Further studies should therefore focus on quantitatively defining defect boundaries across different bioink-printing condition combinations.

2.1.3. Hardware configuration

Defects in bioprinting also emerge from hardware configuration. Hardware configuration, principally nozzle geometry and nozzle alignment, governs two distinct failure pathways: one related to the shear stress field inside the nozzle, and the other related to the positional accuracy of the extruded filament. A central challenge in extrusion-based bioprinting is the shear stress generated as bioink is forced through the narrow nozzle cross-section. Excessive shear stress not only damages cell viability but can also develop unexpected extrusion behavior [94]. Early research examining the influence of pressure, temperature, and nozzle geometry on strand diameter found that, at the same pressure, conical needles produce a higher shear stress compared to the cylindrical counterparts, as illustrated in Figure 3 [52]. Conical needles, however, offered superior cell viability at low pressure [52, 93]. Subsequent simulation models corroborated this finding and further revealed that increasing nozzle length can improve cell viability, albeit at the cost of reduced printing accuracy [96].

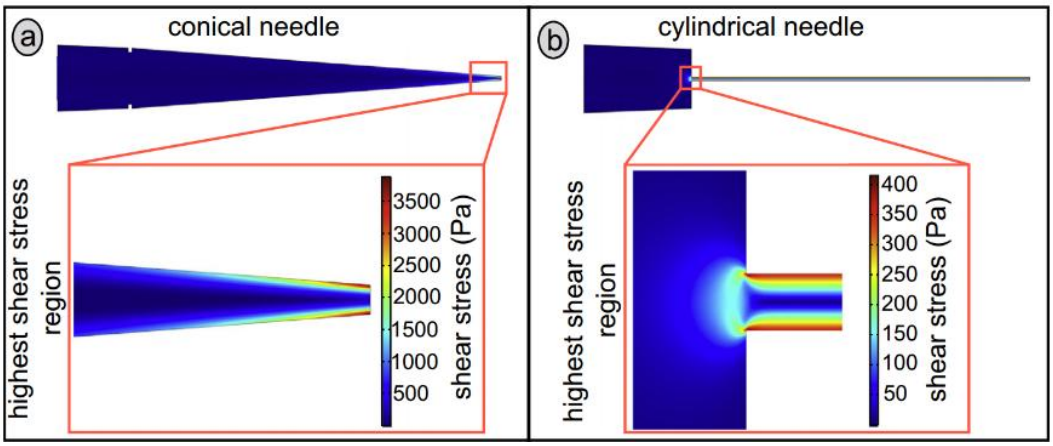


Figure 3. Finite element simulations of shear stress development in (a) conical and (b) cylindrical nozzle, showing higher shear stress in the conical needle [52].

Beyond nozzle geometry, hardware limitations such as nozzle misalignment and tip displacement errors introduce dimensional inaccuracies, particularly at tight corners and small radii of curvature, where fine motion control of the printer axes becomes critical [97, 98]. Compounding this, the material model developed to predict extrusion rate has struggled to achieve sufficient accuracy, further contributing to dimensional errors in the final construct. Moreover, the arrangement of the extrusion system and process selection also affects the material deposition in the case of multi-material extrusion [109]. This study showed the challenges in single-nozzle and multi-nozzle extrusion processes and how they may lead to extrusion-related defects such as discontinuity, misalignment, or unwanted material mixing. Additionally, the resolution of bioprinter defines the deviation between the actual printing trajectory and the reference trajectory, which results in dimensional error in printing samples with complex shape [99].

These findings highlight hardware configuration as an important determinant of process reliability. Quantitative characterization and calibration of printer geometry and mechanical components, together with integrated sensing and error-compensation strategies, are essential for minimizing hardware-induced deposition errors and improving reproducibility across different printing combinations.

2.1.4. Design parameters

Construct design determines the spatial demands placed on the deposited filament, including changes of angles of printing direction, unsupported span length, and the spacing between adjacent strands. When these requirements are not matched to the rheological capability of the bioink, geometric deposition errors are the immediate result.

In extrusion-based bioprinting, sharp corners in the print path require the extrusion head to decelerate sharply and rapidly change direction. At corners where the angle is inconsistent with the bioink viscosity and the printing speed, the nozzle continues to extrude material. As a result, sharp corners in the design often face overlapping issues, resulting in filament fusion, as illustrated in Figure 2(D), which can also damage the uniformity of the layer height [69]. Furthermore, this study notes that the infill density and pattern lead to strand fusion at the sharp corners if the filament distance is significantly lower than the

optimal threshold. In addition, when the angle of corner and printing parameters are not optimized for the bioink viscosity, filament fusion and merging may take place [67].

Scaffold design also determines the unsupported span length across which filaments must bridge. When the design prescribes long gaps between support points, the deposited filament becomes increasingly susceptible to deformation under its own weight. Previous studies demonstrated that filament sagging increases with increasing gap length [67]. A systematic experimental study further investigated filament collapse across different unsupported span lengths due to specific scaffold designs or printing paths [68]. In line with this, it was further demonstrated that increasing fiber spacing may compromise the mechanical strength of the sample [100].

Collectively, achieving the intended design does not necessarily ensure a defect-free construct, as some design parameters inherently increase the susceptibility to filament accumulation, fusion, sagging, or collapse. This highlights an important distinction between intended design and printable design, where the latter must account for the rheological and physical characteristics of the deposited bioink material.

2.2. Failure modes in the nozzle

The nozzle is a critical physical site at which the combined influence of material properties, hardware geometry, and process parameters first resolves into observable failure in extrusion-based bioprinting. Upstream mismatches among these root-cause factors, identified in Section 2.1, manifest at the nozzle as two primary failure modes: clogging, which disrupts the continuity of extrusion, and filament curling, which disrupts the positional accuracy of deposition. Both failure modes propagate downstream to produce the filament-level defects described in Section 2.3.

2.2.1. Nozzle clogging

Nozzle clogging is one of the most frequently reported failures in the extrusion-based bioprinting process, which can be triggered by multiple mechanisms. As the bioink is extruded through the nozzle outlet, the bioink material properties and applied pressure are responsible for the smooth flow of bioink. Clogging occurs when the resistance to flow through the nozzle tip exceeds the available extrusion pressure due to jamming of particles, premature gel, or cell aggregates at the concentration, or yield-stress plug. As a result, the bioink cannot be driven forward at the commanded rate, and the filament output ceases or becomes intermittent. An inadequately sized nozzle tip may restrict bioink flow and generate excessive shear stress along the nozzle wall, simultaneously risking clogging and compromising cell viability [49]. Similarly, highly viscous bioink needs a higher extrusion force, and the absence of this required force, too small nozzle diameter, or temperature-induced increase in material stiffness may trigger nozzle clogging at the outlet.

Material composition further contributes to this challenge. A study identified cell-sedimentation as one of the reasons behind the nozzle clogging [60]. When cells settle within the reservoir or barrel, the local concentration of solids near the nozzle tip rises, increasing effective viscosity and promoting clogging. Bioink preparation further influences flow through the nozzle, as cell-bioink mixing can introduce entrapped air bubbles (Figure 4) into the extrusion cartridge which can contribute to nozzle clogging, particularly in highly flow-resistant bioinks [110, 111]. Nozzle clogging was also encountered in coaxial extrusion for multi-material bioprinting [86].

The consequences of clogging extend beyond a simple interruption of extrusion. Partial clogging where flow is restricted but not fully blocked produces intermittent under-extrusion, which manifests as filament breakage or inconsistent strand width along the print path (Section 2.3.1). Full clogging terminates the print, requiring mechanical cleaning or nozzle replacement. In cell-laden extrusion-based bioprinting, the shear stress generated at the point of partial clogging, especially when the bioink is forced through an effectively narrowed orifice, can exceed the threshold for cell membrane damage, reducing cell viability (Section 5.1).

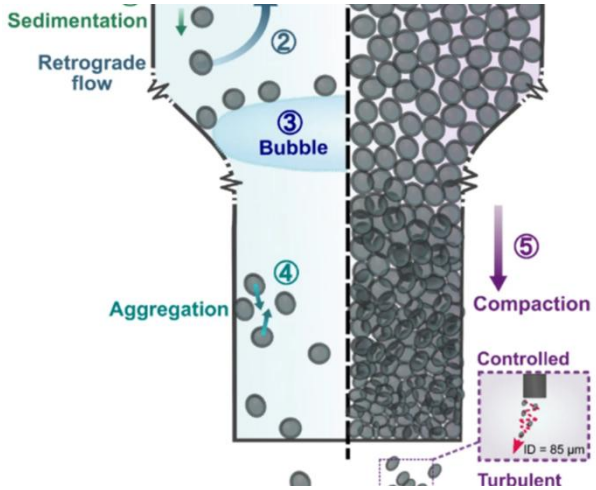


Figure 4. Air bubble trapped in extrusion-based microcapillary tip while cell deposition [112].

2.2.2. Filament curling at nozzle-tip

Filament curling occurs when the extruded filament buckles in the gap between the nozzle tip and the substrate, often twisting into a pig-tail-like shape before it touches down and stabilizes on the layer below, as shown in Figure 2(B). It has been reported for soft material 3D printing, including bioprinting [39, 113]. This behavior is closely associated with the rheological response of the bioink during and immediately after extrusion. Notably, bioink viscosity has been identified as a critical factor behind lateral buckling of bioink at the nozzle tip, resulting in filament curling [114]. In particular, shear-thinning behavior of the ink shortens the toe region of the deposition, increasing the likelihood of lateral buckling of the strand at the nozzle exit. Another study reports that excessive viscosity with higher concentrations of methacrylate mucin (MuMA) results in filament curling for composite bioink [58]. In addition, high concentrations of fibroin and gelatin methacryloyl may increase bioink viscosity to an extent that promotes wrinkle formation at the nozzle tip [60]. A similar phenomenon has also been reported in [10], where bioink warping at the nozzle tip was attributed to the non-uniform rheological behavior of the bioink material. Collectively, these findings suggest that filament curling represents a nozzle-exit instability arising when the rheological state of the bioink and the imposed extrusion conditions are poorly matched, in particular when the extrusion velocity exceeds the stage speed.

2.3. Filament-level defects

The root-cause factors of extrusion-based bioprinting defects described in Section 2.1, acting through the nozzle-level failures discussed in Section 2.2, ultimately produce structural deviations at the filament scale. These filament-level defects

represent the most direct and observable consequence of the underlying imbalances. Their significance extends beyond individual strands. The accumulation of such deviations across consecutive layers can propagate and lead to global structural inaccuracies in the final construct. The following sections describe common defects that are observed at the filament level, several of which are illustrated in Figure 2.

2.3.1. Inconsistent filament diameter

Filament diameter, represented by strand diameter and line width in different studies, is highly sensitive to the rheological properties of the bioink and the selected printing parameters. Higher extrusion pressure reduces the viscosity of shear-thinning bioinks in the nozzle, increasing the flow rate nonlinearly with pressure [52, 78]. At constant printing speed, the increased volume of extruded bioink, combined with slow recovery of viscosity after the deposition, causes lateral spreading and increases the strut diameter [52, 68, 78]. This underscores the need to select appropriate printing speed and dispensing pressure depending on the rheological properties of the bioink [67], as any mismatch may lead to an erroneous strand size compared to the target values [28, 79, 104], as illustrated in Figure 2(A).

Time-dependent viscosity changes further compound this problem. A study on alginate-gelatin (AG) bioink identified time-dependent viscosity change, temperature, pressure, and mismatch from printing speed as factors contributing to filament diameter variation [55]. The authors reported that the viscosity of the AG bioink decreased initially, leading to an increased flowrate and consequently a larger filament diameter. In addition, the viscoelastic properties of the bioinks have also been shown to promote lateral filament spreading after extrusion, further contributing to diameter variation along the printed line [56]. Collectively, these findings highlight that filament diameter consistency is not governed by a single parameter, but the dynamic interplay between bioink rheology and process parameters.

Diameter inconsistency is not merely a geometric imprecision. Excessively wide filaments can merge with adjacent strands, closing intended pores and producing strand interaction errors, as described in Section 2.3.2. Conversely, filaments that are narrower than the target width may create gaps in the bioconstructs, thereby compromising mechanical integrity. Filament diameter, therefore, serves as a key indicator of the overall print quality and a sensitive diagnostic variable for detecting mismatches in printing conditions.

2.3.2. Filament fusion

Filament fusion is one of the major filament-level defects in bioprinting that results from deposition errors or strand-to-strand interactions. It is defined as the pore closure between two filaments [68] due to capillary forces and material spread due to gravity [67], as demonstrated in Figure 2(C-F). This defect is strongly influenced bioink composition, extrusion pressure and geometric design. An early study analyzed the effect of hydroxyapatite (HA) concentration in alginate-gelatin bioink on filament fusion [66]. The results showed that increasing HA concentration raised the hydrogel's viscosity, and filament fusion occurred at sharp corners where the filament spacing was minimal. In a subsequent study, it has been reported that increasing the concentration of carboxymethyl cellulose (CMC) with alginate enhanced the mechanical properties of the hydrogel, resulting in proper gelation during extrusion [59]. The findings from this study demonstrated that material composition affects the gelation status, which can lead to pore merging and subsequent filament fusion, as shown in Figure 5. Over-deposition, another key factor contributing to filament merging [10], occurs when excess material is extruded, causing adjacent strands to

merge and compromising the printability of the bioink. In contrast to unintended filament merging, strategically modulating the strand-to-strand interaction can be exploited constructively. A recent study systematically varied gelatin methacryloyl (GelMA) concentration and printing parameters to identify conditions in which neighboring filaments fuse in a controlled manner to form a continuous membrane [115]. This demonstrates that the same filament interaction mechanism that constitutes a defect in scaffold printing can be an asset in membrane fabrication, provided that the governing parameters are accurately controlled.

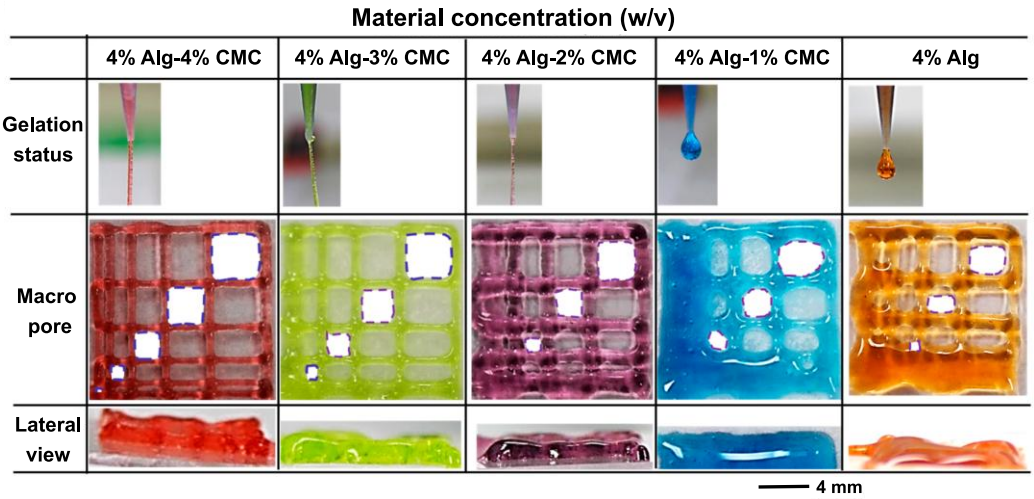


Figure 5. Effect of bioink composition on the gelation status and filament fusion [59]

2.3.3. Filament delamination

Filament fusion errors arise from excessive interaction between strands, whereas filament delamination represents the opposite– insufficient bonding between adjacent layers. This defect typically originates from inadequate deposition of material, excessive layer height, and insufficient fusion between successive layers [83]. Material properties play a central role in governing interlayer adhesion. Premature gelation or insufficient crosslinking density may prevent proper bonding during layer-by-layer deposition. This results in structurally weak interfaces that are prone to separation. Several crosslinking strategies have been investigated to address this issue. Post-crosslinking has been proposed as a means of enhancing shape fidelity, retaining the imparted shape without any separation in the filament [68]. Another study demonstrates that application of partial cross-linking after each layer strengthens interlayer bonds throughout the build process [74]. Process continuity and hardware-related factors further compound the risk of filament delamination. As discussed in Section 2.2.2, filament curling at the nozzle tip can introduce discontinuities in extrusion, leading directly to filament delamination within the printed layer. Collectively, these findings suggest that mitigating filament delamination requires simultaneous consideration of crosslinking behavior, deposition consistency, and hardware reliability.

2.3.4. Filament collapse and breakage

Filament collapse and breakage represent structural failure at the filament level, arising when the deposited strand cannot sustain its own weight or withstand the mechanical demands of the printing process. These phenomena are governed by

gravitational, mechanical, or rheological constraints, and are particularly pronounced in extrusion-based bioprinting, where unsupported spans are unavoidable.

An early study emphasizes that the viscoelastic properties of bioink play a critical role in filament rupture [51]. This study compared the filament structure and its collapse with beam mechanics to characterize structural failure. Soft bioink material goes into deformation after deposition, and filament sagging may occur due to the viscoelastic nature of the bioink, which results in filament collapse. In another study, a model was developed to connect yield stress with filament collapse [67]. This study showed that the severity of filament collapse increased as the filament gap widened. Additionally, this study revealed that higher yield stress in bioink leads to lower filament sagging after deposition, preventing filament collapse. Similarly, elastic modulus has been identified as an indicator of post-deposition stability, with low elastic modulus bioinks exhibiting greater susceptibility to filament collapse after deposition [68]. This combined influence of material properties and unsupported span length is clearly illustrated by the filament collapse test [59]. Increasing carboxymethylcellulose (CMC) concentration enhanced the hydrogel's viscosity and mechanical stiffness and improved its resistance to deformation even at higher unsupported filament gap, as demonstrated in Figure 6.

Gelation conditions introduce another dimension to this failure mode [47]. Rapid gelation of bioink may provide sufficient stiffness to resist filament collapse, yet bioink may fail to adhere to the previous layer, producing delamination. Slow gelation may enable bioink to support its own weight initially, but it can gradually sag as the viscous component relaxes. This will result in filament collapse if the gelation fails to progress rapidly enough to halt the deformation. The crosslinking rate must therefore be tuned to provide structural support during the time window between deposition and the arrival of the next layer, while remaining sufficiently fluid at the moment of layer contact to enable interlayer bonding.

Filament breakage is a related but mechanistically distinct failure. It occurs when the tensile stress in the elongating filament caused by the motion of the nozzle away from a fixed contact point exceeds the tensile strength of the extruded material [56]. This failure is most common during rapid print movements, when the nozzle accelerates away before the filament has been cleanly separated from the deposition point. Low viscosity bioinks and incompletely gelled formulations are particularly susceptible [116], as their tensile strength is insufficient to withstand the stretching imposed by rapid nozzle movement.

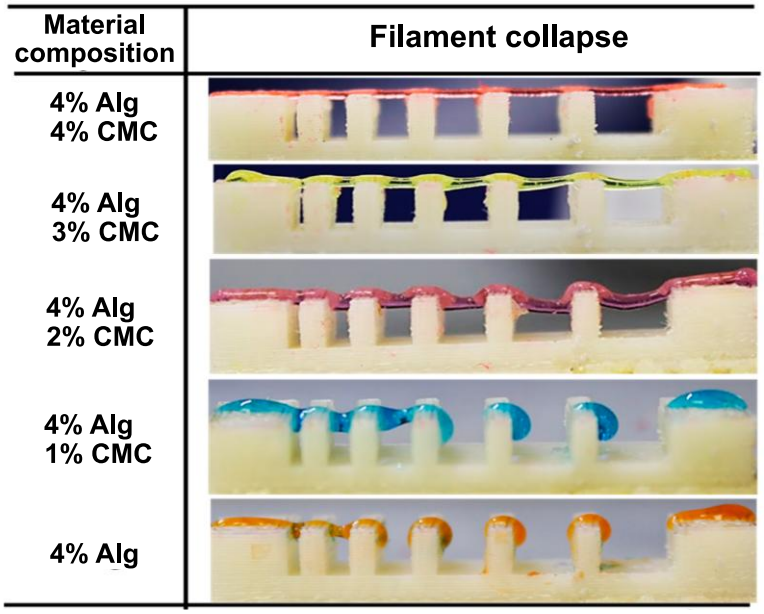


Figure 6. Effect of carboxymethyl cellulose (CMC) concentration in alginate-based hybrid hydrogel on the deflection of suspended filament in filament collapse test [59].

2.4. Critical synthesis of defect formation

The literature reviewed in Sections 2.1–2.3 demonstrates that defect formation in extrusion-based bioprinting is rarely governed by a single factor or pathway. Instead, combinations of bioink material properties, process parameters, hardware configuration, and design parameters, can converge on the same defect, while a single factor can propagate through several failure modes to produce different filament-level defects. Filament collapse, for instance, can arise from the rheological and mechanical properties of the bioink as well as from an excessive unsupported span. Because the same observed defect can have different origins, detecting it is not sufficient to identify its cause, and monitoring a specific defect requires two considerations. First, the values of the governing variables at which the defect is initiated should be estimated. For filament sagging and collapse, for example, the critical condition is set by the rheological parameters of the bioink relative to the unsupported span and the filament size [51, 67]. If the governing variables are monitored against their critical values for each defect type, the corresponding defect type can be anticipated before it forms, or at least before it has progressed substantially, rather than detected only after it has become visible. Second, the stage at which the cause or the developing failure can be observed should be identified. Causes located in the bioink, such as gelation state, are best observed before or during extrusion, by impedance or flow sensing; failures that develop at the nozzle exit, such as curling, form while the strand crosses the nozzle-tip gap and require sensing near the tip; and failures that develop after deposition, such as sagging, fusion and delamination, evolve between successive layers and are accessible to layer-wise or volumetric imaging. These two considerations form the basis for selecting appropriate process monitoring and defect detection techniques, as discussed in the following section. Section 3 surveys the methods available at each stage, compares and maps them to the defect classes they detect.

3. Process monitoring and defect detection techniques

Ensuring the structural integrity of bioprinted constructs requires monitoring techniques capable of detecting the diverse range of defects and process anomalies discussed in the preceding sections. Process monitoring and defect detection methodologies in bioprinting encompass techniques that operate across different stages of printing process, either in situ to capture defects as they form or post-process to evaluate the final construct after printing is completed. Because of the unique principle of the printing workflow of extrusion-based bioprinting and different bio-ink properties, a variety of techniques have been utilized. These techniques are commonly categorized based on their working principles and sensing modalities, ranging from vision-based (Section 3.1) and volumetric imaging (Section 3.2) to impedance measurements (Section 3.3), and ultrasonic and flow-based monitoring (Section 3.4). The following subsections summarize, for each method, their working principles, measured quantity, the stages and types of defects they address, and the main limitation. Section 3.5 then relates the methods to the defect classes of Section 2 (Table 4) and compares them (Table 5).

3.1. Vision-based monitoring and surface optical profilometry

Vision- and optical-based methods are among the most frequently adopted approaches in bioprinting, owing to their non-contact and non-destructive nature and compatibility with a wide range of soft bioink materials. They measure shape fidelity, filament dimensions and surface geometry during or after printing and, except for video-based vibrometry, observe mainly the surface. This section covers optical imaging and machine vision, microscopy, thermography, video-based methods and laser profilometry.

3.1.1. Optical imaging and machine vision analysis

Camera-based imaging has traditionally been among the most frequently reported methods for defect detection in extrusion-based bioprinting. These approaches provide insights into critical aspects of the printed constructs, such as shape fidelity, irregularities, precise layer alignment, and anomalies during material deposition. These techniques harness camera systems to capture high-resolution images of the printing process, which enables defect detection at both micro- and macro-scales. When combined with sophisticated computational image analysis, they allow for a non-invasive assessment of printing quality. By continuously monitoring the printing process, computer vision systems can identify deviations from the intended design and detect geometric inaccuracies at the surface level.

Early efforts focused on quantifying the geometry of extruded strand as a practical indicator for print quality, recognizing that shape accuracy of the printed sample and filament formation is directly governed by bioink rheology [117, 118]. An image-based approach was developed to measure the strand size and area in pneumatic extrusion-based bioprinting using a microplate reader [119]. While effective for opaque bioink materials that are commercially available, this method faced limitations in detecting the line width accurately when transparent bioinks with higher water content were used. This limitation immediately revealed the sensitivity of optical approaches to material properties. Recognizing this limitation, subsequent work introduced a coaxial camera system that is mounted close to the printhead to capture axial images at in situ conditions, extending the extruded line monitoring to detect defects due to over-extrusion in systems using commercially available bioinks [120]. A high-definition camera was installed near the printhead, which moves over the construct after each layer is printed and captures coaxial images of the sample. This method compared binarized images of a printed square lattice pattern with the corresponding

binarized image from the model, from which the 'over-extrusion' metric was developed to quantify defects. Notably, layer drifting phenomena were also detected in this approach, enabling layer-by-layer defect detection. Furthermore, another image-based approach used the pore index as a parameter to identify the effect of uneven extrusion based on the pore sizes of the printed layers [121]. Despite this advancement, the cameras remained sensitive to ambient lighting conditions and bioink transparency. Most recently, computer vision-based approach was implemented with an integrated camera to capture the images of extrusion outputs at in situ conditions to quantify area and spatial fidelity in embedded bioprinting [122]. A bioprinting system was developed in this study, which included a high-resolution camera installed beneath the extrusion nozzle, enabling the real-time monitoring of the outputs from the nozzle. This integrated approach offers reconstruction of high-resolution images and real-time tracking of nozzle flow, unlike the traditional camera-based approach [120, 123], where the camera is installed at an angular position and relatively larger distances. Machine-vision measurements have also been fed back to the toolpath: helix paths were corrected when edge deviations exceeded 1 mm [124, 125], and robotic printing reduced detectable layer-width deviations to 0.15 mm [126]; these closed-loop uses are compared in Section 4.2.

Collectively, optical imaging and machine vision methods have evolved from simple geometric measurements toward in-process monitoring and correction (Figure 7) [41, 127–131]. On the other hand, their performance remains tied to the experimental conditions, particularly lighting consistency and bioink transparency. For instance, visible-light approaches remain sensitive to ambient lighting conditions and transparent bioinks, while higher-resolution imaging is required for precise measurement. Additional challenges arise for complex and stacked designs, where distinguishing individual strand becomes increasingly difficult, while processing higher-resolution images requires computational demand for real-time application. While several approaches have been introduced to classify and quantify filament level defects, integrating this information into corrective control remains less explored, highlighting research opportunities in increasing robustness of these approaches.

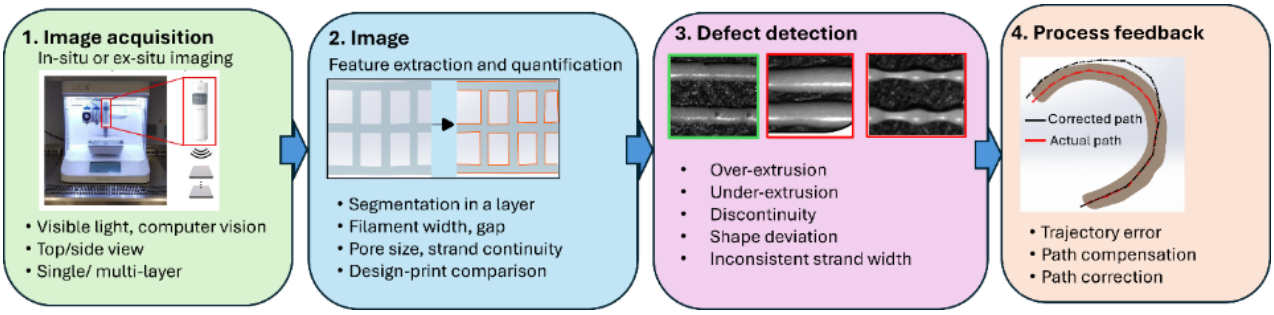


Figure 7. Progression of optical imaging and machine vision approaches in extrusion-based bioprinting. Image in (1) and (3) are reused from [120].

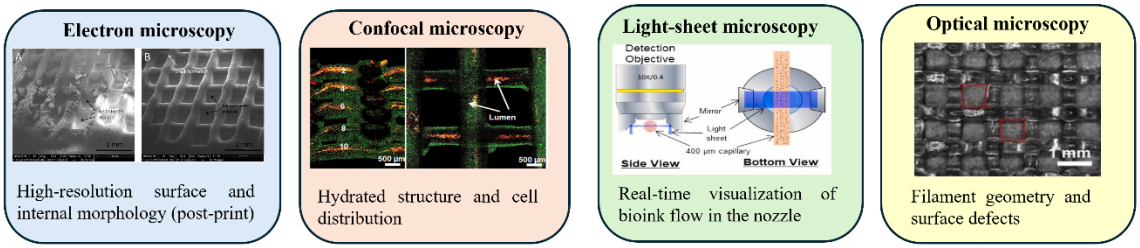
3.1.2. Microscopic visualization

While machine vision methods excel at capturing surface-level geometric deviations, they are limited in their ability to resolve finer structural details. Microscopic visualization helps address this limitation by providing high-resolution, contactless imaging of morphology and geometric deviations at scales that are inaccessible to standard cameras. Two different kinds of microscopic imaging have been utilized in bioprinting: (i) optical microscopy, including fluorescence, confocal, and stereomicroscopy, and (ii) electron microscopy. These methods differ in resolution, depth of field, and magnification.

Optical microscopy has been applied across a range of bioprinting processes to monitor the printing outcomes. The electrohydrodynamic bioprinting process involves extrusion of bioink containing living cells in the presence of high-voltage application [132, 133]. Digital microscopy was used to extract unstable jet modes from jet centroid and size [134], demonstrating the potential to be implemented in extrusion-based bioprinting as well. Similar to the jet monitoring approach, another study used light-sheet fluorescence microscopy for real-time monitoring of hydrogel flow in extrusion-based bioprinting [135]. This approach offers fluid flow profiles of the bioink within the extrusion nozzle, and the findings were used to adjust printing conditions. Additionally, bioink printability was assessed in extrusion-based bioprinting by comparing the images obtained from a laser confocal microscope [47]. This research revealed how gelation rate influences extrusion behavior at the nozzle tip and the integrity of the final structure. Stereomicroscopy has similarly been used to assess the printability by imaging fiber formation and detecting defects such as fiber detachment, merging, and blending across stacked layers [78]. Building on these findings, a systematic study used optical microscopy to relate nozzle pressure, printing speed, and bioink dilution to extrusion width, providing a practical framework for detecting over- and under-extrusion through parameter optimization [136]. In line with this, microscopic images have also been used to assess extruded filament based on the geometry of the filament [137].

The effectiveness of optical microscopy is limited when imaging hydrogel with opaque microparticle due to light scattering [138]. As a result, scanning electron microscopy (SEM) has been introduced for surface morphological [139] and sub-surface analysis at both macro- and micro-scale for different hydrogel conditions [140]. Printing defects such as strand shrinkage, surface roughness, and crack formation have been detected under *ex situ* conditions using this technique. Cryo-SEM, a variant of SEM in which samples are rapidly frozen, has been applied to polysaccharide hydrogels to capture surface cracking after sublimation and analyze porosity distribution [141]. In addition, a recent study clarified that microstructural metrics, especially pore size, can be influenced by dehydration and freezing artifacts and may therefore not represent the native state of bioprinted hydrogel scaffold [142].

Collectively, microscopic visualization methods complement machine vision approaches by enabling structural defect detection at finer length scales. On the other hand, the need for extensive sample preparation in electron microscopy and the requirement to interrupt printing for in situ optical imaging remain practical constraints that motivate the development of more seamlessly integrated monitoring solutions. The capabilities and limitations of these approaches, from detailed post-print characterization toward more integrated in-situ visualization are illustrated in Figure 8. These limitations highlight the need for non-destructive, integrated imaging approaches that combine microscopic resolution with larger area and real-time monitoring capabilities.



Typical resolution	~1-100 nm	~200 nm	~1-5 µm	~1-10 µm
Field view/depth	Small (localized)	Limited (tens to hundred of µm)	Nozzle region (localized)	Moderate (mm-scale)
In-situ capability	No (post-print)	Limited	Yes (localized)	Yes
Sample preparation	Extensive (dying, coating)	Minimal (often requires labeling)	Minimal	Minimal
Key advantages	High structural detail	Hydrated structure, cell imaging	Real-time flow visualization	Simple, fast assessment
Limitations	Artifacts (shrinkage, deformation)	Shallow imaging depth, labeling often required	Limited to small region, special setup	Limited contrast for transparent hydrogels

Figure 8. Comparison of microscopic visualization approaches used in extrusion-based bioprinting process. Images are reused from [135, 140, 142, 143]

3.1.3. Thermographic imaging

Thermographic imaging exploits the thermal signature of deposited materials to enable defect detection, particularly when printing transparent bioinks where conventional optical contrast is limited. An early study utilized thermal imaging as a process monitoring approach in thermally controlled extrusion bioprinting process, where the infrared thermography was used to optimize and validate the printing parameters [107]. Thermal images were captured using a thermal camera to analyze the selected region of interest of the thermally controlled bioprinting unit. Notably, the thermal signature at the nozzle tip indicated the presence of nozzle clogging in this setup, demonstrating that thermal data can provide process information beyond temperature measurement alone. Building on this work, a recent study has implemented thermal imaging for in situ inspection and monitoring of multi-layered bioprinted constructs [144]. This method analyzed temperature gradients from thermal signatures to determine the deviations in the shape of the most recently printed layer, thereby addressing limitations of visible-range imaging. Additionally, this method enabled the detection of layer geometry variations resulting from non-uniform material extrusion during printing. More recently, the approach has been extended toward fully in-line monitoring by integrating G-code trajectory information into the thermal analysis pipeline. This integration enabled real-time frame-by-frame segmentation of the extruded biomaterial and direct comparison against the nominal geometry [145]. As a result, color-coded maps were generated to identify correct depositions, under-extrusion, and over-extrusion along the printing path, establishing a foundation for future closed-loop feedback control.

Thermal imaging provides a real-time, non-contact representation of the temperature field of the extrusion process in bioprinting, which enables continuous process monitoring. Existing studies demonstrate that this method can detect under-extrusion, improper distribution of material, and deviations in shape fidelity of the printed samples. Additionally, the sensitivity of this method to thermal contrast provides an advantage for monitoring transparent bioinks that are difficult to distinguish using visible light imaging. On the other hand, this capability depends on the temperature contrast between newly deposited bioink and the substrate, which decreases with time. The relatively low spatial resolution of thermal cameras also limits the

detection of small-scale defects, while increasing magnification can reduce the field of view and introduce imaging artifacts. These limitations create a trade-off between thermal contrast, spatial detail, and field of view. Moreover, current approaches require broader validation across different bioinks, thermal conditions, and complex multilayer geometries. As thermal imaging hardware continues to improve and G-code integration enables tighter coupling between sensing and control, this approach is well-positioned to support the next generation of closed-loop bioprinting systems.

3.1.4. Video-based method

Video-based approaches offer the extraction of motion, deformation, and geometric features [146, 147] in a non-contact manner by analyzing consecutive frames from videos of an object, which contain subtle information related to shape evolution, material distribution, and dynamic response of the printed sample. The information obtained from these recordings can be utilized to detect the anomalies at the surface and, indirectly through changes in the dynamic response, within the printed constructs. An early application of this approach focused on a persistent geometric challenge in extrusion-based bioprinting [148], namely achieving accurate material distribution at the corner regions, where bioink rheology makes precise control of strand diameter difficult [149]. By recording the extrusion process through a glass substrate using an industrial camera, three distinct types of corner defects were identified through frame-by-frame analysis of a hexagonal print pattern. These defects include smoothing, swelling, and ringing features. Building on this, another study used the recorded videos of bioprinting process to generate a dataset, enabling the determination of extrusion condition of the process [150].

The utility of video-based monitoring extends beyond geometric assessment to the characterization of embedded internal defects. The vibration signal signature of a bioprinted construct provides a holistic response of its structural state, capturing the complex interplay between material properties and geometry configurations. Defects in a bioprinted construct can introduce deviations in its modal properties, as established for vibration-based damage detection in engineering structures [151]. Thus, identifying these modal property changes can provide an effective diagnostic window into the inherent structural integrity and fidelity of the printed sample. High-speed video recordings contain rich dynamic response information of the sample, which can be used to estimate its modal properties using a phase-based motion estimation approach [151–153]. This concept has been applied to bioprinted constructs to detect internal void [154], nozzle pressure defect and embedded defect [155]. These findings, as illustrated in Figure 9, indicate that dynamic video analysis can reveal internal structural anomalies.

Video-based vibrometry detects changes in the global modal signature of a construct relative to a defect-free baseline. This technique is relatively simple, contactless, and non-destructive, but its sensitivity and defect detection resolution of this method needs to be investigated further for its broader implementation in the fabrication process. Furthermore, validation against an independent reference, such as micro-CT of the same samples, would be needed to establish the smallest detectable defect.

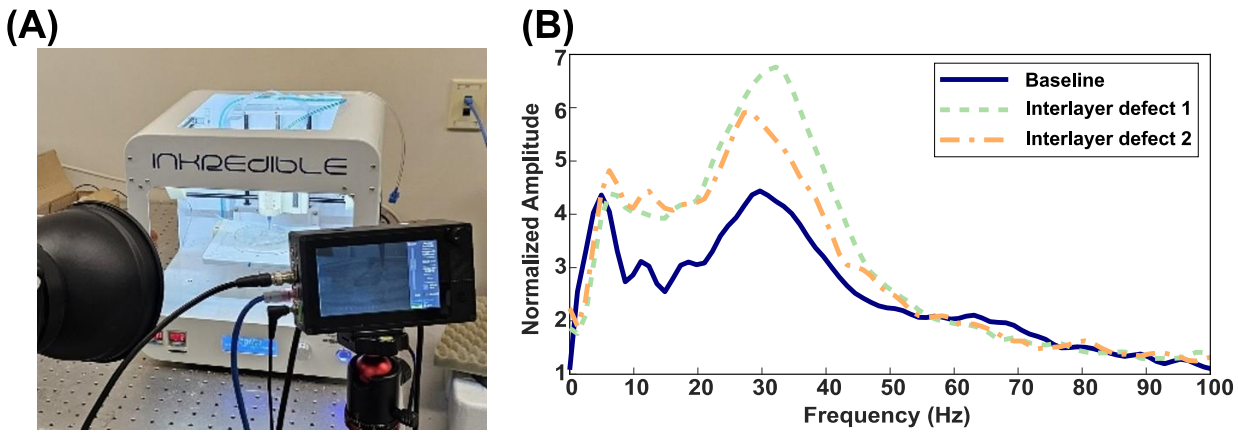


Figure 9. (A) Experimental setup for video-based vibration analysis approach for extrusion-based bioprinting (B) Frequency spectra obtained from phase-based motion estimation technique applied on the recorded video of the bioprinted construct indicating difference in modal characteristics between healthy and defective samples [155]

3.1.5. Laser-based dimensional approach

Laser displacement sensors scan the deposited strand and return a height profile, from which filament position, width and cross-sectional area are computed without contact. The potential of laser scanning for dimensional error correction was first demonstrated in direct-write bioprinting, which shares the same extrusion principle as extrusion-based bioprinting. This method offers relatively simple printing conditions [156], but suffers from limited spatial resolution [157]. A non-contact laser scanner was used to measure material deposition errors at the single-layer level, and the measured error was fed back to modify the reference trajectory for subsequent prints [97]. This closed-loop correction was then verified through repeated laser scanning, providing a direct link between in situ measurement and print quality improvement. The approach was subsequently extended to multi-layer printing, where extrusion width was measured and corrected simultaneously with deposition location, achieving a 2D normalized error below 15% [98]. This approach was further advanced by inferring the cross-sectional area from the laser profiles and the volumetric flow rate, which was used to adjust the extrusion pressure to compensate for over- and under-extrusions in real time [158].

Collectively, laser-based approaches have evolved from single-layer dimensional error measurement to closed-loop dimensional control, demonstrating the advantage of non-contact, quantitative measurement of deposited geometry, including material position, filament width, and surface profile. The integration of a laser displacement scanner with the printing platform enables successive laser profiles to be combined into a 3D point cloud, as illustrated in Figure 10. On the other hand, current implementations largely rely on scanning the deposited layer after a printing iteration, followed by data processing and correction in a subsequent iteration. Real-time correction within the same printing cycle may require additional data processing and implementation complexity. Furthermore, the requirement for controlled scanner motion along with the printing process and reconstruction of the measured profiles introduces additional integration and processing requirements. Thus, extending the laser-based dimensional sensing from iteration-to-iteration geometric correction toward faster in-process measurement, while maintaining sufficient spatial coverage and measurement accuracy for complex multilayer constructs can be an important research direction.

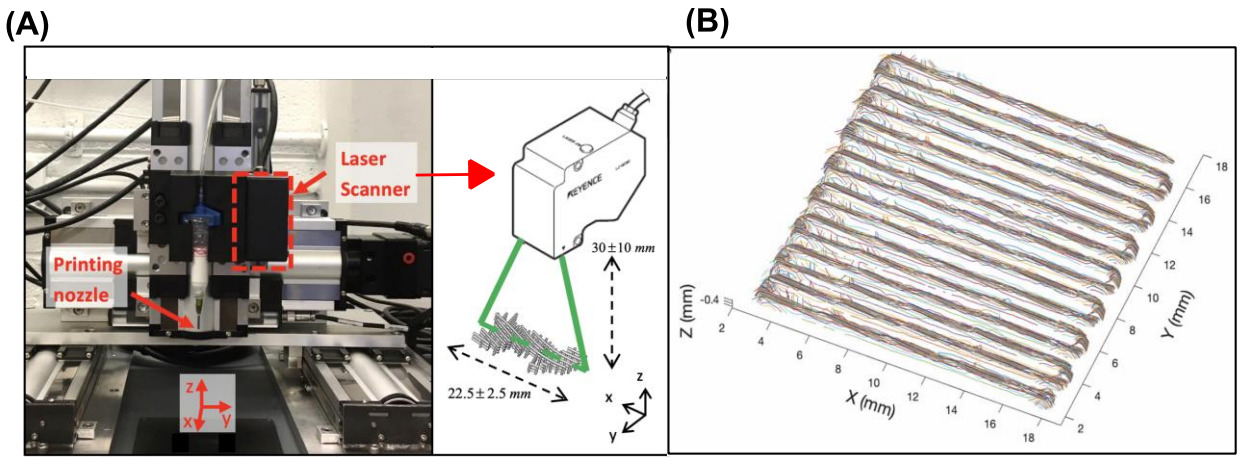


Figure 10. Laser-based dimensional sensing in extrusion-based bioprinting: (A) Integration of laser displacement scanner with the printing platform and scanning configuration [97] (B) Reconstructed 3D point cloud of the deposited filament pattern obtained from successive laser profiles [98].

3.2. Volumetric and subsurface imaging

Ensuring the internal fidelity of bioprinted constructs requires advanced evaluation approaches that can inherently capture volumetric and subsurface information within the printed sample. Conventional surface-level inspection methods often fail to detect subsurface structures, particularly due to the opacity of many bioink materials. Optical coherence tomography, X-ray computed tomography, and magnetic resonance imaging have been demonstrated for bioprinted constructs in the studies reviewed here, enabling non-destructive analysis of the internal structural integrity of bioprinted samples.

3.2.1. Optical coherence tomography

Optical coherence tomography (OCT) is a non-invasive imaging technique that utilizes low-coherence interferometry with near-infrared light to generate high-resolution cross-sectional and volumetric images by measuring the time delay and intensity of backscattered or reflected lights [159]. Originally developed for ophthalmology and subsequently adopted in cardiology, dermatology, and industrial inspections [160, 161], OCT provides micrometer-scale resolution at imaging depths of 1-3 mm, making it well suited for probing the internal structure of hydrogel-based bioprinted constructs. In recent years, OCT has been increasingly used in bioprinting to detect internal defects such as voids, delamination, and pore irregularities, which are not visible through conventional imaging techniques.

Early application of OCT in bioprinting focused on morphological characterization of printed scaffolds. Swept-source optical coherence tomography (SS-OCT) enabled global and local morphological assessment [162], and addressed the limitations of digital microscopy by detecting pore fusion, undefined micropores, and closed pores within the hydrogel scaffolds. Subsequently, an SS-OCT probe integrated with the extrusion nozzle enabled real-time, full-depth, wide-field imaging and quantification of material volume, porosity, pore connectivity to determine layer thickness, filament, and pore size [163]. The approach was further extended to freeform reversible embedding of suspended hydrogels (FRESH) bioprinting,

enabling in-process detection of internal defects caused by air bubbles and channel occlusion from over-extrusion, with average surface deviations below 50 μm [138].

The progression from characterization to active defect detection and correction represents the next logical step in OCT-enabled monitoring. Integration of OCT with feedback control enabled in situ detection of layer thickness, filament size, pore size, and filament breakage. These defects were corrected by adjusting the printing path, extrusion pressure, and printing speed [23]. Building on the previous work [163], OCT-based defect detection mapping was developed using the structural similarity index, enabling the identification of broken filaments and under-extrusion, followed by correction through feedback control mechanism [164]. More recently, OCT has been used as an offline quality assessment tool for FRESH-printed scaffolds, where it verified whether the internal fluidic channels remained open and matched the intended design [165]. 3D image-based comparison with the intended design identified layer straightness, filament diameter, and channel shape deformation, with deviations below 20 μm. In addition, OCT has been employed in multi-material extrusion bioprinting to monitor real-time deformation of hydrogel structures and structural evolution through filament fusion, lateral pore ratio, and scaffold porosity [166].

Maintaining the internal fidelity of bioprinted structures is essential for the transportation of nutrients and oxygen to embedded cells [166, 167]. In recent years, OCT has been increasingly integrated into bioprinting for real-time in situ process monitoring and quality control, addressing the limited subsurface visibility from traditional camera-based approaches, by providing non-destructive volumetric and subsurface imaging and quantitative assessment of filament dimensions, layer thickness, pore architecture, porosity, and interconnectivity. OCT applications range from post-print structural characterization to in-situ defect detection and feedback-based correction, as demonstrated in Figure 11. However, layer-wise volumetric data acquisition may interrupt the printing process, limiting continuous process monitoring. Additionally, quantitative analysis remains sensitive to image quality and segmentation accuracy, which is affected by the bioink properties. Therefore, a key research priority is the development of faster OCT acquisition and analysis methods for uninterrupted volumetric monitoring during the printing process.

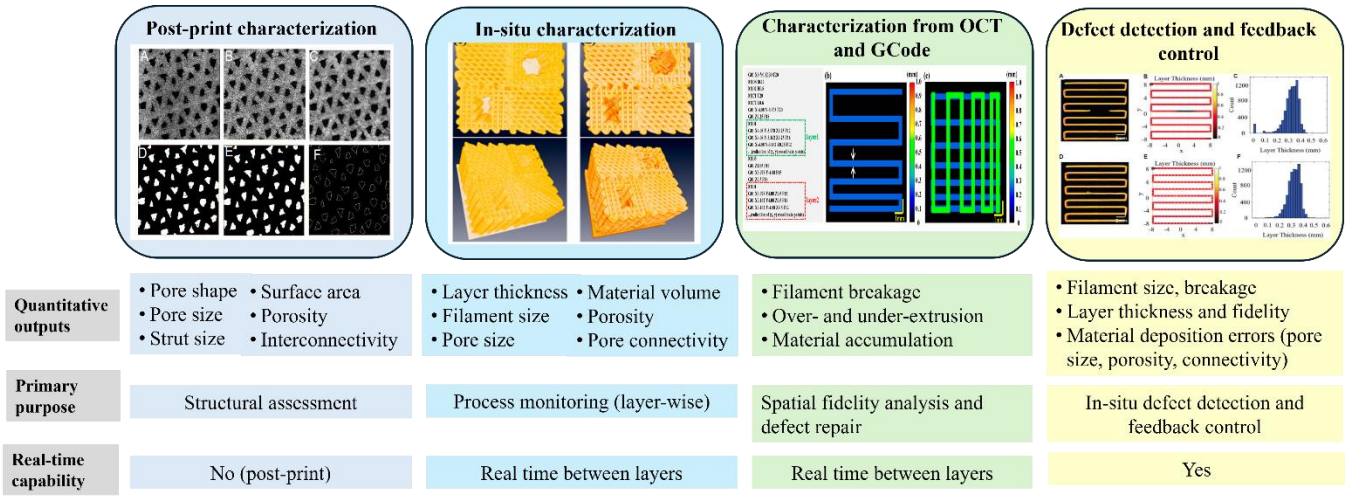


Figure 11. Comparison of OCT-based approaches for structural assessment and process monitoring in extrusion-based bioprinting. Inset images are reused from [162], [163], [164], and [23] respectively.

3.2.2. X-ray and micro-computed tomography,

X-ray-based imaging methods enable non-destructive evaluation of bioprinted constructs by exploiting the differences in X-ray attenuation or phase shift as the beam passes through the material. Given the water-rich composition of hydrogels, X-ray attenuation contrast is inherently low, making imaging dependent on crystalline domains, embedded particles, or phase-contrast effects. Early studies addressed this by using X-ray diffraction profiles to characterize free water and crystalline aggregates within polymeric hydrogel networks [168], while small-angle X-ray scattering synchrotron radiation enabled nano- and micro-scale structural characterization [169]. Subsequently, synchrotron X-ray imaging was applied to bioglass-enriched hydrogels material to determine particle size and distribution under hydrated condition, supporting their potential application in bone regeneration [170].

As bioprinting advanced, computed tomography (CT) and micro-computed tomography (micro-CT) techniques were introduced to analyze the three-dimensional architecture of printed constructs [177], enabling quantification of pore distribution, pore size, and surface area [173]. Notably, micro-CT was used to analyze the degradation behavior of radiopaque constructs fabricated by an extrusion-based bioprinter, quantifying porosity, strut dimension, and local mass density, revealing spatially non-uniform degradation [174]. Expanding this further, synchrotron propagation-based CT was developed to assess scaffold fidelity, diameter deformation, and pore dimensions [175]. Unlike conventional attenuation-based CT, this approach uses refraction-based phase contrast to improve visualization of soft, low-density hydrogels [176]. Combined with compressive loading, it enabled structural deformation from changes in strand size, porous spacing, and layer position. As noted above, Micro-CT often suffers from insufficient contrast in hydrogel applications [177]. While various contrast agents have been applied to address this issue [178], recent work has incorporated gold nanoparticles (Au-NPs) into bioinks to enhance the image contrast and improve visualization of the bioprinted scaffold's internal microstructure [179].

Collectively, X-ray-based methods enable structural integrity assessment of bioprinted constructs across multiple length scales, ranging from nanoscale network characterization to three-dimensional scaffold architecture, internal defects, and

degradation. Their key capabilities, spatial resolutions, limitations, and applicability are summarized in Table 2. On the other hand, the inherently low X-ray attenuation in hydrated hydrogels often requires specialized synchrotron infrastructure or contrast agents, both of which add experimental complexity, influence material properties and limit broader accessibility. These methods also involve trade-offs among imaging resolution, contrast, sample size, material modification, and experimental accessibility. These practical constraints motivate the continued development of faster and more accessible contrast strategies and imaging configurations that enable quantitative assessment of hydrated constructs with minimal bioink modification and greater compatibility with standard bioprinting workflows.

Table 2. Comparison of X-ray based approaches in structural assessment of bioprinted constructs

X-ray approach	Reported resolution	Main capability	Key limitation	Reference
μ-CT	100 nm to a few mm	3D scaffold geometry, pore architecture	Low contrast, radiation dose for cell-laden constructs	[171, 173, 179]
Contrast enhanced μ-CT	Sample dependent	3D structure and degradation	Contrast-agent distribution; agent may alter the bioink	[174, 179]
Synchrotron/Phase-contrast CT	μm scale	Hydrated bioink structure	Acquisition complexity	[170, 175]

3.2.3. Magnetic resonance imaging

Magnetic resonance imaging (MRI) is a non-destructive imaging technique that provides high-contrast visualization of internal structures by detecting radiofrequency signals emitted as hydrogen nuclei return to equilibrium after excitation in a magnetic field. Its ability to generate volumetric images makes it particularly suitable for hydrogen-rich hydrogels. Beyond its use in evaluating patient-specific implant designs [180] and internal cavity structures of scaffolds for brain tissue engineering [181], MRI has also been employed as a powerful tool for structural integrity assessment of bioprinted constructs.

Early works focused on utilizing MRI primarily for structural characterization, including monitoring water movement during the extrusion of microcrystalline cellulose pastes [182]. Subsequently, MRI was implemented to determine geometric deviations in extrusion-bioprinted cubic scaffold composed of alginate, GelMA, and calcium phosphate-based bioinks [183]. MRI cross-sectional imaging enabled quantitative slice-by-slice evaluation of scaffold geometry (as illustrated in Figure 12), identifying defects such as swelling, strand merging, porosity associated with air bubbles, and layer collapse. MRI has also been employed to monitor hydrogel degradation and cartilage regeneration over time using ultrasmall superparamagnetic iron oxide particles as contrast agents, where temporal signal change enabled non-destructive monitoring of scaffold degradation and cartilage regeneration [184].

Further developments have focused on improving spatial resolution and imaging contrast. Integration of MRI coil with a non-magnetic bioreactor enabled monitoring of tissue growth with a planar resolution of 75 μm [185]. Similarly, incorporating superparamagnetic iron oxide nanoparticles into GelMA-based bioinks enhanced MRI contrast and improved the assessment of the printed scaffold fidelity [186].

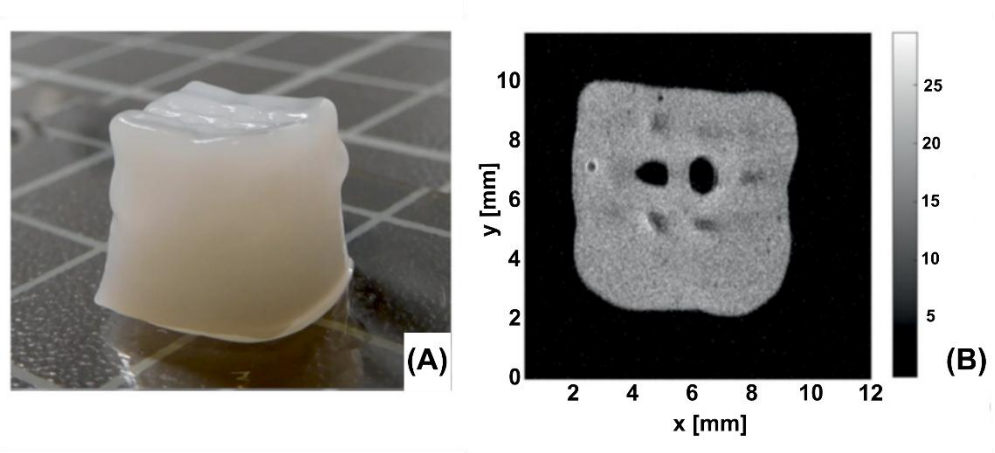


Figure 12. (A) Actual image of alginate GelMA scaffolds on a grid of 10×10 mm^2 and (B) representative slice from pseudo 3D (2.5D) MRI measurements [183]

Overall, MRI provides non-destructive volumetric assessment of bioprinted constructs, facilitating the identification of internal defects, including voids, material degradation, and air bubbles, which are difficult to detect through conventional imaging. On the other hand, the integration of MRI with extrusion-based bioprinting remains constrained by trade-offs between spatial resolution and acquisition time, together with equipment complexity and challenges in integrating MRI hardware with printing platforms. Consequently, current approaches are better suited to post-print characterization than continuous in-process monitoring. A key challenge is therefore to develop a bioprinter-compatible MRI system capable of detecting internal defects without substantially modifying the bioink or interrupting the printing process to enable real-time defect detection.

3.3. Dielectric impedance spectroscopy

Dielectric impedance spectroscopy (DIS) is an impedance-based approach that has emerged as a sensitive, label-free approach for monitoring the electrical and biological state of bioprinted constructs. It measures frequency-dependent complex electrical impedance between electrodes, exploiting the capacitive behavior of intact cell membranes to characterize cellular and matrix states within hydrogels.

An early study established DIS as a process monitoring technique by examining β-dispersion parameters, associated with capacitive properties of cell membranes [187]. Changes in permittivity and the Cole-Cole dispersion parameter were correlated with cell viability, metabolic activity, and spatial distribution within alginate constructs. Reduction in these parameters was linked to process-induced damage from excessive extrusion pressure or unfavorable thermal conditions, establishing DIS as an early-warning indicator of compromised quality during fabrication. This approach was subsequently extended into a manufacturability framework combining DIS, failure mode analysis and process modeling for layer-by-layer quality assessment during bioprinting [188].

These foundational studies motivated efforts to embed impedimetric sensing directly within the printing hardware. A multifunctional hollow fiber serving as both extrusion nozzle and impedance sensor enabled continuous monitoring of bioink

properties during extrusion [189]. Continuous measurement of impedance across 10^2-10^6 Hz enabled real-time classification of cell type, viability, and differentiation state, demonstrating the feasibility of in-nozzle quality control.

Given that DIS systems generate high-dimensional frequency spectra, automated interpretation of DIS spectra was also investigated using supervised machine learning, with the k-nearest neighbors algorithm achieving classification accuracies approaching 99% in distinguishing both cell type and culture duration in cell-seeded polycaprolactone scaffolds [190]. More recently, syringe-integrated impedance sensing enabled pre-extrusion assessment of bioink quality, where impedance and phase angle exhibited strong linear correlations with viable cell count and concentration [191, 192]. This enables non-conforming or compromised bioinks to be identified before printing, adding a preventive quality control step at the earliest stage of the fabrication process. Together, these studies indicate that sensor location determines the quality assessment information accessible through DIS: construct-level measurements assess the biofabricated sample, nozzle-integrated sensing monitors bioink during extrusion, and syringe-integrated sensing evaluates bioink before extrusion. This is further illustrated in Table 3.

Table 3. Comparison of DIS-based sensing configurations for quality monitoring in extrusion-based bioprinting

Monitoring stage	Sensing location	Quantified parameters	Key strength	Limitation	Reference
Pre-extrusion	Syringe	• Cell concentration • Cell viability	Real-time, label-free assessment before extrusion	Demonstrated for specific bioink conditions	[191, 192]
In-line extrusion	Extrusion nozzle	• Cell type • Cell viability • Differentiation state	Direct monitoring of cellular state during extrusion	Filament geometry is not assessed, limited validation across bioinks	[189]
Post-deposition	Electrodes interfaced with construct	• Viable cell number • Spatial distribution • Proliferation	Non-destructive assessment of biological quality of bioprinted construct	Impedance signal depends on geometry, layer and electrode configuration	[187, 190]

Collectively, DIS-based monitoring offers a non-destructive assessment of cellular viability and bioink quality, complementing imaging methods that primarily evaluate printed geometry. Dielectric responses depend on cell concentration, viability, composition, sensor configuration, and construct geometry, complicating interpretation across different printing conditions. Future research should therefore focus on standardized sensing configurations, robust interpretation of dielectric signatures, and integration with bioprinting system to enable real-time biological quality assessment and process correction.

3.4. Ultrasound and flow-based sensing approaches

Ultrasound has emerged as a non-destructive modality for structural quality evaluation of bioprinted constructs, offering penetration beyond the optical range and sensitivity to both mechanical and compositional changes in soft, optically opaque materials [193–195]. It operates by transmitting acoustic waves in the kHz to MHz range into the construct and interpreting the reflected and transmitted signals to infer internal structure, stiffness, and, in some cases, biological state. As a non-destructive method that can be integrated with printing platforms, ultrasound enables repeated measurements on the same sample,

supporting in-process monitoring, in vitro maturation studies, and, in some cases, post-implantation assessment [193, 195, 196].

An early study reported that ultrasound can be implemented in low-cost monitoring process of bioprinted samples, offering internal visualization and quality assessment [195]. Another study developed a real-time in situ ultrasound monitoring system for soft hydrogel 3D printing with subwavelength resolution, coupling an ultrasound probe through the printing stage to monitor interlayer bonding, effective elastic properties, surface profile, and defects such as nozzle-induced scratches and non-uniform layers during extrusion [196]. The workflow of this in-situ process monitoring is illustrated in Figure 13. In a recent study, ultrasound-based monitoring was extended to dynamic mechanical characterization by developing a bioprinting system with ultrasound shear-wave elastography to assess the elasticity of alginate-based and GelMA scaffolds [197]. This method enabled quantitative estimation of storage modulus and spatial elasticity mapping, with strong agreement with conventional rheometry. Furthermore, the continuous tracking of changes in storage modulus during fabrication offers a potential means of identifying anomalous stiffness evolution and spatial mechanical heterogeneity, supporting in-process structural quality assessment of bioprinted scaffolds. This progression from off-line characterization to in-process monitoring, including time-dependent mechanical assessment, mirrors the development trajectory observed in optical and laser-based approaches discussed earlier.

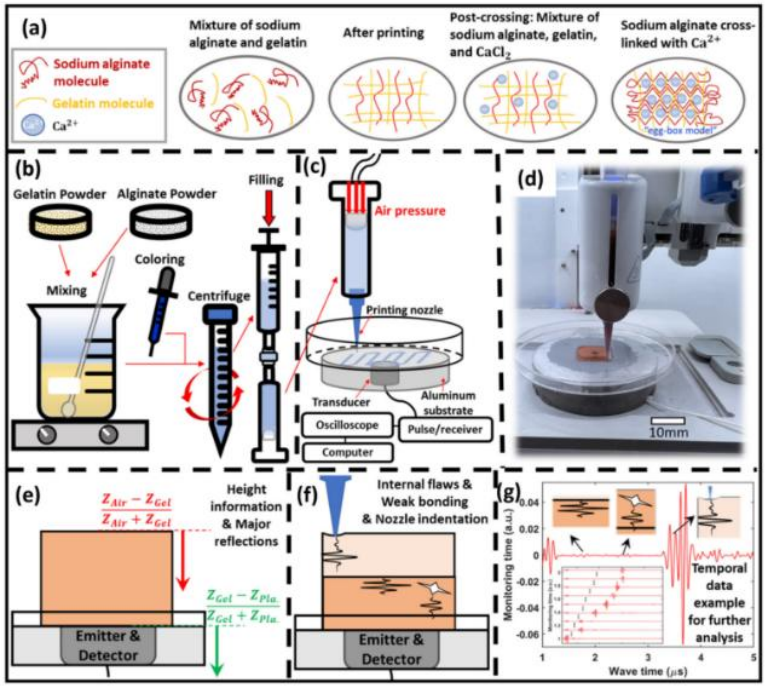


Figure 13. (a) Polymer chains illustration of gelatin-alginate hydrogel before and after printing, and before and after crosslinking. (b) Hydrogel preparation steps include mixing, heating, centrifugation and syringe loading. (c) Schematic diagram of ultrasound monitoring experimental setup and (d) Raw image of ultrasound monitoring setup during printing. (e) Illustration of the two primary reflections from the lower and upper hydrogel surfaces. (f) Detection of internal flaws and nozzle scratching. (g) Representative temporal data captured during continuous ultrasound monitoring indicating internal flaws. [196]

Ultrasound-based monitoring also faces several limitations related to spatial resolution, acoustic coupling requirements, and signal interpretation, particularly in heterogeneous or complex hydrogel structures. Additionally, single-element transducers provide measurements only within a localized region, limiting their ability to detect defects across the entire printed construct. Achieving full-field monitoring requires more advanced transducer arrays, increasing hardware complexity, signal processing requirements, and integration challenges with extrusion-based bioprinting.

In contrast to ultrasound, which determines the condition of the deposited construct, flow sensing targets the material delivery stage of extrusion-based bioprinting. By measuring the volumetric flow of bioink during extrusion, it provides an opportunity to identify and compensate for process disturbances before they propagate into dimensional variations in the deposited filament. Flow sensor-based monitoring has been therefore introduced to overcome the limitations of conventional open-loop pneumatic control in extrusion-based bioprinting, in which a fixed air pressure is assumed to produce a consistent material flow rate. In practice, changes in cartridge fill level, temperature, and bioink viscosity can alter the flow rate, resulting in variations in strand diameter and deposited volume even when the extrusion pressure remains the same. Flow sensing shifts the control objective from constant pressure to constant volumetric flow, enabling more reproducible deposition across varying process conditions. In this approach, a microfluidic liquid flow meter is often placed between the syringe and the nozzle to measure the actual volumetric flow rate in real time. The measured flow is then fed into a feedback controller that continuously adjusts the applied pneumatic pressure to track a specified target flow rate. An early study demonstrating this strategy showed that identical pressure setpoints can produce markedly different flow rates across devices or as the fill level decreases [198]. Switching from pressure control to flow-rate control substantially reduced variability in printed alginate strand dimensions, with the coefficient of variation decreasing by an order of magnitude. Consequently, the inline flow sensing is a candidate process-analytical tool for aligning biofabrication outcomes across platforms, while cross-laboratory comparisons have not yet been reported. Building on this concept, a subsequent study implemented a Python-based proportional-integral-derivative controller that uses flow-sensor feedback for active error correction [199]. The system detected transient flow reductions caused by bioink inhomogeneities or viscosity changes and responded by briefly increasing pressure to restore the desired flow. The same control framework also reduced the trial-and-error associated with changing nozzle diameters, as the controller automatically identified the pressure required to achieve the desired flow rate for each nozzle geometry. Collectively, these two studies from the same research group illustrate how flow sensing can convert extrusion-based bioprinting from an open-loop pressure-driven process into a closed-loop, flow-regulated system, addressing a major source of deposition variability.

Flow sensing approaches are limited by sensor compatibility with viscoelastic bioinks, material-dependent calibration requirements, and challenges in integrating real-time feedback control into bioprinting systems. Additionally, their primary focus on extrusion flow characteristics limits their applicability to comprehensive structural quality assessment of bioprinted constructs.

3.5. Comparative analysis of monitoring methods and defects in bioprinting

The methods discussed in Sections 3.1 through 3.4 operate across complementary sensing physical principles and length scales, collectively addressing the broad spectrum of defect types encountered in bioprinted constructs. Most structural evaluations of bioprinted constructs are performed at the surface level. Optical imaging is the most frequently reported approach that leverages its ability to detect surface-level anomalies, such as filament size inconsistency and dimensional error.

Microscopy extends this capability to a finer spatial scale (filament fusion, filament delamination, surface roughness, and crack formations). Thermography records surface temperature field and detects subsurface features indirectly. Volumetric information comes from optical coherence tomography, computed tomography, and magnetic resonance imaging, which resolves internal features such as porosity, filament collapse, layer delamination, and strand fusion, while ultrasound provides additional sensitivity to internal interfaces, including interlayer bonding, and material stiffness. Complementing these approaches, two further modalities observe the process rather than the geometry. Dielectric impedance spectroscopy provides the state of cells and bioink in the syringe, nozzle or construct, and flow sensing reports the delivered flow rate, which governs deposition consistency. Each method targets different objects of analysis, ranging from cellular components and extruded filaments to printed scaffolds and overall geometry, while quantifying distinct physical and biological parameters.

Table 4 maps each defect class of Section 2 to the methods that have been shown to detect it, with the supporting studies and the stage of each demonstration, while Table 5 compares the methods by observable, reported resolution, evidence base, use of machine learning and demonstrated closed-loop correction. The evidence base is thin and not comparable across methods. Most methods are supported by five or fewer bioprinting studies, often from a single group; resolutions are reported in incompatible terms, such as pixel size, axial resolution or the smallest deviation detected; and cross-method validation is limited to isolated comparisons. Detection limits and probabilities of detection therefore cannot yet be compared across methods. While the methods reviewed here represent the current state of the art, the field of quality assessment method is broad and continues to evolve. Several well-established monitoring techniques from adjacent engineering disciplines, such as acoustic emission, electrical impedance tomography, and fiber Bragg grating sensors, have yet to be systematically explored in the context of bioprinting and may offer promising avenues for future investigation. Reviews of in-process monitoring in metal additive manufacturing demonstrate a potential for such transfer [200–202].

Table 4. Defect classes and quality attributes of Section 2 and the monitoring methods that have detected them in bioprinted constructs or bioink hydrogels. Each entry lists the supporting studies by the stage of demonstration: P, pre-extrusion (syringe); N, in the nozzle or feed line; I, in-process at the deposited strand or layer; L, layer-wise between layers; O, offline after printing; n.s., stage not specified. —, no demonstration found among the reviewed studies.

Method	Under-/over-extrusion, diameter	Filament fusion	Delamination	Sagging, collapse	Breakage, discontinuity	Construct-level deviation	Internal voids, porosity	Surface, micro-structure	Cellular state
Optical imaging and machine vision	I [122, 128, 203–205]; L [120, 121, 127]; O [119]	I [205], L [28]	—	—	L [127]	I [128]; L [120]; O [206]; n.s. [124–126]	—	—	I [207]; O [208]
Microscopy	O [136, 137]	O [78]	—	—	—	—	O [141, 142]	O [139, 140]	N [135]; O [47]
Thermography	I [145]; L [144]	—	—	—	—	I [145]; L [144]	—	—	—
Video-based methods	I [131, 150]; O [209]	—	—	—	—	I [148]	I [210]; O [154]	—	—
Laser profilometry	I [158]; L [98]	—	—	—	—	L [97, 98]	—	—	—
Optical coherence tomography	I [138]; L [23, 164]; O [165]	I [166]; O [162]	—	—	L [23, 164]	I [138]; L [163]; O [165]	I [138]; L [163]; O [162]	—	—
X-ray, micro-CT	—	—	—	—	—	O [175]	O [174, 175, 179]	O [168–170]	—
Magnetic resonance imaging	—	O [183]	—	O [183]	—	O [183, 186]	O [183]	—	O [184, 185]
Ultrasound	—	—	I [196]	—	—	I [196]	I [196]	I [196]	—
Dielectric impedance spectroscopy	—	—	—	—	—	—	—	—	P [191]; N [189]; L [188]; O [187, 190]
Flow sensing	N [198, 199]	—	—	—	—	—	—	—	—

Table 5. Comparison of monitoring methods for extrusion-based bioprinting. Stage codes as in Table 4. Resolution and performance values are given as reported in the cited studies and are not directly comparable, because they refer to different quantities; n.r., not reported.

Method	Stage	Reported resolution or performance	Target object	Analyzing parameters
Optical imaging and machine vision	I, L, O	Layer-width deviation of 0.15 mm detected [126]; path errors >1 mm corrected [124, 125]	Extruded filament/jet	Filament width, effect of printing temperature [122, 126, 211]
			Printed Geometry-macro scale	Line geometry, over- and under-extrusion metric, trajectory deviation, printability, cell-viability, laser power, scan speed, pore index [119–121, 124, 125, 127, 206, 212–214]
Microscopic visualization	N, O	Micrometer (optical) to sub-micrometer (SEM) scale; detection limits n.r.	Cellular components	Droplet velocity, cell count [65, 215]
			Extruded filament/jet	Bioink rheology, printability, dead/live cell ratio [134]
			Hydrogel/biomaterial matrix	Extrusion pressure, speed, and line width [65, 140]
			Layer & process dynamics	Yield stress, shear-thinning, recovery behavior, fiber formation, layer stacking, rheology, pore size, swelling rate, and live/dead cells observation [47, 78, 215]
			Microstructure/pore network	Pore size, and distribution, pore morphology [141, 207]
			Printed geometry-macro scale	Filament width, height, viscosity, etc. [128, 136, 137]
Thermographic and infrared imaging	N, I, L	n.r.	Cellular components	Cellular behavior, printability [208]
			Extruded filament/jet	Filament width, position, area [144]
			Hydrogel/biomaterial matrix	Printing parameters, rheological parameters, structural parameters [107]
Video-based	I, O	n.r.	Printed geometry-macro scale	Deviation in position, width, vibration characteristics [154, 209, 210]
			Front view of printing process	Layer height, extrusion flow, infill density [131, 150]
Laser-based	I, L	Two-dimensional normalized error <15% after correction [98]	Extruded filament/jet	Geometric error, process parameter, pressure, speed, nozzle size [98, 158]
			Layer & process dynamics	Deviation in path [97]
			Tissue constructs	Spheroid geometry & growth, cell viability [18]
	I, L, O		Hydrogel/biomaterial matrix	Pore size, shape, strut size [162]
			Layer & process dynamics	Filament size, layer thickness [23]

Method	Stage	Reported resolution or performance	Target object	Analyzing parameters
Optical coherence tomography		Surface deviation <50 μm [138] and <20 μm [165]	Microstructure/pore network	Porosity, pore ratio, dynamic deformation [166]
			Printed geometry-macro scale	Layer-to-layer thickness, filament size, pore size, OCT image quality, geometric fidelity, deviation from the model [138, 163–165]
X-ray CT, micro-CT	O	<1 μm [171, 173]	Nano- and micro-structure of the hydrogel network	Free water and crystalline aggregates, crystalline size, and spectral intensity [168]
			Gellan gum-bioglass hydrogel composites	Particle size, distribution [170]
			Bioprinted scaffold	Porosity, strut dimension, local mass density, diameter deformation, and pore size [174, 175]
Magnetic resonance imaging	O, including bioreactor	75 μm in plane [185]	Extruded filament/jet	Water intensity using varying parameters [182]
			Hydrogel/biomaterial matrix	MRI-based, histological, and in-vitro parameters, the strand's geometrical feature [184]
			Microstructure/pore network	Porous size, hole area, and scaffold height [183]
			Tissue constructs	Electromagnetic field & simulation parameters, MRI-imaging parameters [186]
Ultrasound-based approach	I, O	Subwavelength resolution [196]	Hydrogel/biomaterial matrix	Ultrasound-based, mechanical, statistical parameters, mineral content inside hydrogel, collagen fiber microstructure, ultrasound parameters, bioink properties, frequency domain, thermal parameters, printing parameters, etc. [216–219, 79, 196]
			Nozzle-material interface	Cell positioning, alignment, and morphology [49]
Dielectric impedance spectroscopy	P, N, L, O	Linear with viable cell count [191]; classification accuracy approaching 99% [190]	Cellular components	Dielectric spectrum, Impedance and process parameters, biological validation parameters, dielectric & flow-related parameters [187, 191]
			Syringe-material interface	Bioink composition, pH, cross-linking and real-time monitoring of cells [192]
	N		Layer & process dynamics	Flow, process, feedback control, material parameters [199]

Method	Stage	Reported resolution or performance	Target object	Analyzing parameters
Flow sensing approaches		Coefficient of variation of strand dimensions reduced by an order of magnitude [198]	Nozzle-material interface	Flow, printing performance, pressure-related, material parameters [198]

4. Machine learning for process monitoring and defect detection in bioprinting

As discussed in the previous sections, process monitoring and quality assessment in bioprinting aim to continuously assess the integrity and fidelity of printed constructs during fabrication. Modern bioprinting platforms generate large volumes of heterogeneous data from multiple sensing modalities, including imaging data (images and videos), electrical signals such as impedance spectra, and process-level signals such as flow rate, extrusion pressure, printing speed, and temperature. Collectively, these datasets describe the evolving state of the printing process and the printed construct. While various classical analytical or physics-based models have been extensively explored to explain specific aspects of the printing process, these traditional approaches often struggle to interpret subtle defect signatures, integrate multimodal sensing signals, and predict failure events before they occur. This limitation is particularly evident in bioprinting, where complex rheological behavior, material heterogeneity, and the layer-by-layer accumulation of errors challenge conventional modeling approaches [39]. Machine learning (ML) has therefore emerged as a powerful tool for extracting information from high-dimensional process data, learning defect signatures from labeled datasets, quantifying anomaly severity, and supporting predictive and adaptive control [220]. While ML has already been explored across multiple areas of bioprinting, including parameter optimization [221], printability, print quality prediction [222], and cell viability estimation [223], the focus of this section is specifically on the role of ML in interpreting monitoring data collected during bioprinting, assessment of printing quality and defect detection, and, ultimately, closed-loop and predictive control. The discussion is organized according to sensing modality and then extended toward integrated control frameworks. Section 4.1 reviews machine learning for interpreting optical and video data, the two modalities with which it has most often been combined; Section 4.2 examines how monitoring has been closed into correction, with or without machine learning; and Section 4.3 compares machine learning approaches by task and validation.

4.1. Data-driven defect identification across monitoring modalities

4.1.1. Optical image-based monitoring

Among the studies reviewed here, optical imaging is the modality most often combined with ML for process monitoring in extrusion-based bioprinting. This technique provides high-resolution visual information about filament morphology and scaffold geometry, allowing ML algorithms to detect deviations from the intended printing pattern [41, 131]. By directly integrating camera-acquired images into machine learning workflows, these frameworks enable automated recognition of deviations from the prescribed printing trajectory, thereby mitigating the limitations of manual, error-prone visual inspection [214].

Early deep learning efforts demonstrated that standard convolutional architectures could be effectively tuned for filament-level defect detection. In one such effort, an anomaly detection system was developed for transparent GelMA hydrogels by capturing layer-by-layer images and extracting patches corresponding to individual filament segments [127]. In this study, a pretrained ResNeXt 50 Convolutional Neural Network (CNN) was applied to classify three types of structural anomalies–discontinuity, irregularity, and non-uniformity–across four infill patterns, achieving an accuracy of over 90% and an F1 score of 0.868. Building on this foundation, subsequent studies moved from labeling to measurement: a dual-task framework was developed to compare printed scaffolds directly against their reference models, simultaneously yielding a quality classification and a continuous structural similarity score [214]. This model, reported in a preprint, achieved an overall accuracy of 92.7% across multiple scaffold geometries. Concurrently, the integration of foundation models, such as Segment Anything Model

(SAM), has facilitated zero-shot filament segmentation without the need for manual annotation. This approach enables the direct extraction of geometric measurements that align closely with results obtained via standard confocal microscopy [128]. An example of AI-based filament segmentation and subsequent geometric feature extraction from in situ images is shown in Figure 14, illustrating how structural features can be directly quantified from raw imaging data. This model could extract filament diameter and spatial deviation directly from in situ images and showed strong agreement with ex-situ confocal microscopy measurements. These advances indicate that image-based monitoring is evolving beyond defect classification toward segmentation and geometric quantification, enabling more detailed quality assessment of the printed construct.

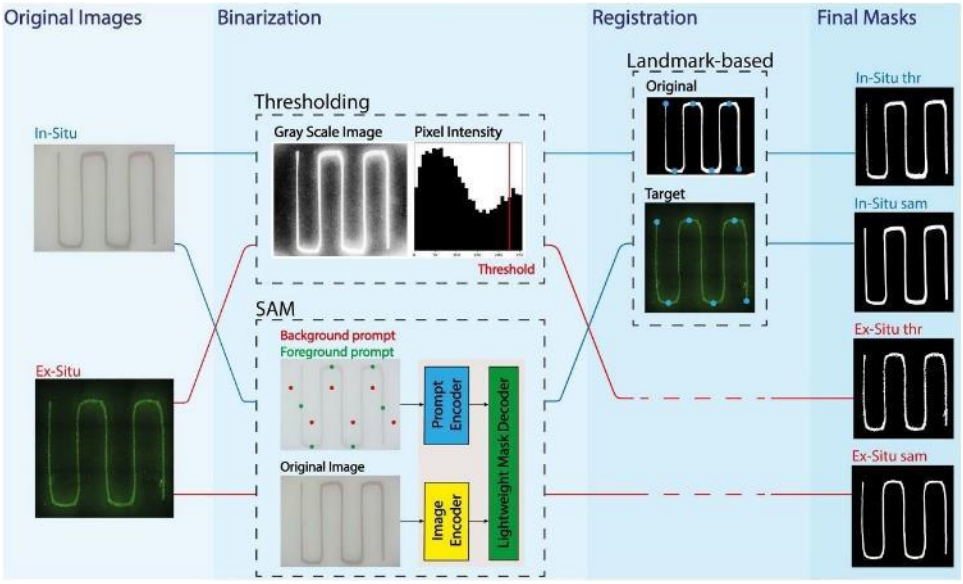


Figure 14. AI-based filament segmentation and geometric feature extraction from in situ bioprinting images [128]

More recent work has further expanded the capabilities of image-based monitoring by incorporating advanced architectures and high-resolution imaging strategies. Transformer-based models have been introduced to capture both local and global structural features from in situ images, improving generalization across the materials and printing conditions tested in [211]. In parallel, AI-powered printability evaluation systems integrating segmentation models, support vector regression, multilayer perceptrons, and regression-based CNNs have been used to quantitatively assess shape fidelity and geometric deviation using metrics such as Hausdorff distance between printed structures and reference CAD geometries [206]. High-resolution imaging in specialized processes, such as two-photon polymerization, has also been integrated with deep learning models to predict structural quality from layer-wise grayscale images. These systems incorporate additional uncertainty estimation to identify ambiguous regions, such as incomplete polymerization or bubble formation [213]. Such advancements extend image-based monitoring toward increasingly complex objectives, including cross-material analysis and confidence-aware prediction.

Collectively, these studies illustrate a clear evolutionary trajectory in image-based monitoring utilizing ML techniques. The field has advanced from single-modality defect classification via CNN architectures toward sophisticated multi-task frameworks capable of structural benchmarking, zero-shot segmentation, and precise geometric quantification. These image-based systems are increasingly being integrated into scaffold and bone tissue engineering applications for real-time, in situ

quality assessment [41, 129, 130]. Perspective articles show promising results that optical ML monitoring may be an important component of next-generation bioprinting process monitoring and control [220, 224].

4.1.2. Video-based anomaly monitoring

Video-based monitoring extends image-based approaches by incorporating temporal information, enabling the detection of transient instabilities that cannot be captured from static images alone. In extrusion-based bioprinting, extrusion instabilities such as under- and over-extrusion develop over successive frames, which makes video data particularly valuable for identifying early-stage process deviations before they manifest as visible geometric defects. Among video-based methods, internal voids and embedded defects have so far been detected only through vibrometry (Section 3.1.4).

Early studies demonstrated that spatiotemporal deep learning architectures can effectively learn normal printing dynamics from video sequences. In a conference paper, a convolutional long short-term memory (ConvLSTM) autoencoder was developed to model stable extrusion behavior using only defect-free video data [150]. The overall architecture of this framework is illustrated in Figure 15(A), where the network learns spatiotemporal patterns of normal extrusion through sequential frame encoding and reconstruction. In this framework, the model reconstructs incoming frame sequences, and deviations from learned patterns are quantified through reconstruction error, which increases in the presence of filament size inconsistencies from under- or over-extrusion. This approach enables continuous anomaly scoring, allowing not only the detection of abnormal events but also the quantification of defect severity. Building on this foundation, subsequent work incorporated supervised learning to directly classify defect states from video streams. To enable real-time quality assessment, a CNN-based monitoring framework was developed to categorize printing conditions into ‘ok,’ ‘under-extrusion,’ and ‘over-extrusion’ using frontal-view video frames collected under varying process conditions [131]. As shown in Figure 15(B), video frames undergo preprocessing and data augmentation before being used to train CNN, improving robustness across variations in lighting, material appearance, and printing conditions. Integrated within an online monitoring loop, this system enabled early identification of process instabilities and early termination of unusable prints. Furthermore, by coupling the classifier output with a process model, the framework adjusted the extrusion parameters across successive prints (run-to-run) and converged toward optimal printing conditions.

Collectively, these studies highlight the progression of video-based monitoring from unsupervised anomaly detection toward real-time classification and control integration. By capturing the temporal evolution of the printing process, video-based machine learning provides a capability for early detection of dynamic instabilities and supports the development of adaptive and automated bioprinting systems.

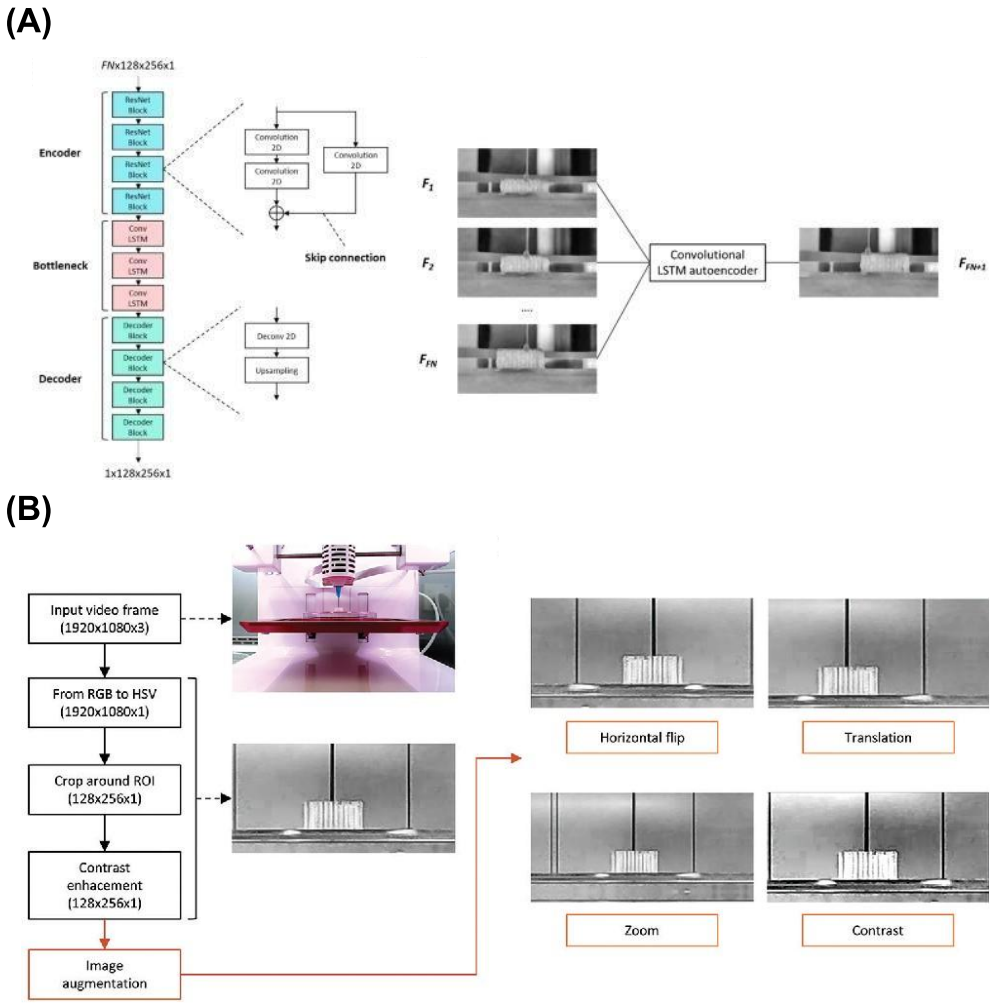


Figure 15. (A) Spatiotemporal deep learning framework for video-based anomaly detection in bioprinting [150]. (B) Deep learning-based video processing pipeline for real-time defect classification [131]

4.2. From monitoring to correction

Defect detection alone does not ensure reliable manufacturing. Traditional process monitoring systems typically operate in a passive mode that only flags a defect, often requiring manual intervention. Early studies accordingly detected errors and stopped or restarted prints [41]. In extrusion-based bioprinting, due to the layer-by-layer nature of fabrication, an uncorrected deviation alters the substrate for every subsequent layer. This section examines how monitoring has been closed into correction, regardless of whether machine learning is involved. The demonstrations differ in when the correction is applied, and four modes of correction can be distinguished (Table 6): in-print feedback, which adjusts pressure, flow rate or speed while a layer is being deposited; layer-wise feedback, which corrects the next layer from a measurement of the last; run-to-run adjustment, which corrects the next print from the outcome of the previous one; and feedforward setting, which sets parameters during printing from a measured process state through a model, without measuring the output it is meant to control. Open-loop parameter

selection before printing is listed for comparison. The timing of the correction determines which defects can be corrected: only in-print feedback can act on a disturbance within the layer in which it arises.

In-print feedback has been demonstrated with three types of sensors. Laser profiles converted to a volumetric flow rate were used to adjust the extrusion pressure during the printing of spatially graded structures [158]. Flow sensing replaced pressure control with flow-rate control [198], and a proportional–integral–derivative controller restored the target flow after transient reductions caused by bioink inhomogeneity [199]. Camera-based feedback has corrected the extrusion flow rate with a convolutional neural network under increasingly complex printing conditions [203] and adjusted the feed rate from the filament width measured by computer vision to hold a target width [204]. In each case a single output, flow rate or width, was regulated through a single actuator. Layer-wise feedback has been demonstrated with OCT, which detected deviations in layer thickness, filament and pore size and filament breakage and corrected the printing path, pressure and speed for subsequent layers [23], and with a G-code-registered OCT defect map [164]. Run-to-run correction has used laser profilometry to modify the reference trajectory and extrusion width of the next print [97, 98], and a CNN classification of video frames as ok, under-extrusion or over-extrusion to adjust the extrusion multiplier across successive prints until the multiplier converged within the printability window [131]. Machine-vision path compensation for helical and robotic printing [124–126] corrected the toolpath from measured deviations, although the reports reviewed here do not state whether the correction was applied within or between prints. Feedforward control has been demonstrated with thermal and geometric measurements used to train models that set the printing speed from the sensed process state [28].

Machine learning can serve three roles in these loops. It can be the sensor model that converts images into the controlled variable, as in CNN classification of the extrusion state [131, 203]; it can supply a continuous error signal, as the reconstruction error of a ConvLSTM autoencoder [150]; or it can also be the process model used to choose the correction, as in feedforward speed setting [28]. Loops without machine learning, such as flow-rate PID control [199] and width feedback by rule-based computer vision [204], show that a calibrated measurement can suffice for single-variable regulation; machine learning becomes useful when the controlled variable cannot be extracted by rule-based image analysis, as in classifying the extrusion state [131, 203], or when the correction depends on a learned process model [28].

Table 6. Closed-loop, feedforward and open-loop correction demonstrated in extrusion-based bioprinting, grouped by correction timing.

Correction timing	Sensor	Measured variable	Controlled variable	Machine learning	Reference
In-print	Laser profilometry	Cross-sectional area → volumetric flow rate	Extrusion pressure	—	[158]
In-print	Flow sensor	Volumetric flow rate	Pressure (flow-rate control)	—	[198]
In-print	Flow sensor	Volumetric flow rate	Pressure (PID controller)	—	[199]
In-print	Camera	Extrusion state	Extrusion flow rate	CNN	[203]

Correction timing	Sensor	Measured variable	Controlled variable	Machine learning	Reference
In-print	Camera	Deposited filament width	Feed rate	—	[204]
Layer-wise	OCT	Layer thickness, filament and pore size, breakage	Path, pressure and speed	—	[23]
Layer-wise	OCT registered to G-code	Defect map: breakage, under-extrusion	Correction of identified defects	—	[164]
Run-to-run	Laser profilometry	Deposition error, extrusion width	Reference trajectory and width	—	[97, 98]
Run-to-run	Video	Extrusion state (ok, under-, over-extrusion)	Extrusion multiplier	CNN with printability-window model	[131]
Run-to-run	Imaging of printed morphology	Morphology score	Parameters of the next print	Bayesian optimization	[221]
Feedforward	IR thermocouple and layer imaging	Thermal and geometric process state	Printing speed	Trained process model	[28]
Before printing (open loop)	Microscopy	Filament geometry	Pressure and speed (selected)	Logistic regression, SVM	[137]

4.2.1. From reactive monitoring to predictive assessment

Conventional feedback primarily operates in a reactive manner, correcting deviations only after they are detected. In contrast, ML-based monitoring can, in principle, identify early anomaly signatures. Early work in this direction demonstrated that image-based deep learning models can capture subtle spatial features associated with emerging process instabilities. Patch-level classification using convolutional neural networks has been shown to identify deviations in filament continuity, regularity, and uniformity at an early stage of formation [127]. Extending this concept to temporal data, ConvLSTM has been applied to detect gradual drift in extrusion rather than discrete failure events [150]. Such early approaches show that both spatial and temporal features extracted from imaging data can serve as early indicators of instability, supporting potential for predictive intervention during printing, which remains to be demonstrated.

A complementary class of methods uses machine learning as a predictive tool to estimate printability and optimal process conditions prior to fabrication. Rheology-informed models incorporating rheological and mechanical properties have been developed to predict printing resolution across different bioinks [225]. Prediction before printing has also been advanced through data-efficient optimization strategies. Bayesian optimization frameworks, for example, have been used to explore high-dimensional process parameter spaces with a limited number of experiments, identifying near-optimal printing conditions based on morphology-driven objective functions [221]. Similarly, lightweight machine learning models trained on sparse datasets

have been shown to generate probabilistic process maps that define stable printing regions and suggest compensatory parameter adjustments under varying conditions [106]. An open-loop extrusion control framework was developed in which logistic regression was used to eliminate defective parameter combinations associated with discontinuous filaments and unstable extrusion, while a support vector machine model subsequently predicted target filament geometry based on process variables [137]. Similarly, transfer learning frameworks coupled with Gaussian process regression have been employed to predict the optimal pressure and printing-speed combinations for new bioinks using only limited target-material datasets [121]. Large-scale ensemble learning studies incorporating XGBoost, LightGBM, and Extra Trees models have been applied to correlate process parameters such as extrusion pressure, nozzle speed, temperature, and biomaterial composition with scaffold-quality and printability metrics [222]. Unlike localized defect-detection frameworks focused on filament-level anomalies, this approach emphasized global process-quality prediction across various printing conditions, demonstrating the potential of ensemble learning for identifying robust operating windows and stable fabrication conditions. In parallel, ML models have been combined with optimization techniques to directly target biological outcomes, such as maximizing cell viability through inverse prediction of crosslinking and process parameters [223]. Collectively, these developments demonstrate a transition from reactive monitoring toward predictive process management. By combining early-stage anomaly detection with physics-informed modeling, data-efficient optimization, and digital twin integration, ML enables proactive adjustment of process parameters. This shift could reduce defect accumulation, minimize material waste, and constrain the process space to conditions more likely to yield structurally and biologically viable constructs.

4.2.2. Toward autonomous biofabrication systems

The convergence of ML-based monitoring, predictive modeling, adaptive control, and digital twin frameworks is motivating work toward autonomous biofabrication systems. In conventional bioprinting workflows, process quality depends heavily on operator expertise, manual parameter tuning, and post hoc inspection. AI-driven process monitoring and control system aims to reduce this dependency by enabling self-correcting systems that learn from data and adapt in real time. At the system level, the integration of monitoring and control has enabled the development of closed-loop bioprinting platforms with automated regulation of selected process parameters. These systems combine real-time sensor feedback, computer vision, and ML inference to dynamically adjust process parameters [45]. While such approaches demonstrate significant potential for improving print fidelity and consistency, challenges remain in ensuring model generalizability across materials and processes, establishing standardized datasets, and meeting regulatory requirements for clinical translation. Beyond process-level autonomy, broader considerations are emerging as critical for real-world deployment. The need for explainable AI, privacy-preserving learning strategies, and standardized data infrastructures has been highlighted as essential for building trust among clinicians and regulatory bodies [226]. Approaches such as federated learning enable collaborative model development across distributed datasets without requiring direct data sharing, addressing privacy concerns in biomedical applications [227].

4.3. Critical synthesis of machine learning approaches in extrusion-based bioprinting: detection, prediction, and intervention

This section brings together the ML studies reviewed in Sections 4.1 and 4.2 to answer practical questions: which capability each study actually demonstrates, how a suitable method can be chosen for a given monitoring task, and what must still be validated before the method can be relied upon. The applications of ML in quality assessment can be distinguished into three

related capabilities. (1) Detection identifies the current print state or geometric deviations from monitoring data, for example by recognizing from an image that a filament is wider than specified. (2) Prediction estimates the outcome expected for given material properties and process settings, providing information that can also support parameter selection for a target outcome. For example, a model may predict filament width from extrusion pressure or be used to estimate the pressure required to achieve a target filament width. (3) Intervention uses monitoring results or model outputs to adjust printing conditions, between prints or during printing, with subsequent measurements used to evaluate the effect; for example, the pressure is lowered automatically when the measured or predicted filament width exceeds its tolerance, and the width is then re-measured. Their roles should therefore be distinguished by the information they receive, the outputs they produce, and how those outputs inform decisions.

Figure 16 summarizes these relationships, separating (a) model development and (b) task-specific inference from (c) subsequent assessment, experimental optimization, or feedback correction. The pathways represent complementary uses of ML rather than a single integrated system demonstrated across all materials and printing platforms. The following paragraphs address detection, prediction, and intervention in turn, followed by a comparison of practical model selection considerations and the validation required for reliable implementation. Table 7 summarizes the representative approaches in terms of their applications, supporting evidence, practical advantages, and limitations.

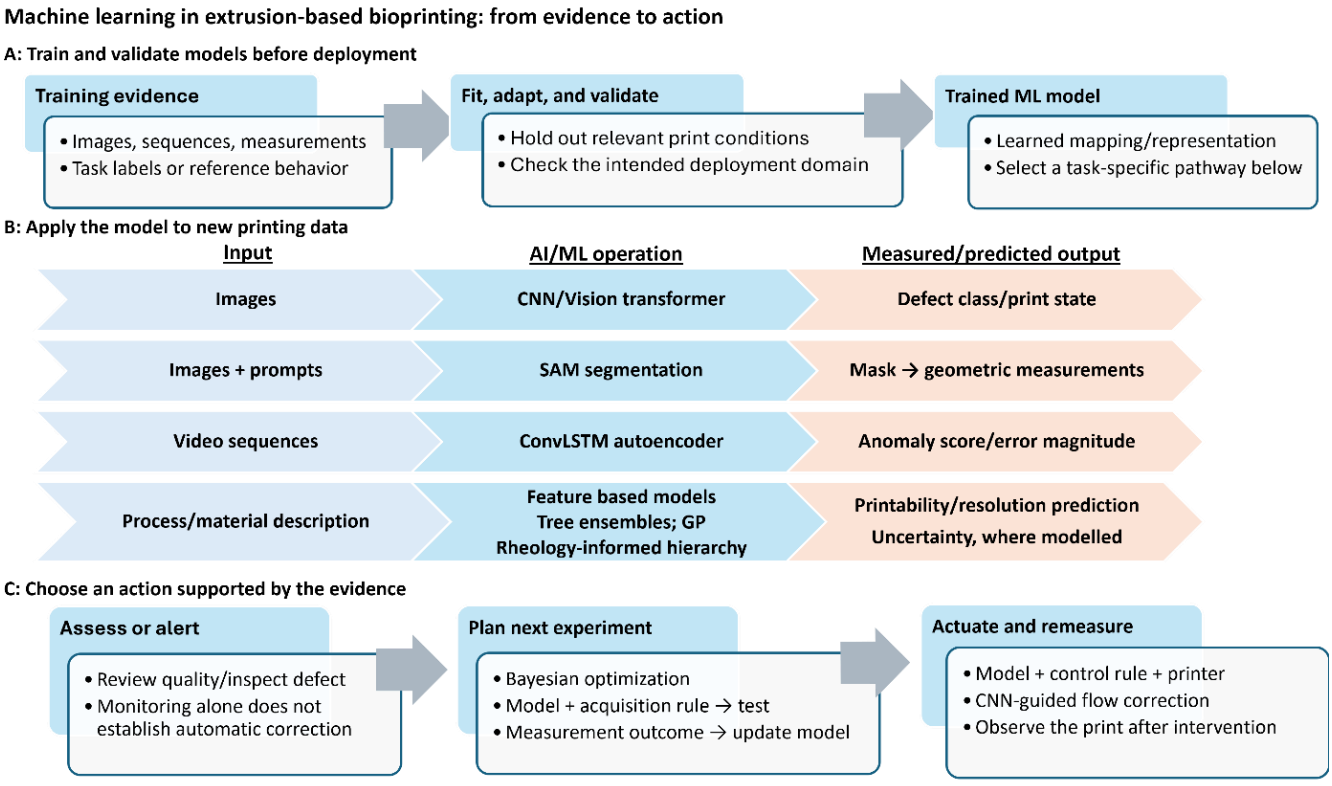


Figure 16. Task-oriented workflow for ML-assisted monitoring and quality assessment in extrusion-based bioprinting. Training and validation precede inference from images, video sequences, or process and material descriptors. Model outputs support quality assessment, selection of subsequent experiments, or process actuation when a control rule and measurement are implemented. Bayesian optimization selects experiments [221], whereas CNN-guided flow correction illustrates intervention during printing [203]

Detection provides information about deviations from the intended printing condition or construct geometry. Image-based models, including CNNs and vision transformers, have been used for extrusion-state classification [203], geometric fidelity evaluation [206], and in-situ monitoring across different materials [211]. These approaches can extract spatial features directly from images, reducing reliance on manually defined descriptors, although their performance depends on the availability and representativeness of training data. When the objective is to measure filament dimensions rather than assign a defect label, segmentation models such as the Segment Anything Model (SAM) provide an alternative approach by identifying filament regions from which geometric measurements can be extracted [128]. Video-based models further extend monitoring by incorporating information from successive frames. For example, a ConvLSTM autoencoder has been used to identify extrusion anomalies by evaluating reconstruction errors in video sequences [150]. Unlike frame-based classification, this approach captures temporal changes in the printing process, but the resulting anomaly score does not necessarily identify the underlying defect mechanism. The selection of an appropriate detection method therefore depends on whether the required output is a defect class, a geometric measurement, or an indication of abnormal process behavior.

Prediction extends quality assessment by estimating printing outcomes from selected material properties and process conditions. Logistic regression and support-vector-based models have been applied to screen printing conditions and estimate filament geometry for open-loop parameter selection [137]. Tree-based ensemble models have also been investigated for predicting printability and scaffold quality from material and process descriptors [222]. In comparison, Gaussian process regression combined with transfer learning has been employed to estimate printing conditions for new bioinks with limited target-material data [121], while rheology-informed hierarchical learning incorporates material properties into printing-resolution prediction [225]. These approaches offer different advantages depending on data availability, prediction targets, and the degree of material variation. Models using structured process variables may be suitable when experimental datasets are limited, whereas more complex approaches may be useful when simpler models cannot adequately represent the relationships in the available data. However, reported performance across different studies cannot be directly compared because their datasets, target variables, and validation procedures differ. Incorporating rheological properties can improve the physical relevance of a model but does not itself establish accurate prediction beyond the investigated materials and operating conditions.

Beyond predicting printing outcomes, machine learning can support process parameter optimization and, when integrated with suitable control mechanisms, corrective intervention. Bayesian optimization, for example, combines modelling with sequential experiment selection to identify suitable printing conditions while reducing the number of experiments required [221]. Unlike feedback correction during printing, Bayesian optimization selects parameter combinations that are evaluated in subsequent experimental trials. In run-to-run adjustment, a CNN-based framework has been used to classify extrusion conditions and update the extrusion multiplier across successive prints [131]. In contrast, CNN-guided flow correction has been demonstrated during printing, where monitoring results were connected to changes in extrusion conditions [203]. Thermal sensing combined with ML has also supported a feedforward adjustment of printing speed based on the measured process state [28]. These studies demonstrate that ML can support both process optimization and corrective adjustment, although the timing of intervention determines which disturbances can be addressed. In particular, predicting suitable parameters before printing, correcting the next print, and adjusting material deposition during printing represent different levels of process integration. A model should therefore be considered part of a demonstrated corrective system only when its output is connected to a defined process adjustment and the resulting printing performance is evaluated.

The selection of an appropriate ML approach depends on the monitoring objective, available data, and requirements for practical implementation. Image-based models are suitable when printing deviations can be reliably identified from visual information, whereas feature-based methods may be preferable when experimental datasets are limited and meaningful process or material descriptors are available. Deep-learning approaches can extract complex spatial features from images and, when temporal architectures are employed, capture changes across video sequences. However, their data requirements, computational demands, and lower intrinsic interpretability may limit practical implementation. For predictive applications, the training data must adequately represent the intended materials and printing conditions. Corrective intervention introduces additional requirements, including an adjustable process variable, a defined relationship between the model output and the commanded adjustment, and measurements to verify the resulting improvement. Transfer learning can reduce target-material training requirements [121], while federated learning supports model training across distributed datasets [227]. However, these are training strategies rather than independent monitoring or control methods, and neither inherently guarantees reliable performance across different bioinks or printing platforms. Table 7 compares representative ML approaches in terms of their applications, data requirements, supporting evidence, practical advantages, limitations, and validation needs.

Table 7. Comparison of representative machine learning approaches for defect detection, quality prediction, and correction in extrusion-based bioprinting, including their inputs, outputs, supporting studies, and main limitations

ML Approach	Input → output and task	Representative evidence	Advantages/suitable use	Limitations and validation needs
Detection: monitoring data → current print state or geometric deviation				
CNN and vision transformer (ViT)	In situ images or individual video frames → extrusion-state or defect class; images → geometric-quality estimate	Defect classification [127]; CNN state classification informing in-print correction [203]; image-based geometric evaluation [206]; ViT cross-material anomaly classification [211]	Extract spatial features without manual descriptors; pretrained models can reduce target-task training demands.	Require representative images and labels; lighting, material appearance and image quality may shift. Classification or geometric regression does not itself demonstrate control.
ConvLSTM autoencoder	Ordered video frames → reconstruction-error anomaly score	Spatiotemporal reconstruction of normal extrusion sequences for anomaly detection [150]	Learns temporal behavior; normal-only training reduces dependence on labeled defect cases.	Anomaly score is not a physical defect measurement or causal diagnosis; thresholds and robustness to process changes require testing.
SAM-based segmentation	In situ images and prompts → masks → calibrated filament geometry	Segmentation and geometric measurements compared with confocal microscopy [128]	Supports geometric metrology with limited task-specific pixel annotation.	Segmentation alone does not label a defect; depends on prompts, image contrast and calibration; surface imagery cannot establish internal geometry.
Prediction and optimization: process/material descriptors → expected quality or selected printing conditions				
Logistic regression; SVM/SVR	Process settings and measured filament geometry → printability screening and geometric prediction used for open-loop setting selection	Logistic regression screening and support-vector-based filament geometry modeling [137]	Useful for structured process data; logistic regression coefficients can aid interpretation.	Feature design and material/process coverage matter; SVM/SVR are not inherently interpretable; selected settings are not evidence of feedback control.
Tree-based ensembles (RF, Extra Trees, XGBoost, LightGBM)	Material/composition and printing descriptors → printability or scaffold-quality class/estimate	Comparison of tree and boosting algorithms using heterogeneous scaffold data [222]	Handle nonlinear interactions in tabulated descriptors; offer feature-importance measures.	Source dataset mixes materials and conditions; feature importance is not causal evidence; validate on unseen bioinks, printers and data sources.

ML Approach	Input → output and task	Representative evidence	Advantages/suitable use	Limitations and validation needs
Gaussian process regression with transfer learning	Source/target material data and process conditions → printability response estimate on a target bioink	Material-to-material transfer learning for extrusion-bioprinting printability response modeling [121]	Can leverage source-material data when target-material experiments are limited; uncertainty estimates can aid experiment planning when calibrated.	Performance depends on source–target similarity and target-domain data; evaluate target prediction error, uncertainty calibration and scalability.
Rheology-informed hierarchical ML	Rheological/material descriptors and printing settings → predicted printing resolution	Rheology-informed printing-resolution prediction [225]	Uses physically meaningful descriptors to link material behavior to resolution.	Including rheological predictors does not enforce governing equations; reliability beyond studied formulations requires separate tests.
Bayesian optimization	Process settings plus experimentally measured printability score → next parameter combinations to test	Sequential printability optimization with morphology-based scoring [221]	Efficient sequential selection can reduce trial-and-error when experiments are costly.	Experimental optimization, not in-print defect detection or feedback correction; sensitive to objective, search bounds and experimental repeatability.
Intervention: model output + control rule → adjustment of the process				
ML-assisted in-print feedback, run-to-run adjustment and feedforward setting	Monitored extrusion state / thermal process measurements → updated flow multiplier or printing speed	CNN-guided in-print flow correction [203]; CNN-based run-to-run extrusion-multiplier changes [131]; thermal/geometric ML feedforward speed setting [28]	Links sensing or inference to a specific process adjustment; timing can be matched to disturbance dynamics.	Different modes must not be equated: feedback measures error, run-to-run adjusts later prints, feedforward uses measured state without output-error feedback. Validate correction benefit, latency and stability.

The practical value of these approaches ultimately depends on validation that reflects their intended applications. Defect detection requires comparison with reliable reference labels or geometric measurements, while predictive models should be evaluated using printing conditions not included in model development. Performance within a single experimental setting should be distinguished from validation using different bioinks, printers, or sensing configurations, particularly when assessing model transferability. For process intervention, model accuracy should also be considered alongside inference delay, intervention frequency, and the resulting improvement in printing quality. Furthermore, structural fidelity cannot serve as a substitute for biological validation. The separate prediction of geometric fidelity and cell viability in an alginate–hyaluronic acid bioink containing PC12 cells [206] illustrates the need to define these outcomes independently. These considerations highlight the requirements for reliable ML-assisted process monitoring and quality assessment and provide a basis for the discussion of coupled structural and cellular quality in the following section.

5. Beyond structure: The interplay between structural and cellular quality

While this review primarily highlights the structural defects in extrusion-based bioprinting, structural and cellular qualities in bioprinting are inseparable in practice. The parameters that govern geometric fidelity, such as nozzle geometry, extrusion pressure, and bioink rheology, simultaneously determine the limits of cell viability, which is a necessary, though not sufficient, condition for a functional construct. This section does not review biological assessment in general; instead, it considers cellular-level outcomes only where they are coupled to the process conditions and monitoring methods reviewed above and identifies the research gaps in this interface.

5.1. Cellular defects in extrusion-based bioprinting

A growing body of evidence demonstrates that printability-related structural parameters, including rheological properties of bioink, scaffold/pore geometry, and process parameters such as nozzle geometry, extrusion pressure, and tip size, directly govern the cellular microenvironment and, consequently, cell fate. The rheological properties that enable stable bioink formation may contribute to the mechanical stress transmitted to the encapsulated cells. For instance, bioinks with a gel-like consistency, that is, a high yield stress and storage modulus, improve shape fidelity, but they require higher extrusion pressure, which raises the wall shear stress on cells in the nozzle and can reduce viability [64]. It is also reported that higher alginate concentration improves shape fidelity and mechanical integrity, and on the other hand, it may reduce cell viability due to the stress developed [65]. Furthermore, the relationship between scaffold/pore geometry and cell viability is well-documented, as is the subsequent influence of cells, in turn, on the mechanical properties of the bioconstructs [76, 77]. In addition to that, process parameters may affect structural and cellular outcomes simultaneously. Nozzle geometry, pressure, and tip size are the primary factors of shear stress development within the nozzle [52, 93, 96], which directly correlates with an elevated dead-to-live cell ratio. A relationship between shear exposure and cell damage has been demonstrated, with effects depending on both the magnitude and duration of the stress [228, 229], along with additional contributions from thermal and radiative sources [50, 70]. Extrusion pressure has been identified as a more critical determinant of cell damage compared to nozzle diameter [61]. Furthermore, stress at the channel center, often neglected relative to wall shear, was shown to make an independent contribution [62]. Moreover, efforts to improve cell distribution through aggressive mixing may damage the very cells being distributed [94], and the small nozzle tips that enhance print resolution simultaneously intensify shear stress and promote clogging [49]. These coupled trade-offs indicate that optimizing structural quality without monitoring cellular outcomes risks producing geometrically accurate but biologically compromised constructs.

5.2. Monitoring approaches for cellular quality

Efforts to monitor cellular quality have progressed from post-fabrication optical inspection toward inline, multi-physics sensing. Fluorescence and confocal microscopy established the baseline–confirming stress-viability relationships in printed constructs [47, 135]. On the other hand, their dependence on optical transparency limited applicability to opaque bioinks. Near-infrared imaging and layer-resolved digital microscopy extended optical monitoring closer to in situ conditions [207, 208, 230], yet still required process interruptions or label preparation. Acoustic and tomographic methods broke through the opacity barrier: OCT tracked hydrogel deformation in real time [166], and spectral ultrasound, combined with machine learning, detected shifts in cellular composition within implanted scaffolds [219]. Acoustic fields also proved useful in the opposite direction, by not just sensing but actively improving cell distribution and reducing clogging during printing [49, 218]. Additionally, dielectric impedance spectroscopy brought these threads together most directly, exploiting the capacitive behavior of cell membranes to produce viability signatures in dense, opaque hydrogels and linking impedance changes to the same pressure- and temperature-induced damage mechanisms identified in process studies [187, 188]. The subsequent integration of DIS into a nozzle-embedded sensor enabled real-time, inline cell monitoring during extrusion [189], representing the closest realization to date of truly in-process cellular quality assurance. For a more detailed discussion, the reader is referred to [77, 231].

6. Open challenges and research gaps

Process monitoring and quality assessment in bioprinting have advanced substantially, yet several critical bottlenecks remain that hinder the transition of bioprinting from a research tool to a clinically viable manufacturing platform. A central limitation is the fragmentation of the process monitoring approaches. Optical imaging, laser sensing, OCT, and related techniques primarily provide information on filament geometry, layer deposition, and structural defects, whereas impedance-based and other biological sensing approaches focus on the cellular or material states. Process sensors, such as flow and pressure measurements, provide another layer of information on the bioink extrusion. These measurements are generally investigated independently, and a major research need is therefore multimodal sensing that synchronizes process variables, deposited filament, material state, and cellular conditions within a common spatial and temporal framework. Such integration could help distinguish defects with similar geometric appearances but different origins of sources. The practical implementation of this approach will require sensor miniaturization, synchronization of measurements acquired at different rates and spatial scales, and integration without interrupting the process and interfering with sterility or structural integrity. State estimation, for example Kalman filtering [232], provides one route to fuse such multirate measurements into a single estimate of the process state, and model predictive control can then optimize the next commands subject to actuator limits.

The underlying challenge in this integration is to establish relationships between process conditions and biological response. During extrusion, cell damage depends on the extrusion pressure, bioink rheology, hardware configurations, flow conditions, temperature, and shear stresses [63]. Computational models have been implemented to estimate these quantities, but their applicability is often limited to certain bioink and hardware configurations, limiting transferability to new printing conditions. Recent approaches have developed predictive frameworks combining rheological models with computationally derived shear stress and experimental viability data to model relationships among shear stress, exposure time, and cell viability [233]. Nevertheless, models trained using several cell types and material conditions require broader validation before they can be implemented to represent much larger bioink-cell-printer design space in extrusion-based bioprinting. Future models should

therefore move beyond purely data-driven correlations toward hybrid or physics-informed frameworks that incorporate rheology, sensor measurements, and biological response while quantifying prediction uncertainty.

AI-assisted monitoring is increasingly extending quality assessment from defect detection toward prediction, interpretation and process optimization. Current approaches combine image-based approaches, process parameters, rheological properties, and simulation-derived features to estimate printability, geometric fidelity and biological viability. On the other hand, the predictive capability of these models remains strongly dependent on the training dataset, limiting the transferability across printers, bioink materials, and operating conditions. Model performance depends heavily on large, homogeneous datasets for data-driven approaches, whereas hybrid models incorporating rheological and physics-based features show robustness within limited data. A key research direction is therefore the development of hybrid AI frameworks that combine sensor measurements with material properties rather than relying solely on correlations within individual datasets.

Building on these advances in multimodal sensing and AI-assisted monitoring, closed-loop feedback is emerging as an important step toward adaptive and reproducible extrusion-based bioprinting. Flow-sensor feedback has been used to regulate extrusion pressure, while computer-vision systems have measured deposited filament width and adjusted feed rate to maintain a target width under varying material conditions [204]. Coordinating multiple quality attributes instead of depending largely on individual outputs remains a challenge to improve extrusion bioprinting from closed-loop feedback system. This is particularly important as improving structural fidelity does not necessarily ensure the biological outcomes in extrusion process. Alterations of one of the process parameters to maintain geometric fidelity can affect the viability of biological components within the constructs. The next step is therefore to develop multimodal, multi-objective closed-loop systems that integrate structural, process, and cellular feedback to guide coordinated parameters adjustment. Such systems will require faster sensing-to-control framework, robust control under varying bioink properties, and validation across different materials, geometries, and printing platforms before they can provide transferable process control.

Standardization is a precondition for comparing monitoring methods and models across laboratories, and two elements are missing. The first is a set of definitions: the defect classes of Table 1 and Table 4 are described differently across studies, and a shared vocabulary with measurable criteria, such as width deviation relative to the nozzle diameter or the fraction of closed pores, would make detection results comparable. For example, resolutions are reported in incompatible terms, such as pixel size, axial resolution or the smallest deviation detected (Table 5). The process categories and vocabulary of ISO/ASTM 52900 may provide a starting point [56, 234]. The second is benchmark datasets and inter-laboratory comparisons. For example, flow sensing has been proposed as a process-analytical tool for aligning outcomes across platforms, but cross-laboratory comparisons have not yet been reported [198], and no shared defect dataset for extrusion bioprinting was identified among the studies in this review.

These technical limitations are further amplified by an immature regulatory and standardization landscape. Unlike conventional medical devices, bioprinted samples contain living cells, which make the standardization and regulatory work challenging [235]. Ethical considerations surrounding data privacy from embedded sensors and machine learning decision-making also warrant regulatory attention. However, the existing regulatory framework, which was designed for 3D-printed medical devices and non-living samples, struggles to accommodate patient-specific and process-dependent bioprinting technologies, thus creating a regulatory vacuum surrounding bioprinting [236]. Without agreed-upon metrics for acceptable structural or cellular deviation, the role of process monitoring techniques in regulatory compliance remains ambiguous.

Classification ambiguities persist at the global level as well. For example, in the European Union, bioprinted constructs with engineered living cells are regulated as combined advanced therapy medicinal products. In the United States, FDA evaluates bioprinted samples under biologics, devices, or combination product pathways, depending on the primary mode of action [237]. Similarly, the existing standards, such as GMP, ISO 13485, and ICH guidelines, were developed for centralized manufacturing and do not fully address decentralized or point-of-care bioprinting contexts [238]. Addressing these gaps will require coordinated progress on multiple fronts. From a regulatory perspective, the field requires process-centric frameworks that incorporate the structural integrity evaluation techniques into formal assessments [235]. These need to be supported by interoperable data formats, validation criteria, and biocompatibility standards tailored for sensor-integrated constructs. Sustained cross-disciplinary collaboration among biologists, engineers, clinicians, and regulators remains essential to establish a quality assurance framework that keeps pace with rapid technical innovation while ensuring safety and accountability.

7. Conclusion

Bioprinting stands at the forefront of regenerative medicine and tissue engineering. It offers the unprecedented ability to fabricate complex, cell-laden structures that can replicate human tissues and organs. However, its successful clinical and commercial translation depends on ensuring structural integrity, mechanical stability, and biological functionality. These objectives are often compromised by printing-related defects and inconsistencies. This review has comprehensively explored how defects form in extrusion-based bioprinting and how they can be detected. Defects arise from mismatches among bioink rheology, process parameters, hardware and design; some first appear at the nozzle as clogging or buckling-induced filament curling, and all manifest as filament-level deviations in size, fusion, delamination, sagging, collapse and breakage that accumulate into construct-level inaccuracy. Several of these failure boundaries can be expressed quantitatively through the wall shear stress, the flow rate–pressure relation, the bending and yield-stress criteria for sagging and the speed ratio for buckling. Among surface methods, optical imaging is the most frequently reported, while microscopy, thermography and laser profilometry add finer resolution, thermal contrast and height profiles. Volumetric methods, namely optical coherence tomography, X-ray computed tomography, magnetic resonance imaging and ultrasound, resolve internal defects, with optical coherence tomography closest to in-process use. Dielectric impedance spectroscopy and flow sensing monitor the state of cells and bioink and the delivered flow rather than geometry. Closed-loop correction has been demonstrated with optical imaging, laser profilometry, optical coherence tomography and flow sensing. Machine learning has been applied mainly to image and video data for defect classification, segmentation and anomaly scoring; demonstrations of machine learning-guided correction remain few and are largely confined to single materials and printers, and dataset size, data splitting and external validation need to be reported for each study. The principal gaps are therefore the absence of standardized defect definitions and shared datasets, the limited validation of sensors and models across laboratories, the coupling between structural and cellular quality, and the integration of multirate sensors into control loops whose timescales match the defects they are meant to correct. Closing them will require collaboration among materials scientists, sensing and control engineers, biologists, clinicians and regulators, together with quality frameworks, such as quality by design, that link measured attributes to process parameters.

8. Conflict of Interest

The authors declare no competing interests.

9. Acknowledgements

This research is supported by the National Science Foundation under Award No. 2301948 and by the faculty research seed grant from the College of Engineering and Computing at Georgia Southern University.

10. References

[1] "Global Observatory on Donation and Transplantation," GODT. Available at: https://www.transplant-observatory.org/, Accessed October 19, 2026.

[2] "Organ Donation Statistics | Organdonor.Gov." Available at: https://www.organdonor.gov/learn/organ-donation-statistics, Accessed October 15, 2026.

[3] Derby, B., 2012, "Printing and Prototyping of Tissues and Scaffolds," Science, **338**(6109), pp. 921–926.

[4] Ng, W. L., and Bartolo, P., 2026, "3D Bioprinting of Tissues and Organs for Systemic Diseases and Localized Injuries," Mil. Med. Res., **13**(1), p. 100006.

[5] Chameettachal, S., Yeleswarapu, S., Sasikumar, S., Shukla, P., Hibare, P., Bera, A. K., Bojedla, S. S. R., and Pati, F., 2019, "3D Bioprinting: Recent Trends and Challenges," J. Indian Inst. Sci., **99**(3), pp. 375–403.

[6] Jergitsch, M., and Mateos-Timoneda, M. A., 2026, "3D Extrusion Bioprinting: Rational Bioink Design and Advanced Fabrication Techniques," Trends Biotechnol., **44**(2), pp. 378–388.

[7] Ng, W. L., and Shkolnikov, V., 2024, "Jetting-Based Bioprinting: Process, Dispense Physics, and Applications," Bio-Des. Manuf., **7**(5), pp. 771–799.

[8] Ng, W. L., Paula, C. T., Serra, A. C., Coelho, J. F., and Bartolo, P., 2026, "Vat Photopolymerization-based Bioprinting: Shaping Next-generation Tissues with Light," Interdiscip. Med., **4**(1), p. e70078.

[9] Hölzl, K., Lin, S., Tytgat, L., Van Vlierberghe, S., Gu, L., and Ovsianikov, A., 2016, "Bioink Properties before, during and after 3D Bioprinting," Biofabrication, **8**(3), p. 032002.

[10] Gillispie, G., Prim, P., Copus, J., Fisher, J., Mikos, A. G., Yoo, J. J., Atala, A., and Lee, S. J., 2020, "Assessment Methodologies for Extrusion-Based Bioink Printability," Biofabrication, **12**(2), p. 022003.

[11] Mirdamadi, E., Tashman, J. W., Shiwarski, D. J., Palchesko, R. N., and Feinberg, A. W., 2020, "FRESH 3D Bioprinting a Full-Size Model of the Human Heart," ACS Biomater. Sci. Eng., **6**(11), pp. 6453–6459.

[12] Kim, M., Kim, Y. J., Kim, Y. S., Roh, T. S., Lee, E.-J., Shim, J.-H., Kang, E. H., Kim, M. J., and Yun, I. S., 2024, "One-Year Results of Ear Reconstruction with 3D Printed Implants," Yonsei Med. J., **65**(8), p. 456.

[13] Ranganathan, P., Han, S. H., Kim, I. G., Oh, D., Kim, Y., Yoon, K.-N., Kim, G., Lee, Y. H., Shirzad, M., and Lee, G., 2025, "Integrated Biofabrication of Artificial Esophageal Scaffolds Using Electrospinning, Embedded DLP, and Extrusion Techniques," Mater. Today Bio, p. 102518.

[14] Mannoor, M. S., Jiang, Z., James, T., Kong, Y. L., Malatesta, K. A., Soboyejo, W. O., Verma, N., Gracias, D. H., and McAlpine, M. C., 2013, "3D Printed Bionic Ears," Nano Lett., **13**(6), pp. 2634–2639.

[15] Nguyen, D. G., Funk, J., Robbins, J. B., Crogan-Grundy, C., Presnell, S. C., Singer, T., and Roth, A. B., 2016, "Bioprinted 3D Primary Liver Tissues Allow Assessment of Organ-Level Response to Clinical Drug Induced Toxicity In Vitro," PLOS ONE, **11**(7), p. e0158674.

[16] Weng, T., Zhang, W., Xia, Y., Wu, P., Yang, M., Jin, R., Xia, S., Wang, J., You, C., Han, C., and Wang, X., 2021, "3D Bioprinting for Skin Tissue Engineering: Current Status and Perspectives," J. Tissue Eng., **12**, p. 20417314211028574.

[17] Wang, X., Zhang, X., Dai, X., Wang, X., Li, X., Diao, J., and Xu, T., 2018, "Tumor-like Lung Cancer Model Based on 3D Bioprinting," 3 Biotech, **8**(12), p. 501.

[18] Hakobyan, D., Médina, C., Dusserre, N., Stachowicz, M.-L., Handschin, C., Fricain, J.-C., Guillermet-Guibert, J., and Oliveira, H., 2020, "Laser-Assisted 3D Bioprinting of Exocrine Pancreas Spheroid Models for Cancer Initiation Study," Biofabrication, **12**(3), p. 035001.

[19] Arjoca, S., Robu, A., Neagu, M., and Neagu, A., 2023, "Mathematical and Computational Models in Spheroid-Based Biofabrication," Acta Biomater., **165**, pp. 125–139.

[20] Welman, T., Michel, S., Segaren, N., and Shanmugarajah, K., 2015, "Bioengineering for Organ Transplantation: Progress and Challenges," Bioengineered, **6**(5), pp. 257–261.

[21] Zoghi, S., 2024, "Advancements in Tissue Engineering: A Review of Bioprinting Techniques, Scaffolds, and Bioinks," Biomed. Eng. Comput. Biol., **15**, p. 11795972241288099.

[22] Arslan-Yildiz, A., Assal, R. E., Chen, P., Guven, S., Inci, F., and Demirci, U., 2016, "Towards Artificial Tissue Models: Past, Present, and Future of 3D Bioprinting," Biofabrication, **8**(1), p. 014103.

[23] Yang, S., Chen, Q., Wang, L., and Xu, M., 2022, "In Situ Defect Detection and Feedback Control with Three-Dimensional Extrusion-Based Bioprinter-Associated Optical Coherence Tomography," Int. J. Bioprinting, **9**(1), p. 624.

[24] Elango, J., and Zamora-Ledezma, C., 2025, "Rheological, Structural, and Biological Trade-Offs in Bioink Design for 3d Bioprinting," Gels, **11**(8), p. 659.

[25] Gillispie, G. J., Han, A., Uzun-Per, M., Fisher, J., Mikos, A. G., Niazi, M. K. K., Yoo, J. J., Lee, S. J., and Atala, A., 2020, "The Influence of Printing Parameters and Cell Density on Bioink Printing Outcomes," Tissue Eng. Part A, **26**(23–24), pp. 1349–1358.

[26] Melchels, F. P. W., Barradas, A. M. C., van Blitterswijk, C. A., de Boer, J., Feijen, J., and Grijpma, D. W., 2010, "Effects of the Architecture of Tissue Engineering Scaffolds on Cell Seeding and Culturing," Acta Biomater., **6**(11), pp. 4208–4217.

[27] Van Bael, S., Chai, Y. C., Truscello, S., Moesen, M., Kerckhofs, G., Van Oosterwyck, H., Kruth, J.-P., and Schrooten, J., 2012, "The Effect of Pore Geometry on the in Vitro Biological Behavior of Human Periosteum-Derived Cells Seeded on Selective Laser-Melted Ti6Al4V Bone Scaffolds," Acta Biomater., **8**(7), pp. 2824–2834.

[28] Gerdes, S., Gaikwad, A., Ramesh, S., Rivero, I. V., Tamayol, A., and Rao, P., 2024, "Monitoring and Control of Biological Additive Manufacturing Using Machine Learning," J. Intell. Manuf., **35**(3), pp. 1055–1077.

[29] Zhang, X., and Zhang, Y., 2015, "Tissue Engineering Applications of Three-Dimensional Bioprinting," Cell Biochem. Biophys., **72**(3), pp. 777–782.

[30] Sun, W., Starly, B., Daly, A. C., Burdick, J. A., Groll, J., Skeldon, G., Shu, W., Sakai, Y., Shinohara, M., Nishikawa, M., Jang, J., Cho, D.-W., Nie, M., Takeuchi, S., Ostrovidov, S., Khademhosseini, A., Kamm, R. D., Mironov, V., Moroni, L., and Ozbolat, I. T., 2020, "The Bioprinting Roadmap," Biofabrication, **12**(2), p. 022002.

[31] Gogoi, D., Kumar, M., and Singh, J., 2024, "A Comprehensive Review on Hydrogel-Based Bio-Ink Development for Tissue Engineering Scaffolds Using 3D Printing," Ann. 3D Print. Med., **15**, p. 100159.

[32] Gungor-Ozkerim, P. S., Inci, I., Zhang, Y. S., Khademhosseini, A., and Dokmeci, M. R., 2018, "Bioinks for 3D Bioprinting: An Overview," Biomater. Sci., **6**(5), pp. 915–946.

[33] Lee, V., Singh, G., Trasatti, J. P., Bjornsson, C., Xu, X., Tran, T. N., Yoo, S.-S., Dai, G., and Karande, P., 2014, "Design and Fabrication of Human Skin by Three-Dimensional Bioprinting," Tissue Eng. Part C Methods, **20**(6), pp. 473–484.

[34] Isaacson, A., Swioklo, S., and Connon, C. J., 2018, "3D Bioprinting of a Corneal Stroma Equivalent," Exp. Eye Res., **173**, pp. 188–193.

[35] Jia, S., Bu, Y., Lau, D.-S. A., Lin, Z., Sun, T., Lu, W. W., Lu, S., Ruan, C., and Chan, C.-H. J., 2023, "Advances in 3D Bioprinting Technology for Functional Corneal Reconstruction and Regeneration," Front. Bioeng. Biotechnol., **10–2022**.

[36] Zheng, X., Huang, J., Lin, J., Yang, D., Xu, T., Chen, D., Zan, X., and Wu, A., 2019, "3D Bioprinting in Orthopedics Translational Research," J. Biomater. Sci. Polym. Ed., **30**(13), pp. 1172–1187.

[37] Chae, S., and Cho, D.-W., 2023, "Biomaterial-Based 3D Bioprinting Strategy for Orthopedic Tissue Engineering," Acta Biomater., **156**, pp. 4–20.

[38] Ricci, G., Gibelli, F., and Sirignano, A., 2023, "Three-Dimensional Bioprinting of Human Organs and Tissues: Bioethical and Medico-Legal Implications Examined through a Scoping Review," Bioengineering, **10**(9), p. 1052.

[39] Yu, K., Yao, Y., Zhang, W., Lu, L., Gao, Q., Zhang, P., and Sing, S. L., 2025, "Defects, Monitoring, and AI-Enabled Control in Soft Material Additive Manufacturing: A Review," Virtual Phys. Prototyp., **20**(1), p. e2588456.

[40] Matavosian, A. A., and Bonassar, L. J., 2025, "Reimagining Bioprinters: Real-Time Monitoring for Quality Control of Bioprinted Constructs and Future Vision," Biofabrication, **17**(4), p. 042008.

[41] Bonatti, A. F., Vozzi, G., and De Maria, C., 2024, "Enhancing Quality Control in Bioprinting through Machine Learning," Biofabrication, **16**(2), p. 022001.

[42] Ramesh, S., Deep, A., Tamayol, A., Kamaraj, A., Mahajan, C., and Madihally, S., 2024, "Advancing 3D Bioprinting through Machine Learning and Artificial Intelligence," Bioprinting, **38**, p. e00331.

[43] Chen, H., Zhang, B., and Huang, J., 2024, "Recent Advances and Applications of Artificial Intelligence in 3D Bioprinting," Biophys. Rev., **5**(3), p. 031301.

[44] Robazzi, J. V. S., Derman, I. D., Gupta, D., Haugh, L., Singh, Y. P., Pal, V., Yilmaz, Y. O., Liu, S., Dias, A. L., and Flauzino, R. A., 2026, "The Synergy of Artificial Intelligence and 3D Bioprinting: Unlocking New Frontiers in Precision and Tissue Fabrication," Adv. Funct. Mater., **36**(1), p. e09530.

[45] Ke, D., 2026, "AI-Driven Closed-Loop Extrusion-Based Bioprinting System: From Dynamic Regulation to Medical Translation," Bioprinting, **54**, p. e00459.

[46] Murphy, S. V., and Atala, A., 2014, "3D Bioprinting of Tissues and Organs," Nat. Biotechnol., **32**(8), pp. 773–785.

[47] Ouyang, L., Yao, R., Zhao, Y., and Sun, W., 2016, "Effect of Bioink Properties on Printability and Cell Viability for 3D Bioplotting of Embryonic Stem Cells," Biofabrication, **8**(3), p. 035020.

[48] Wenger, L., Radtke, C. P., Gerisch, E., Kollmann, M., Niemeyer, C. M., Rabe, K. S., and Hubbuch, J., 2022, "Systematic Evaluation of Agarose-and Agar-Based Bioinks for Extrusion-Based Bioprinting of Enzymatically Active Hydrogels," Front. Bioeng. Biotechnol., **10**, p. 928878.

[49] Sriphutkiat, Y., Kasetsirikul, S., Ketpun, D., and Zhou, Y., 2019, "Cell Alignment and Accumulation Using Acoustic Nozzle for Bioprinting," Sci. Rep., **9**(1), p. 17774.

[50] Manzoli, S., Merotto, E., Piccoli, M., Gobbo, P., Todros, S., and Pavan, P. G., 2025, "An Overview of 3D Bioprinting Impact on Cell Viability: From Damage Assessment to Protection Solutions," J. Funct. Biomater., **16**(12), p. 436.

[51] Therriault, D., White, S. R., and Lewis, J. A., 2007, "Rheological Behavior of Fugitive Organic Inks for Direct-Write Assembly," Appl. Rheol., **17**(1), pp. 10112–10121.

[52] Billiet, T., Gevaert, E., De Schryver, T., Cornelissen, M., and Dubruel, P., 2014, "The 3D Printing of Gelatin Methacrylamide Cell-Laden Tissue-Engineered Constructs with High Cell Viability," Biomaterials, **35**(1), pp. 49–62.

[53] Mouser, V. H., Melchels, F. P., Visser, J., Dhert, W. J., Gawlitta, D., and Malda, J., 2016, "Yield Stress Determines Bioprintability of Hydrogels Based on Gelatin-Methacryloyl and Gellan Gum for Cartilage Bioprinting," Biofabrication, **8**(3), p. 035003.

[54] Gao, T., Gillispie, G. J., Copus, J. S., Pr, A. K., Seol, Y.-J., Atala, A., Yoo, J. J., and Lee, S. J., 2018, "Optimization of Gelatin–Alginate Composite Bioink Printability Using Rheological Parameters: A Systematic Approach," Biofabrication, **10**(3), p. 034106.

[55] Ahmadi Soufivand, A., Faber, J., Hinrichsen, J., and Budday, S., 2023, "Multilayer 3D Bioprinting and Complex Mechanical Properties of Alginate-Gelatin Mesostructures," Sci. Rep., **13**(1), p. 11253.

[56] Lamberger, Z., Schubert, D. W., Buechner, M., Cabezas, N. C., Schrüfer, S., Murenu, N., Schaefer, N., and Lang, G., 2024, "Advanced Optical Assessment and Modeling of Extrusion Bioprinting," Sci. Rep., **14**(1), p. 13972.

[57] Holland, I., 2025, "Extrusion Bioprinting: Meeting the Promise of Human Tissue Biofabrication?," Prog. Biomed. Eng., **7**(2), p. 023001.

[58] Sasikumar, S. C., Goswami, U., and Raichur, A. M., 2024, "3D Bioprinting with Visible Light Cross-Linkable Mucin-Hyaluronic Acid Composite Bioink for Lung Tissue Engineering," ACS Appl. Bio Mater., **7**(8), pp. 5411–5422.

[59] Habib, A., Sathish, V., Mallik, S., and Khoda, B., 2018, "3D Printability of Alginate-Carboxymethyl Cellulose Hydrogel," Materials, **11**(3), p. 454.

[60] Chen, N., Zhu, K., Zhang, Y. S., Yan, S., Pan, T., Abudupataer, M., Yu, G., Alam, M. F., Wang, L., and Sun, X., 2019, "Hydrogel Bioink with Multilayered Interfaces Improves Dispersibility of Encapsulated Cells in Extrusion Bioprinting," ACS Appl. Mater. Interfaces, **11**(34), pp. 30585–30595.

[61] Nair, K., Gandhi, M., Khalil, S., Yan, K. C., Marcolongo, M., Barbee, K., and Sun, W., 2009, "Characterization of Cell Viability during Bioprinting Processes," Biotechnol. J. Healthc. Nutr. Technol., **4**(8), pp. 1168–1177.

[62] Müller, S. J., Fabry, B., and Gekle, S., 2023, "Predicting Cell Stress and Strain during Extrusion Bioprinting," Phys. Rev. Appl., **19**(6), p. 064061.

[63] Boularaoui, S., Al Hussein, G., Khan, K. A., Christoforou, N., and Stefanini, C., 2020, "An Overview of Extrusion-Based Bioprinting with a Focus on Induced Shear Stress and Its Effect on Cell Viability," Bioprinting, **20**, p. e00093.

[64] Cooke, M. E., and Rosenzweig, D. H., 2021, "The Rheology of Direct and Suspended Extrusion Bioprinting," APL Bioeng., **5**(1).

[65] Zhang, J., Wehrle, E., Vetsch, J. R., Paul, G. R., Rubert, M., and Müller, R., 2019, "Alginate Dependent Changes of Physical Properties in 3D Bioprinted Cell-Laden Porous Scaffolds Affect Cell Viability and Cell Morphology," Biomed. Mater., **14**(6), p. 065009.

[66] Wüst, S., Godla, M. E., Müller, R., and Hofmann, S., 2014, "Tunable Hydrogel Composite with Two-Step Processing in Combination with Innovative Hardware Upgrade for Cell-Based Three-Dimensional Bioprinting," Acta Biomater., **10**(2), pp. 630–640.

[67] Ribeiro, A., Blokzijl, M. M., Levato, R., Visser, C. W., Castilho, M., Hennink, W. E., Vermonden, T., and Malda, J., 2017, "Assessing Bioink Shape Fidelity to Aid Material Development in 3D Bioprinting," Biofabrication, **10**(1), p. 014102.

[68] Schwab, A., Levato, R., D'este, M., Piluso, S., Eglin, D., and Malda, J., 2020, "Printability and Shape Fidelity of Bioinks in 3D Bioprinting," Chem. Rev., **120**(19), pp. 11028–11055.

[69] Malekpour, A., and Chen, X., 2022, "Printability and Cell Viability in Extrusion-Based Bioprinting from Experimental, Computational, and Machine Learning Views," J. Funct. Biomater., **13**(2), p. 40.

[70] Xu, H.-Q., Liu, J.-C., Zhang, Z.-Y., and Xu, C.-X., 2022, "A Review on Cell Damage, Viability, and Functionality during 3D Bioprinting," Mil. Med. Res., **9**(1), p. 70.

[71] Cohen, D. L., Lo, W., Tsavaris, A., Peng, D., Lipson, H., and Bonassar, L. J., 2011, "Increased Mixing Improves Hydrogel Homogeneity and Quality of Three-Dimensional Printed Constructs," Tissue Eng. Part C Methods, **17**(2), pp. 239–248.

[72] Huang, G., Zhao, Y., Chen, D., Wei, L., Hu, Z., Li, J., Zhou, X., Yang, B., and Chen, Z., 2024, "Applications, Advancements, and Challenges of 3D Bioprinting in Organ Transplantation," Biomater. Sci., **12**(6), pp. 1425–1448.

[73] Derakhshanfar, S., Mbeleck, R., Xu, K., Zhang, X., Zhong, W., and Xing, M., 2018, "3D Bioprinting for Biomedical Devices and Tissue Engineering: A Review of Recent Trends and Advances," Bioact. Mater., **3**(2), pp. 144–156.

[74] Placone, J. K., and Engler, A. J., 2018, "Recent Advances in Extrusion-based 3D Printing for Biomedical Applications," Adv. Healthc. Mater., **7**(8), p. 1701161.

[75] GhavamiNejad, A., Ashammakhi, N., Wu, X. Y., and Khademhosseini, A., 2020, "Crosslinking Strategies for 3D Bioprinting of Polymeric Hydrogels," Small, **16**(35), p. 2002931.

[76] Simińska-Stanny, J., Tournier, P., Shavandi, A., and Habib, S. J., 2026, "Geometrical Designs in Volumetric Bioprinting to Study Cellular Behaviors in Engineered Constructs," Adv. Healthc. Mater., **15**(6), p. e03550.

[77] Li, B., Wang, Z., Huang, C., Xu, L., Huang, S., Qu, M., Xu, Z., Zhang, D., Guo, B., and Jin, T., 2025, "A Comprehensive Review on the Printing Efficiency, Precision, and Cell Viability in 3D Bioprinting," Med. Eng. Phys., p. 104448.

[78] Paxton, N., Smolan, W., Böck, T., Melchels, F., Groll, J., and Jungst, T., 2017, "Proposal to Assess Printability of Bioinks for Extrusion-Based Bioprinting and Evaluation of Rheological Properties Governing Bioprintability," Biofabrication, **9**(4), p. 044107.

[79] Aliabouzar, M., Ley, A. W. Y., Meurs, S., Putnam, A. J., Baker, B. M., Kripfgans, O. D., Fowlkes, J. B., and Fabiilli, M. L., 2022, "Micropatterning of Acoustic Droplet Vaporization in Acoustically-Responsive Scaffolds Using Extrusion-Based Bioprinting," Bioprinting, **25**, p. e00188.

[80] Rossi, A., Pescara, T., Gambelli, A. M., Gaggia, F., Asthana, A., Perrier, Q., Basta, G., Moretti, M., Senin, N., and Rossi, F., 2024, "Biomaterials for Extrusion-Based Bioprinting and Biomedical Applications," Front. Bioeng. Biotechnol., **12**, p. 1393641.

[81] Tansell, A. V., Mahmoodi, N., Crolla, J. P., Dyson, R. J., Luo, G. J., and Thomas-Seale, L. E. J., 2025, "Exploiting Nozzle Geometry to Predict Resolution in Extrusion-Based Bioprinting: Mathematical Modelling of a Power-Law Fluid," R. Soc. Open Sci., **12**(11).

[82] Rastin, H., Ormsby, R. T., Atkins, G. J., and Losic, D., 2020, "3D Bioprinting of Methylcellulose/Gelatin-Methacryloyl (MC/GelMA) Bioink with High Shape Integrity," ACS Appl. Bio Mater., **3**(3), pp. 1815–1826.

[83] Hinton, T. J., Jallerat, Q., Palchesko, R. N., Park, J. H., Grodzicki, M. S., Shue, H.-J., Ramadan, M. H., Hudson, A. R., and Feinberg, A. W., 2015, "Three-Dimensional Printing of Complex Biological Structures by Freeform Reversible Embedding of Suspended Hydrogels," Sci. Adv., **1**(9), p. e1500758.

[84] Ma, J., Qi, C., Liu, Z., Meng, S., and Kong, T., 2024, "Instability-Driven 3D Bioprinting for Engineering Composite Bio-Inks," Eng. Regen., **5**(3), pp. 350–360.

[85] van der Valk, P. C., and Mirzaali, M. J., 2025, "Non-Planar Additive Manufacturing with Hydrogels: A Review of Flow Control and Toolpath Strategies," Npj Soft Matter, **1**(1), p. 5.

[86] Xu, Y., Wang, C., Yang, Y., Liu, H., Xiong, Z., Zhang, T., and Sun, W., 2022, "A Multifunctional 3D Bioprinting System for Construction of Complex Tissue Structure Scaffolds: Design and Application," Int. J. Bioprinting, **8**(4), p. 617.

[87] Iberite, F., Badiola-Mateos, M., Loggini, S., Paci, C., Ruspi, J., Iachetta, D., Mannini, A., Gruppioni, E., and Ricotti, L., 2024, "3D Bioprinting of Thermosensitive Inks Based on Gelatin, Hyaluronic Acid, and Fibrinogen: Reproducibility and Role of Printing Parameters," Bioprinting, **39**, p. e00338.

[88] Abdollahi, A., Malek-Khatabi, A., Razavi, M. S., Sheikhi, M., Abbaspour, K., Rezagholi, Z., Atashi, A., Rahimzadegan, M., Sadeghi, M., and Javar, H. A., 2023, "The Recent Advancement in the Chitosan-Based Thermosensitive Hydrogel for Tissue Regeneration," J. Drug Deliv. Sci. Technol., **86**, p. 104627.

[89] Yu, K., Gao, Q., Lin, Z., Wang, F., Zhang, P., Liu, Y., and Lu, L., 2024, "Investigation of the Temperature Gradient Control in the Printing Space for the Material Extrusion of Medical Biodegradable Hydrogel," Comput. Biol. Med., **168**, p. 107722.

[90] Gómez-Blanco, J. C., Mancha-Sánchez, E., Marcos, A. C., Matamoros, M., Díaz-Parralejo, A., and Pagador, J. B., 2020, "Bioink Temperature Influence on Shear Stress, Pressure and Velocity Using Computational Simulation," Processes, **8**(7), p. 865.

[91] Li, Q., Zhang, B., Xue, Q., Zhao, C., Luo, Y., Zhou, H., Ma, L., Yang, H., and Bai, D., 2021, "A Systematic Thermal Analysis for Accurately Predicting the Extrusion Printability of Alginate–Gelatin-Based Hydrogel Bioinks," Int. J. Bioprinting, **7**(3), p. 394.

[92] Rahman, T. T., Wood, N., Pei, Z., and Qin, H., 2024, "Effects of Extreme Temperature on Human Bronchial Epithelial Cells in 3D Printed Samples," Bioengineering, **11**(12), p. 1201.

[93] Townsend, J. M., Beck, E. C., Gehrke, S. H., Berkland, C. J., and Detamore, M. S., 2019, "Flow Behavior Prior to Crosslinking: The Need for Precursor Rheology for Placement of Hydrogels in Medical Applications and for 3D Bioprinting," Prog. Polym. Sci., **91**, pp. 126–140.

[94] Kuzucu, M., Vera, G., Beaumont, M., Fischer, S., Wei, P., Shastri, V. P., and Forget, A., 2021, "Extrusion-Based 3D Bioprinting of Gradients of Stiffness, Cell Density, and Immobilized Peptide Using Thermogelling Hydrogels," ACS Biomater. Sci. Eng., **7**(6), pp. 2192–2197.

[95] Magalhães, I. P., Oliveira, P. M. de, Dernowsek, J., Casas, E. B. L., and Casas, M. S. L., 2019, "Investigation of the Effect of Nozzle Design on Rheological Bioprinting Properties Using Computational Fluid Dynamics," Matér. Rio Jan., **24**(3), p. e12401.

[96] Chand, R., Muhire, B. S., and Vijayavenkataraman, S., 2022, "Computational Fluid Dynamics Assessment of the Effect of Bioprinting Parameters in Extrusion Bioprinting," Int. J. Bioprinting, **8**(2), p. 545.

[97] Armstrong, A. A., Norato, J., Alleyne, A. G., and Wagoner Johnson, A. J., 2019, "Direct Process Feedback in Extrusion-Based 3D Bioprinting," Biofabrication, **12**(1), p. 015017.

[98] Armstrong, A. A., Alleyne, A. G., and Wagoner Johnson, A. J., 2020, "1D and 2D Error Assessment and Correction for Extrusion-Based Bioprinting Using Process Sensing and Control Strategies," Biofabrication, **12**(4), p. 045023.

[99] Lee, A., Hudson, A. R., Shiwarski, D. J., Tashman, J. W., Hinton, T. J., Yerneni, S., Bliley, J. M., Campbell, P. G., and Feinberg, A. W., 2019, "3D Bioprinting of Collagen to Rebuild Components of the Human Heart," Science, **365**(6452), pp. 482–487.

[100] Godau, B., Stefanek, E., Gharaie, S. S., Amereh, M., Pagan, E., Marvdashti, Z., Libert-Scott, E., Ahadian, S., and Akbari, M., 2022, "Non-Destructive Mechanical Assessment for Optimization of 3D Bioprinted Soft Tissue Scaffolds," Iscience, **25**(5).

[101] Jungst, T., Smolan, W., Schacht, K., Scheibel, T., and Groll, J., 2016, "Strategies and Molecular Design Criteria for 3D Printable Hydrogels," Chem. Rev., **116**(3), pp. 1496–1539.

[102] Daskalakis, P., Kanakousaki, E., Ntoulias, C., Peponaki, K., Kavatzikidou, P., Manousaki, A., Vlassopoulos, D., Ranella, A., and Stratakis, E., 2025, "3D Bioprinting with High-Viscosity Bioinks: A Custom-Designed Extrusion Head for High-Resolution Cellulose Acetate Scaffolds," Int. J. Bioprinting, **11**(3), pp. 337–357.

[103] Balters, L., and Reichl, S., 2025, "A Design of Experiment to Evaluate the Printability for Bioprinting by Using Deep Learning Image Similarity," J. Biomed. Mater. Res. A, **113**(7), p. e37961.

[104] Gerdes, S., Mostafavi, A., Ramesh, S., Memic, A., Rivero, I. V., Rao, P., and Tamayol, A., 2020, "Process–Structure–Quality Relationships of Three-Dimensional Printed Poly (Caprolactone)-Hydroxyapatite Scaffolds," Tissue Eng. Part A, **26**(5–6), pp. 279–291.

[105] Roehm, K. D., and Madihally, S. V., 2018, "Bioprinted Chitosan-Gelatin Thermosensitive Hydrogels Using an Inexpensive 3D Printer," Biofabrication, **10**(1), p. 015002.

[106] Fu, Z., Angeline, V., and Sun, W., 2021, "Evaluation of Printing Parameters on 3D Extrusion Printing of Pluronic Hydrogels and Machine Learning Guided Parameter Recommendation," Int. J. Bioprinting, **7**(4), p. 434.

[107] Moncal, K. K., Ozbolat, V., Datta, P., Heo, D. N., and Ozbolat, I. T., 2019, "Thermally-Controlled Extrusion-Based Bioprinting of Collagen," J. Mater. Sci. Mater. Med., **30**(5), p. 55.

[108] Cai, B., Kilian, D., Ramos Mejia, D., Rios, R. J., Ali, A., and Heilshorn, S. C., 2024, "Diffusion-based 3D Bioprinting Strategies," Adv. Sci., **11**(8), p. 2306470.

[109] Liu, W., Zhang, Y. S., Heinrich, M. A., De Ferrari, F., Jang, H. L., Bakht, S. M., Alvarez, M. M., Yang, J., Li, Y., and Trujillo-de Santiago, G., 2017, "Rapid Continuous Multimaterial Extrusion Bioprinting," Adv. Mater., **29**(3), p. 1604630.

[110] Strauß, S., Grijalva Garces, D., and Hubbuch, J., 2023, "Analytics in Extrusion-Based Bioprinting: Standardized Methods Improving Quantification and Comparability of the Performance of Bioinks," Polymers, **15**(8), p. 1829.

[111] Koch, F., Thaden, O., Tröndle, K., Zengerle, R., Zimmermann, S., and Koltay, P., 2021, "Open-Source Hybrid 3D-Bioprinter for Simultaneous Printing of Thermoplastics and Hydrogels," HardwareX, **10**, p. e00230.

[112] Fathi, S., Lei, I. M., Cao, Y., and Huang, Y. Y. S., 2023, "Microcapillary Cell Extrusion Deposition with Picolitre Dispensing Resolution," Bio-Des. Manuf., **6**(1), pp. 1–11.

[113] Xin, S., Deo, K. A., Dai, J., Pandian, N. K. R., Chimene, D., Moebius, R. M., Jain, A., Han, A., Gaharwar, A. K., and Alge, D. L., 2021, "Generalizing Hydrogel Microparticles into a New Class of Bioinks for Extrusion Bioprinting," Sci. Adv., **7**(42), p. eabk3087.

[114] Talluri, D. J., Nguyen, H. T., Avazmohammadi, R., and Miri, A. K., 2022, "Ink Rheology Regulates Stability of Bioprinted Strands," J. Biomech. Eng., **144**(7), p. 074503.

[115] Luo, Y., Li, D., Lin, C., Zhou, X., Ma, J., and Zhang, B., 2025, "Three-Dimensional Bioprinting of Gelatin Methacryloyl Hydrogel with a Tri-Layered Vascularized Architecture for Full-Thickness Skin Regeneration," Int. J. Bioprinting, **11**(4), pp. 328–349.

[116] Theus, A. S., Ning, L., Hwang, B., Gil, C., Chen, S., Wombwell, A., Mehta, R., and Serpooshan, V., 2020, "Bioprintability: Physiomechanical and Biological Requirements of Materials for 3D Bioprinting Processes," Polymers, **12**(10), p. 2262.

[117] Soltan, N., Ning, L., Mohabatpour, F., Papagerakis, P., and Chen, X., 2019, "Printability and Cell Viability in Bioprinting Alginate Dialdehyde-Gelatin Scaffolds," ACS Biomater. Sci. Eng., **5**(6), pp. 2976–2987.

[118] Gao, Q., Niu, X., Shao, L., Zhou, L., Lin, Z., Sun, A., Fu, J., Chen, Z., Hu, J., Liu, Y., and He, Y., 2019, "3D Printing of Complex GelMA-Based Scaffolds with Nanoclay," Biofabrication, **11**(3), p. 035006.

[119] Strauß, S., Meutelet, R., Radosevic, L., Gretzinger, S., and Hubbuch, J., 2021, "Image Analysis as PAT-Tool for Use in Extrusion-Based Bioprinting," Bioprinting, **21**, p. e00112.

[120] Gugliandolo, S. G., Margarita, A., Santoni, S., Moscatelli, D., and Colosimo, B. M., 2022, "In-Situ Monitoring of Defects in Extrusion-Based Bioprinting Processes Using Visible Light Imaging," Procedia CIRP, **110**, pp. 219–224.

[121] Bracco, F., Zanderigo, G., Paynabar, K., and Colosimo, B., 2025, "Leveraging Transfer Learning for Efficient Bioprinting," Biofabrication, **17**(3), p. 035022.

[122] Sergis, V., Kelly, D., Pramanick, A., Britchfield, G., Mason, K., and Daly, A. C., 2025, "In-Situ Quality Monitoring during Embedded Bioprinting Using Integrated Microscopy and Classical Computer Vision," Biofabrication, **17**(2), p. 025004.

[123] Prendergast, M. E., and Burdick, J. A., 2022, "Computational Modeling and Experimental Characterization of Extrusion Printing into Suspension Baths," Adv. Healthc. Mater., **11**(7), p. 2101679.

[124] Liu, C., Liu, J., Yang, C., Tang, Y., Lin, Z., Li, L., Liang, H., Lu, W., and Wang, L., 2022, "Computer Vision-Aided 2D Error Assessment and Correction for Helix Bioprinting," Int. J. Bioprinting, **8**(2), p. 547.

[125] Liu, C., Yang, C., Liu, J., Tang, Y., Lin, Z., Li, L., Liang, H., Lu, W., and Wang, L., 2022, "Error Assessment and Correction for Extrusion-Based Bioprinting Using Computer Vision Method," Int. J. Bioprinting, **9**(1), p. 644.

[126] Barjuei, E. S., Shin, J., Kim, K., and Lee, J., 2024, "Precision Improvement of Robotic Bioprinting via Vision-Based Tool Path Compensation," Sci. Rep., **14**(1), p. 17764.

[127] Jin, Z., Zhang, Z., Shao, X., and Gu, G. X., 2023, "Monitoring Anomalies in 3D Bioprinting with Deep Neural Networks," ACS Biomater. Sci. Eng., **9**(7), pp. 3945–3952.

[128] Zanderigo, G., Afghah, F., Colosimo, B. M., and Raman, R., 2025, "Modular and AI-Driven in Situ Monitoring Platform for Real-Time Process Analysis in Embedded Bioprinting," Device, **3**(11).

[129] Sun, J., Yao, K., Huang, K., and Huang, D., 2022, "Machine Learning Applications in Scaffold Based Bioprinting," Mater. Today Proc., **70**, pp. 17–23.

[130] Liu, C., Wang, L., Lu, W., Liu, J., Yang, C., Fan, C., Li, Q., and Tang, Y., 2022, "Computer Vision-Aided Bioprinting for Bone Research," Bone Res., **10**(1), p. 21.

[131] Bonatti, A. F., Vozzi, G., Chua, C. K., and De Maria, C., 2022, "A Deep Learning Quality Control Loop of the Extrusion-Based Bioprinting Process," Int. J. Bioprinting, **8**(4), p. 620.

[132] Gasperini, L., Maniglio, D., Motta, A., and Migliaresi, C., 2015, "An Electrohydrodynamic Bioprinter for Alginate Hydrogels Containing Living Cells," Tissue Eng. Part C Methods, **21**(2), pp. 123–132.

[133] He, J., Zhang, B., Li, Z., Mao, M., Li, J., Han, K., and Li, D., 2020, "High-Resolution Electrohydrodynamic Bioprinting: A New Biofabrication Strategy for Biomimetic Micro/Nanoscale Architectures and Living Tissue Constructs," Biofabrication, **12**(4), p. 042002.

[134] Sun, J., Jing, L., Fan, X., Gao, X., and Liang, Y. C., 2018, "Electrohydrodynamic Printing Process Monitoring by Microscopic Image Identification," Int. J. Bioprinting, **5**(1), p. 164.

[135] Poologasundarampillai, G., Haweet, A., Jayash, S. N., Morgan, G., Moore, J. E., and Candeo, A., 2021, "Real-Time Imaging and Analysis of Cell-Hydrogel Interplay within an Extrusion-Bioprinting Capillary," Bioprinting, **23**, p. e00144.

[136] Sedigh, A., DiPiero, D., Shine, K. M., and Tomlinson, R. E., 2022, "Enhancing Precision in Bioprinting Utilizing Fuzzy Systems," Bioprinting, **25**, p. e00190.

[137] Arduengo, J., Hascoet, N., Chinesta, F., and Hascoet, J.-Y., 2024, "Open-Loop Control System for High Precision Extrusion-Based Bioprinting through Machine Learning Modeling," J. Mach. Eng., **24**(1), pp. 103–117.

[138] Tashman, J. W., Shiwarski, D. J., Coffin, B., Ruesch, A., Lanni, F., Kainerstorfer, J. M., and Feinberg, A. W., 2022, "In Situ Volumetric Imaging and Analysis of FRESH 3D Bioprinted Constructs Using Optical Coherence Tomography," Biofabrication, **15**(1), p. 014102.

[139] Van Der Valk, D. C., Van Der Ven, C. F. T., Blaser, M. C., Grolman, J. M., Wu, P.-J., Fenton, O. S., Lee, L. H., Tibbitt, M. W., Andresen, J. L., Wen, J. R., Ha, A. H., Buffolo, F., Van Mil, A., Bouten, C. V. C., Body, S. C., Mooney, D. J., Sluijter, J. P. G., Aikawa, M., Hjortnaes, J., Langer, R., and Aikawa, E., 2018, "Engineering a 3D-Bioprinted Model of Human Heart Valve Disease Using Nanoindentation-Based Biomechanics," Nanomaterials, **8**(5), p. 296.

[140] Koch, M., and Włodarczyk-Biegun, M. K., 2020, "Faithful Scanning Electron Microscopic (SEM) Visualization of 3D Printed Alginate-Based Scaffolds," Bioprinting, **20**, p. e00098.

[141] Aston, R., Sewell, K., Klein, T., Lawrie, G., and Grøndahl, L., 2016, "Evaluation of the Impact of Freezing Preparation Techniques on the Characterisation of Alginate Hydrogels by Cryo-SEM," Eur. Polym. J., **82**, pp. 1–15.

[142] Franco, A., Van Durme, B., Van Vlierberghe, S., and Dupont-Gillain, C., 2024, "Misleading Pore Size Measurements in Gelatin and Alginate Hydrogels Revealed by Confocal Microscopy," Tissue Eng. Part C Methods, **30**(7), pp. 307–313.

[143] Chu, H., Zhang, K., Rao, Z., Song, P., Lin, Z., Zhou, J., Yang, L., Quan, D., and Bai, Y., 2023, "Harnessing Decellularised Extracellular Matrix Microgels into Modular Bioinks for Extrusion-Based Bioprinting with Good Printability and High Post-Printing Cell Viability," Biomater. Transl., **4**(2), p. 115.

[144] Gugliandolo, S. G., Prioglio, E., Moscatelli, D., and Colosimo, B. M., 2024, "A New Solution for in Situ Monitoring of Shape Fidelity in Extrusion-Based Bioprinting via Thermal Imaging," Int. J. Bioprinting, **10**(3), pp. 394–407.

[145] Prioglio, E., Zanderigo, G., and Colosimo, B. M., 2026, "In-Line Process Monitoring of Extrusion-Based Bioprinting Using In-Situ Thermal Imaging," Procedia CIRP, **138**, pp. 1207–1212.

[146] Chen, J. G., Wadhwa, N., Cha, Y.-J., Durand, F., Freeman, W. T., and Buyukozturk, O., 2014, "Structural Modal Identification Through High Speed Camera Video: Motion Magnification," *Topics in Modal Analysis I, Volume 7*, J. De Clerck, ed., Springer International Publishing, Cham, pp. 191–197.

[147] Chen, J. G., Davis, A., Wadhwa, N., Durand, F., Freeman, W. T., and Büyüköztürk, O., 2017, "Video Camera–Based Vibration Measurement for Civil Infrastructure Applications," J. Infrastruct. Syst., **23**(3), p. B4016013.

[148] Friedrich, L., and Begley, M., 2020, "Corner Accuracy in Direct Ink Writing with Support Material," Bioprinting, **19**, p. e00086.

[149] Gharraei, R., Bergstrom, D., and Chen, X. (Daniel), 2024, "Extrusion Bioprinting from a Fluid Mechanics Perspective," ACC Sci. Publ., **10**(6).

[150] Bonatti, A. F., Vozzi, G., Kai Chua, C., and De Maria, C., 2022, "A Deep Learning Approach for Error Detection and Quantification in Extrusion-Based Bioprinting," Mater. Today Proc., **70**, pp. 131–135.

[151] Sarrafi, A., Mao, Z., Niezrecki, C., and Poozesh, P., 2018, "Vibration-Based Damage Detection in Wind Turbine Blades Using Phase-Based Motion Estimation and Motion Magnification," J. Sound Vib., **421**, pp. 300–318.

[152] Wadhwa, N., Rubinstein, M., Durand, F., and Freeman, W. T., 2013, "Phase-Based Video Motion Processing," ACM Trans. Graph., **32**(4), pp. 1–10.

[153] Sands, M., and Kim, J., 2023, "A Low-Cost and Open-Source Measurement System to Determine the Young's and Shear Moduli and Poisson's Ratio of Soft Materials Using a Raspberry Pi Camera Module and 3D Printed Parts," HardwareX, **13**, p. e00386.

[154] Taylor, R., and Kim, J., 2023, "Monitoring Volumetric Defects in 3D Bioprinting Using Video-Based Vibrometry," American Society of Mechanical Engineers Digital Collection.

[155] Rahman, M. A., Khan, M. A. H., Mai, T., and Kim, J., 2026, "Non-Contact and Non-Destructive Detection of Structural Defects in Bioprinted Constructs Using Video-Based Vibration Analysis," Bioprinting, **58**, p. e00490.

[156] Vijayavenkataraman, S., Yan, W.-C., Lu, W. F., Wang, C.-H., and Fuh, J. Y. H., 2018, "3D Bioprinting of Tissues and Organs for Regenerative Medicine," Adv. Drug Deliv. Rev., **132**, pp. 296–332.

[157] Dababneh, A. B., and Ozbolat, I. T., 2014, "Bioprinting Technology: A Current State-of-the-Art Review," J. Manuf. Sci. Eng., **136**(061016).

[158] Armstrong, A. A., Pfeil, A., Alleyne, A. G., and Wagoner Johnson, A. J., 2021, "Process Monitoring and Control Strategies in Extrusion-Based Bioprinting to Fabricate Spatially Graded Structures," Bioprinting, **21**, p. e00126.

[159] Huang, D., Swanson, E. A., Lin, C. P., Schuman, J. S., Stinson, W. G., Chang, W., Hee, M. R., Flotte, T., Gregory, K., Puliafito, C. A., and Fujimoto, J. G., 1991, "Optical Coherence Tomography," Science, **254**(5035), pp. 1178–1181.

[160] Swanson, E. A., and Fujimoto, J. G., 2017, "The Ecosystem That Powered the Translation of OCT from Fundamental Research to Clinical and Commercial Impact [Invited]," Biomed. Opt. Express, **8**(3), pp. 1638–1664.

[161] Fu, M.-Y., Yin, Z.-H., Yao, X.-Y., Xu, J., Liu, Y., Dong, Y., and Shen, Y.-C., 2024, "The Progress of Optical Coherence Tomography in Industry Applications," Adv. Devices Instrum., **5**, p. 0053.

[162] Wang, L., Xu, M., Zhang, L., Zhou, Q., and Luo, L., 2016, "Automated Quantitative Assessment of Three-Dimensional Bioprinted Hydrogel Scaffolds Using Optical Coherence Tomography," Biomed. Opt. Express, **7**(3), p. 894.

[163] Yang, S., Wang, L., Chen, Q., and Xu, M., 2021, "In Situ Process Monitoring and Automated Multi-Parameter Evaluation Using Optical Coherence Tomography during Extrusion-Based Bioprinting," Addit. Manuf., **47**, p. 102251.

[164] Fan, B., Yang, S., Wang, L., and Xu, M., 2024, "Spatially Resolved Defect Characterization and Fidelity Assessment for Complex and Arbitrary Irregular 3D Printing Based on 3D P-OCT and GCode," Sensors, **24**(11), p. 3636.

[165] Shiwarski, D. J., Hudson, A. R., Tashman, J. W., Bakirci, E., Moss, S., Coffin, B. D., and Feinberg, A. W., 2025, "3D Bioprinting of Collagen-Based High-Resolution Internally Perfusable Scaffolds for Engineering Fully Biologic Tissue Systems," Sci. Adv., **11**(17), p. eadu5905.

[166] Yang, S., Li, Y., Ye, J., Wang, L., and Xu, M., 2025, "Three-Dimensional Bioprinting Utilizing Sacrificial Material Support and Longitudinal Printability Evaluation through Volumetric Imaging," Biomater. Adv., **169**, p. 214188.

[167] Chen, E. P., Toksoy, Z., Davis, B. A., and Geibel, J. P., 2021, "3D Bioprinting of Vascularized Tissues for in Vitro and in Vivo Applications," Front. Bioeng. Biotechnol., **Volume 9-2021**.

[168] Ricciardi, R., Auriemma, F., De Rosa, C., and Lauprêtre, F., 2004, "X-Ray Diffraction Analysis of Poly (Vinyl Alcohol) Hydrogels, Obtained by Freezing and Thawing Techniques," Macromolecules, **37**(5), pp. 1921–1927.

[169] Mansur, H. S., Oréfice, R. L., and Mansur, A. A., 2004, "Characterization of Poly (Vinyl Alcohol)/Poly (Ethylene Glycol) Hydrogels and PVA-Derived Hybrids by Small-Angle X-Ray Scattering and FTIR Spectroscopy," Polymer, **45**(21), pp. 7193–7202.

[170] Gorodzha, S., Douglas, T. E., Samal, S. K., Detsch, R., Cholewa-Kowalska, K., Braeckmans, K., Boccaccini, A. R., Skirtach, A. G., Weinhardt, V., and Baumbach, T., 2016, "High-resolution Synchrotron X-ray Analysis of Bioglass-enriched Hydrogels," J. Biomed. Mater. Res. A, **104**(5), pp. 1194–1201.

[171] Keklikoglou, K., Arvanitidis, C., Chatzigeorgiou, G., Chatzinikolaou, E., Karagiannidis, E., Koletsa, T., Magoulas, A., Makris, K., Mavrothalassitis, G., and Papanagnou, E.-D., 2021, "Micro-CT for Biological and Biomedical Studies: A Comparison of Imaging Techniques," J. Imaging, **7**(9), p. 172.

[172] Moosmann, J., Ershov, A., Weinhardt, V., Baumbach, T., Prasad, M. S., LaBonne, C., Xiao, X., Kashef, J., and Hofmann, R., 2014, "Time-Lapse X-Ray Phase-Contrast Microtomography for in Vivo Imaging and Analysis of Morphogenesis," Nat. Protoc., **9**(2), pp. 294–304.

[173] Tuan, H. S., and Hutmacher, D. W., 2005, "Application of Micro CT and Computation Modeling in Bone Tissue Engineering," Comput.-Aided Des., **37**(11), pp. 1151–1161.

[174] Datta, S., Jana, S., Das, A., Chakraborty, A., Chowdhury, A. R., and Datta, P., 2020, "Bioprinting of Radiopaque Constructs for Tissue Engineering and Understanding Degradation Behavior by Use of Micro-CT," Bioact. Mater., **5**(3), pp. 569–576.

[175] Ning, L., Zhu, N., Smith, A., Rajaram, A., Hou, H., Srinivasan, S., Mohabatpour, F., He, L., Mclnnes, A., Serpooshan, V., Papagerakis, P., and Chen, X., 2021, "Noninvasive Three-Dimensional In Situ and In Vivo Characterization of Bioprinted Hydrogel Scaffolds Using the X-Ray Propagation-Based Imaging Technique," ACS Appl. Mater. Interfaces, **13**(22), pp. 25611–25623.

[176] Gureyev, T., Nesterets, Y. I., Baran, P., Taba, S., Mayo, S., Thompson, D., Arhatari, B., Mihocic, A., Abbey, B., and Lockie, D., 2019, "Propagation-based X-ray Phase-contrast Tomography of Mastectomy Samples Using Synchrotron Radiation," Med. Phys., **46**(12), pp. 5478–5487.

[177] Appel, A., Anastasio, M. A., and Brey, E. M., 2011, "Potential for Imaging Engineered Tissues with X-Ray Phase Contrast," Tissue Eng. Part B Rev., **17**(5), pp. 321–330.

[178] Keklikoglou, K., Faulwetter, S., Chatzinikolaou, E., Wils, P., Brecko, J., Kvaček, J., Metscher, B., and Arvanitidis, C., 2019, "Micro-Computed Tomography for Natural History Specimens: A Handbook of Best Practice Protocols," Eur. J. Taxon., (522).

[179] Ramirez, S. P., Hernandez, I., Balcorta, H. V., Kumar, P., Kumar, V., Poon, W., and Joddar, B., 2023, "Microcomputed Tomography for the Microstructure Evaluation of 3D Bioprinted Scaffolds," ACS Appl. Bio Mater., **7**(12), pp. 7799–7808.

[180] Haleem, A., and Javaid, M., 2018, "Role of CT and MRI in the Design and Development of Orthopaedic Model Using Additive Manufacturing," J. Clin. Orthop. Trauma, **9**(3), pp. 213–217.

[181] Fu, F., Qin, Z., Xu, C., Chen, X., Li, R., Wang, L., Peng, D., Sun, H., Tu, Y., Chen, C., Zhang, S., Zhao, M., and Li, X., 2017, "Magnetic Resonance Imaging-Three-Dimensional Printing Technology Fabricates Customized Scaffolds for Brain Tissue Engineering," Neural Regen. Res., **12**(4), p. 614.

[182] Tomer, G., Newton, J. M., and Kinchesh, P., 1999, "Magnetic Resonance Imaging (MRI) as a Method to Investigate Movement of Water During the Extrusion of Pastes," Pharm. Res., **16**(5), pp. 666–671.

[183] Schmieg, B., Gretzinger, S., Schuhmann, S., Guthausen, G., and Hubbuch, J., 2022, "Magnetic Resonance Imaging as a Tool for Quality Control in Extrusion-Based Bioprinting," Biotechnol. J., **17**(5), p. 2100336.

[184] Chen, Z., Yan, C., Yan, S., Liu, Q., Hou, M., Xu, Y., and Guo, R., 2018, "Non-Invasive Monitoring of in Vivo Hydrogel Degradation and Cartilage Regeneration by Multiparametric MR Imaging," Theranostics, **8**(4), pp. 1146–1158.

[185] Gnanago, J.-L., Gerges, T., Chastagnier, L., Petiot, E., Semet, V., Lombard, P., Christophe, M., Cabrera, M., and Lambert, S. A., 2021, "Compact MRI Bioreactor for Real-Time Monitoring 3D Printed Tissue-Engineered Constructs.," *2021 ISMRM & SMRT Annual Meeting and Exhibition*.

[186] Theus, A. S., Ning, L., Kabboul, G., Hwang, B., Tomov, M. L., LaRock, C. N., Bauser-Heaton, H., Mahmoudi, M., and Serpooshan, V., 2022, "3D Bioprinting of Nanoparticle-Laden Hydrogel Scaffolds with Enhanced Antibacterial and Imaging Properties," iScience, **25**(9).

[187] Narayanan, L. K., Thompson, T. L., Shirwaiker, R. A., and Starly, B., 2018, "Label Free Process Monitoring of 3D Bioprinted Engineered Constructs via Dielectric Impedance Spectroscopy," Biofabrication, **10**(3), p. 035012.

[188] Narayanan, L. K., 2019, *Manufacturability Considerations in Biofabrication–Functional Mapping, Risk Assessment and Dielectric Impedance Spectroscopy-Based Non-Destructive Quality Evaluation*, North Carolina State University.

[189] Haring, A. P., Jiang, S., Barron, C., Thompson, E. G., Sontheimer, H., He, J.-Q., Jia, X., and Johnson, B. N., 2020, "3D Bioprinting Using Hollow Multifunctional Fiber Impedimetric Sensors," Biofabrication, **12**(3), p. 035026.

[190] Shohan, S., Harm, J., Hasan, M., Starly, B., and Shirwaiker, R., 2021, "Non-Destructive Quality Monitoring of 3D Printed Tissue Scaffolds via Dielectric Impedance Spectroscopy and Supervised Machine Learning," Procedia Manuf., **53**, pp. 636–643.

[191] Matavosian, A. A., Griffin, A. C., Bhuiyan, D. B., Lyness, A. M., Bhatnagar, V., and Bonassar, L. J., 2025, "Real-Time Assessment of Cell Concentration and Viability Onboard a Syringe Using Dielectric Impedance Spectroscopy for Extrusion Bioprinting," Biofabrication, **17**(2), p. 025018.

[192] Matavosian, A. A., Griffin, A., and Bonassar, L. J., 2026, "Alginate Bioink Properties Influence Real-Time Impedance Monitoring of Cells during Extrusion Bioprinting," Biofabrication, **18**(2), p. 025031.

[193] Kim, K., and Wagner, W. R., 2016, "Non-Invasive and Non-Destructive Characterization of Tissue Engineered Constructs Using Ultrasound Imaging Technologies: A Review," Ann. Biomed. Eng., **44**(3), pp. 621–635.

[194] Dalecki, D., Mercado, K. P., and Hocking, D. C., 2016, "Quantitative Ultrasound for Nondestructive Characterization of Engineered Tissues and Biomaterials," Ann. Biomed. Eng., **44**(3), pp. 636–648.

[195] Zhou, Y., 2016, "The Application of Ultrasound in 3D Bio-Printing," Molecules, **21**(5).

[196] Yang, T., Jin, Y., Smith, L. M., Dahotre, N. B., and Neogi, A., 2024, "Real-Time in-Situ Ultrasound Monitoring of Soft Hydrogel 3D Printing with Subwavelength Resolution," Commun. Eng., **3**(1), p. 162.

[197] Kim, G., Oh, D., Kim, D., Lee, G., Park, S.-H., Yoon, C., and Nam, S. Y., 2025, "Suspended Bioprinting with In-Situ Elasticity Monitoring Using the Assessment of Shear Wave Phase Velocity," Addit. Manuf., **99**, p. 104667.

[198] Strauß, S., Schroth, B., and Hubbuch, J., 2022, "Evaluation of the Reproducibility and Robustness of Extrusion-Based Bioprinting Processes Applying a Flow Sensor," Front. Bioeng. Biotechnol., **10**.

[199] Wenger, L., Strauß, S., and Hubbuch, J., 2022, "Automated and Dynamic Extrusion Pressure Adjustment Based on Real-Time Flow Rate Measurements for Precise Ink Dispensing in 3D Bioprinting," Bioprinting, **28**, p. e00229.

[200] Fang, Q., Xiong, G., Zhou, M., Tamir, T. S., Yan, C.-B., Wu, H., Shen, Z., and Wang, F.-Y., 2024, "Process Monitoring, Diagnosis and Control of Additive Manufacturing," IEEE Trans. Autom. Sci. Eng., **21**(1), pp. 1041–1067.

[201] Yeshiwas, T. A., Tiruneh, A. B., and Sisay, M. A., 2025, "A Review Article on the Assessment of Additive Manufacturing," J. Mater. Sci. Mater. Eng., **20**(1), p. 85.

[202] Wang, P., Wu, Z., Ten, J. J. S., Huang, J., and Nai, M. L. S., 2026, "Towards Intelligent Defect Detection in Metal Powder Bed Fusion: A Review of in Situ Monitoring, Data Pre-Processing, and Machine Learning," Mater. Sci. Eng. R Rep., **167**, p. 101112.

[203] Kelly, D., Sergis, V., Ventura i Blanco, L., Mason, K., and Daly, A. C., 2025, "Autonomous Control of Extrusion Bioprinting Using Convolutional Neural Networks," Adv. Funct. Mater., **35**(30), p. 2424553.

[204] Arduengo, J., Hascoët, N., Chinesta, F., and Hascoet, J.-Y., 2025, "Closed-Loop Control of Extrusion-Based Bioprinting through Real-Time Computer Vision," J. Mach. Eng., **25**.

[205] Zanderigo, G., Bracco, F., Semeraro, Q., and Colosimo, B. M., 2023, "In-Situ Printability Maps (IPM): A New Approach for in-Situ Printability Assessment with Application to Extrusion-Based Bioprinting," Bioprinting, **36**, p. e00320.

[206] Zhang, C., Elvitigala, K. C. M. L., and Sakai, S., 2026, "AI-Powered Printability Evaluation Framework for 3D Bioprinting Using Hausdorff Distance Metrics," Biofabrication, **18**(1), p. 015015.

[207] Margarita, A., Gugliandolo, S. G., Santoni, S., Moscatelli, D., and Colosimo, B. M., 2025, "A Novel Solution for Real-Time in-Situ Cell Distribution Monitoring in 3D Bioprinting via Fluorescence Imaging," Biofabrication, **17**(2).

[208] Kim, S. H., Kwon, J. S., Cho, J. G., Park, K. G., Lim, T. H., Kim, M. S., Choi, H. S., Park, C. H., and Lee, S. J., 2021, "Non-Invasive in Vivo Monitoring of Transplanted Stem Cells in 3D-Bioprinted Constructs Using near-Infrared Fluorescent Imaging," Bioeng. Transl. Med., **6**(2), p. e10216.

[209] Rahman, M. A., Khan, M. A. H., and Kim, J., 2024, "Nozzle Pressure Defect Detection in Extrusion-Based Bio 3D Printing Using Video-Based Motion Estimation," *ASME 2024 Conference on Smart Materials, Adaptive Structures and Intelligent Systems*, American Society of Mechanical Engineers, Atlanta, Georgia, USA, p. V001T05A008.

[210] Khan, M. A. H., Rahman, M. A., and Kim, J., 2025, "In-Situ Condition Monitoring of Extrusion-Based 3d Bio-Printing Using Phase-Based Motion Estimation," American Society of Mechanical Engineers Digital Collection.

[211] Zhang, J., Yu, K., Yao, Y., Lu, L., Gao, Q., Zhang, P., Shang, G., and Sing, S. L., 2026, "A Transformer-Based Framework for Cross-Material in Situ Monitoring in Extrusion-Based Bioprinting," Adv. Eng. Inform., **71**, p. 104323.

[212] Ramya, V., Rohith, S. L., and Ananthi, G., 2024, "Automated Defect Classification in 3D Bioprinting Using Liquid Neural Networks," IEEE, pp. 1–5.

[213] Bastianini, B., 2024, "Predictive Modeling and In-Situ Optimization of Two-Photon Bioprinting Using Deep Learning Techniques."

[214] Dey, M. K., Ikponmwoba, E., John, P., Belgodere, J. A., Semmes, I., Park, D. S., Monroe, W. T., and Devireddy, R., "Ai Driven Dual-Task Deep Learning Framework for Automated Scaffold Quality Assessment in Extrusion Based 3d Bioprinting," Available SSRN 5374136.

[215] Diamantides, N., Dugopolski, C., Blahut, E., Kennedy, S., and Bonassar, L. J., 2019, "High Density Cell Seeding Affects the Rheology and Printability of Collagen Bioinks," Biofabrication, **11**(4), p. 045016.

[216] Walker, J. M., Myers, A. M., Schluchter, M. D., Goldberg, V. M., Caplan, A. I., Berilla, J. A., Mansour, J. M., and Welter, J. F., 2011, "Nondestructive Evaluation of Hydrogel Mechanical Properties Using Ultrasound," Ann. Biomed. Eng., **39**(10), pp. 2521–2530.

[217] Gudur, M., Rao, R. R., Hsiao, Y.-S., Peterson, A. W., Deng, C. X., and Stegemann, J. P., 2012, "Noninvasive, Quantitative, Spatiotemporal Characterization of Mineralization in Three-Dimensional Collagen Hydrogels Using High-Resolution Spectral Ultrasound Imaging," Tissue Eng. Part C Methods, **18**(12), pp. 935–946.

[218] Chansoria, P., Narayanan, L. K., Schuchard, K., and Shirwaiker, R., 2019, "Ultrasound-Assisted Biofabrication and Bioprinting of Preferentially Aligned Three-Dimensional Cellular Constructs," Biofabrication, **11**(3), p. 035015.

[219] Bushnell, G. G., Hong, X., Hartfield, R. M., Zhang, Y., Oakes, R. S., Rao, S. S., Jeruss, J. S., Stegemann, J. P., Deng, C. X., and Shea, L. D., 2020, "High Frequency Spectral Ultrasound Imaging to Detect Metastasis in Implanted Biomaterial Scaffolds," Ann. Biomed. Eng., **48**(1), pp. 477–489.

[220] Yu, C., and Jiang, J., 2020, "A Perspective on Using Machine Learning in 3D Bioprinting," Int. J. Bioprinting, **6**(1), p. 253.

[221] Ruberu, K., Senadeera, M., Rana, S., Gupta, S., Chung, J., Yue, Z., Venkatesh, S., and Wallace, G., 2021, "Coupling Machine Learning with 3D Bioprinting to Fast Track Optimisation of Extrusion Printing," Appl. Mater. Today, **22**, p. 100914.

[222] Rafieyan, S., Ansari, E., and Vasheghani-Farahani, E., 2024, "A Practical Machine Learning Approach for Predicting the Quality of 3D (Bio) Printed Scaffolds," Biofabrication, **16**(4), p. 045014.

[223] Mohammadrezaei, D., Podina, L., Silva, J. D., and Kohandel, M., 2024, "Cell Viability Prediction and Optimization in Extrusion-Based Bioprinting via Neural Network-Based Bayesian Optimization Models," Biofabrication, **16**(2), p. 025016.

[224] Ning, H., Zhou, T., and Joo, S. W., 2023, "Machine Learning Boosts Three-Dimensional Bioprinting," Int. J. Bioprinting, **9**(4), p. 739.

[225] Oh, D., Shirzad, M., Kim, M. C., Chung, E. J., and Nam, S. Y., 2023, "Rheology-Informed Hierarchical Machine Learning Model for the Prediction of Printing Resolution in Extrusion-Based Bioprinting," Int. J. Bioprinting, **9**(6), pp. 308–324.

[226] Mueller, E., Desai, S., Lundberg, M. S., Somara, S., Kengla, C., Schmidt, J., and Mitra, K., 2026, "Integrating 3D Bioprinting and AI in Healthcare," Curr. Stem Cell Rep., **12**(1), p. 1.

[227] Ramya, V., Vinothini, N., Levin Rohith, S., and Ananthi, G., 2026, "DenseNet-Driven Federated Learning for Enhanced Fault Detection in 3D Bioprinting," *Innovative and Intelligent Computing for Global Sustainability*, Springer, pp. 9–17.

[228] Grigioni, M., Daniele, C., Morbiducci, U., D'Avenio, G., Di Benedetto, G., and Barbaro, V., 2004, "The Power-law Mathematical Model for Blood Damage Prediction: Analytical Developments and Physical Inconsistencies," Artif. Organs, **28**(5), pp. 467–475.

[229] Grigioni, M., Morbiducci, U., D'Avenio, G., Benedetto, G. D., and Gaudio, C. D., 2005, "A Novel Formulation for Blood Trauma Prediction by a Modified Power-Law Mathematical Model," Biomech. Model. Mechanobiol., **4**(4), pp. 249–260.

[230] Suh, Y. J., Lim, T. H., Choi, H. S., Kim, M. S., Lee, S. J., Kim, S. H., and Park, C. H., 2020, "3D Printing and NIR Fluorescence Imaging Techniques for the Fabrication of Implants," Materials, **13**(21), p. 4819.

[231] West-Livingston, L. N., Park, J., Lee, S. J., Atala, A., and Yoo, J. J., 2020, "The Role of the Microenvironment in Controlling the Fate of Bioprinted Stem Cells," Chem. Rev., **120**(19), pp. 11056–11092.

[232] Kalman, R. E., 1960, "A New Approach to Linear Filtering and Prediction Problems," J. Basic Eng., **82**(1), pp. 35–45.

[233] Zhang, C., Elvitigala, K. C. M. L., Mubarok, W., Okano, Y., and Sakai, S., 2024, "Machine Learning-Based Prediction and Optimisation Framework for as-Extruded Cell Viability in Extrusion-Based 3D Bioprinting," Virtual Phys. Prototyp., **19**(1), p. e2400330.

[234] "ISO/ASTM 52900:2021," ISO. Available at: https://www.iso.org/standard/74514.html, Accessed October 21, 2026.

[235] Mladenovska, T., Choong, P. F., Wallace, G. G., and O'Connell, C. D., 2023, "The Regulatory Challenge of 3D Bioprinting," Regen. Med., **18**(8), pp. 659–674.

[236] Li, P., Faulkner, A., and Medcalf, N., 2020, "3D Bioprinting in a 2D Regulatory Landscape: Gaps, Uncertainties, and Problems," Law Innov. Technol., **12**(1), pp. 1–29.

[237] Hourd, P., Medcalf, N., Segal, J., and Williams, D. J., 2015, "A 3D Bioprinting Exemplar of the Consequences of the Regulatory Requirements on Customized Processes," Regen. Med., **10**(7), pp. 863–883.

[238] "3D Bio-Printed Products: ICMRA Members Discuss Potential Regulatory Frameworks." Available at: https://www.raps.org/news-and-articles/news-articles/2019/10/3d-bio-printed-products-icmra-members-discuss-pot, Accessed October 19, 2026.